Improving bipolar electrode sensors by improving electrochemiluminescence efficiency of Ru(bpy)$_3$Cl$_2$

by

Waliul Islam Khan

A thesis submitted to the Graduate Faculty of
Auburn University
in partial fulfillment of the
requirements for the Degree of
Master of Science

Auburn, Alabama
December 12, 2020

Keywords: Bipolar Electrochemistry, Electrochemiluminescence,
Surface Plasmon Resonance, Gold Nanorods

Approved by

Dr. Curtis Shannon, Chair, Emeritus Professor of Chemistry and Biochemistry
Dr. Christopher Easley, Professor of Chemistry and Biochemistry
Dr. Byron Farnum, Assistant Professor of Chemistry and Biochemistry
Dr. Wei Zhan, Associate Professor of Chemistry and Biochemistry

Abstract

    Bipolar electrochemistry belongs to the branch of electrochemistry where cathodic and anodic processes can be coupled. As there is no direct contact establishes between the bipolar electrodes and electrical connection, the best way to measure the current produced in the bipolar electrode system is by analyzing the electrochemiluminescence produces by passing the current the voltage across the bipolar electrode system from an external source such as a potentiostat. $Ru(bpy)_3Cl_2$ is the preferred reagent which shows ECL (electrochemiluminescence) as it is electrochemically stable, but it has very lower ECL efficiency 3.5-6%. So, the motivation of the research came from the improvement of the sensitivity of the ECL based sensor. ECL based Bipolar electrochemistry have applications in different fields such as clinical diagnostics including thyroid, hormone, tumor, cardiac, diabetes diseases & other diseases causing infections, food testing, water testing, detection of biowarfare, detection of electrolytes and heavy metals, in detecting explosives, in batteries.

    This dissertation is organized as follows. The first chapter is the introduction in which the basic principle of bipolar electrochemistry and electrochemiluminescence and their application to different fields are discussed.

    Chapter 2 discusses the results I found and the possible explanation supporting the results.

    Chapter 3 discusses the improvements possible related to the research field for further research.

Chapter 4 is the conclusion and discusses the importance of bipolar electrochemistry and electrochemistry, the overall research done and how the research should be further progressed in the future.

Table of Contents

List of Tables

List of Figures

xiv

Chapter One

Introduction

Bipolar electrochemistry is an electrochemical system based on coupling anodic and cathodic processes. In the sensor based on bipolar electrochemistry, a material is placed inside the cell which is known as bipolar electrode. When voltage is applied along the driving electrode, current is generated across the bipolar electrode. But there is no direct way of measuring current across the bipolar electrode as it has no external connection. Amongst, all the possible way of measuring current across the bipolar electrode, ECL is the most popular one. ECL belongs to the formation of light from the excited state of a substance which is formed by transferring electrons from the species generated on the surface of an electrode. The best reagent for producing ECL is $Ru(bpy)_3^{2+}$ and its derivatives as they are highly soluble in water, highly stable electrochemically and can be repeatedly generated in ECL reaction [1]. However, the efficiency of ECL solution made of $Ru(bpy)_3^2$ is very low, 3.5-6% [2]. Bipolar sensing has many applications in the field of battery, solar cells, in electrosynthesis, sensing different organic, inorganic molecules including DNA, cancer cells, heavy metals etc. So, my present work is dedicated to improve sensitivity of the bipolar electrode.

The target of improving sensitivity of the bipolar electrochemical sensor can be achieved by increasing bipolar electrochemical sensitivity based on surface plasmon resonance effect of gold nanorods.

1.1 Background:

Bipolar electrode is a conducting substrate in solution which has no direct electrical contact and which can act both as cathode and anode upon applying a voltage higher than a threshold voltage.
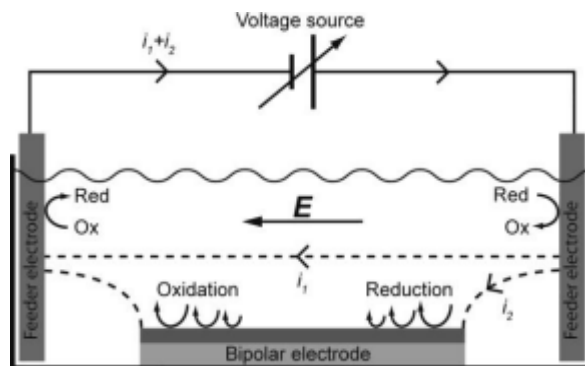
Figure 1. 1 Experimental setup of a bipolar electrode showing the redox processes [3]

(Reprinted with permission from Ref.3. Copyright © 2009, Analytical Chemistry)

In the bipolar electrode cell, upon applying voltage across the feeder electrode, electric field is produced which initiates faradic processes at the cathode and anode of a bipolar electrode due to interfacial potential difference between bipolar electrode and the solution. Since the potential difference is maximum at the terminal of cathode and anode, rate of faradic processes are maximum at the terminals. For maintaining electroneutrality, reactions occurring at cathodic pole and anodic poles are interrelated. In the cathodic pole of a bipolar electrode, a substance can be reduced and in the anodic pole ECL can be generated due to the oxidation of the electrochemiluminescence solution. As two different types of reactions occur at the same bipolar electrode, interaction between the reduced species and ECL +oxidation can be avoided in the bipolar electrode system.

In the absence of a bipolar electrode, when a voltage is applied across the feeder electrodes an uniform electric field is generated in solution. But when a bipolar electrode

is placed in the solution, there is a decrease of electric field across the bipolar electrode. As the current is flowing in opposite direction across the bipolar electrode compared with that of the feeder electrode, electric field generated in the cell is reduced along the bipolar electrode which is known as depolarization. Due to this depolarization effect, an interfacial potential difference was experienced along the bipolar electrode. This potential difference varies linearly with distance across the bipolar electrode.
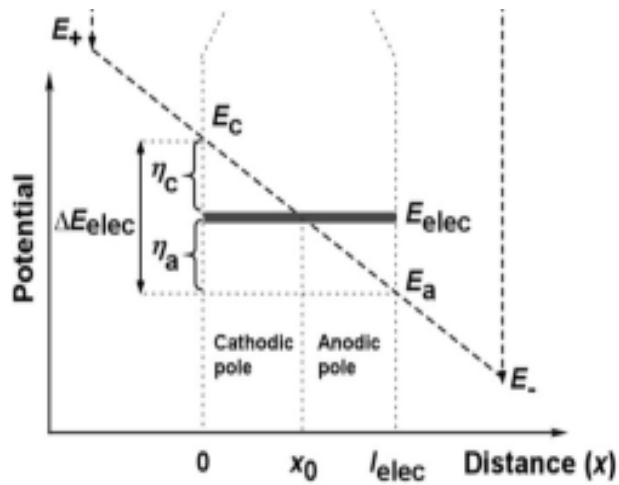
Figure 1. 2 Variation of interfacial potential difference across the bipolar electrode [4]

(Reprinted with permission from Ref.4. Copyright © 2009, Analytical Chemistry)

In the electrochemical cell having bipolar electrode, current is carried by ionic mobility in the solution and faradic process generate electronic flow across the bipolar electrode. Now, if we consider R_s as the resistance of the solution and R_e as the resistance of the bipolar electrode, then the fraction of current passing through the bipolar electrode is

$i_{bpe}/i_{channel} = 1 - i_s/i_{channel} = R_s/(R_e + R_s)$ (1) [5]

Here, i_{bpe} and $i_{channel}$ are the current passing through the bipolar electrode and through the solution respectively. From the equation (1) we can see that bipolar electrode

experiences the maximum amount of current when Rs is higher.

Now, if the voltage applied between the feeder electrodes E_{tot} and voltage lost across the bipolar electrode is ΔE. Then,

$\Delta E = (E_{tot}/l_{channel})*l_{elec}$

Where $l_{channel}$ is the length of the microchannel and the length of the bipolar electrode is l_{elec}. From this equation, we can see that rate of ECL can be increased by increasing the length of bipolar electrode[6]. ECL can also be increased by increasing the area of the cathodic pole, because to ensure electrical balance more overpotential is required in the anodic pole, which eventually increases the ECL intensity.
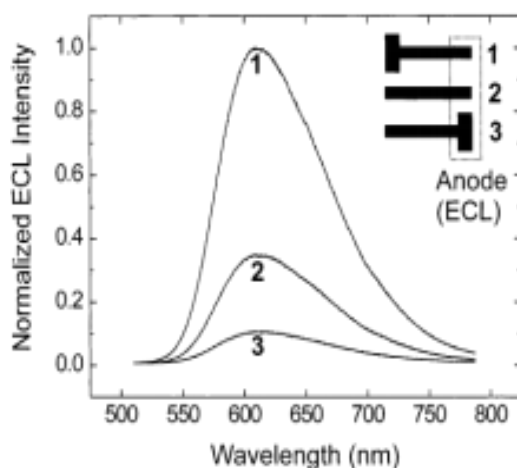
Figure 1. 3 ECL intensity change based on length of anodic pole of BPE [6]

(Reprinted with permission from Ref.6. Copyright © 2002, American Chemical Society)

The advantages of bipolar electrodes are that they offer higher sensitivity for detection, with a lower background signal. It is easy to operate and it is cheaper to be used. The overpotentials occur at cathodic and anodic pole also somewhere at the electrode there is no difference in the potential between the solution potential and electrode potential. It's position depends on the types of reactions occurring at the bipolar electrode. To have faradic reactions to occur, the height of the solution in the cell should be low and the electrolyte concentration should

be kept low so that current pass through more easily across the bipolar electrode and ions passing

through the solution is low. [7]

For a bipolar electrode of length L, the potential difference between the anodic pole

and cathodic pole is

$\Delta E = \eta_a - \eta_c = EL$

Where η_a is the anodic overpotential, η_c is the cathodic overpotential and E is the

applied potential. Based on this equation, for a smaller bipolar anode, higher voltage needs to be

applied from external power supply to cause the faradic reactions. [8]

The potential across the bipolar electrode can be measured by

a) by putting a reference electrode at different points of a bipolar electrode and analyzing

potential across the reference electrode and the point at bipolar electrode,

b) By putting two electrodes closer to the anodic pole and cathodic pole of the bipolar anode

respectively and measuring potential difference between them [9]

c) Electric field at different positions in a cell can be measured from series of microbands [10]

Current density across the cell was measured by applying current in a cell having

two closely placed reference electrodes and it was found that current density was maximum at the

two terminals of the bipolar electrode [9]
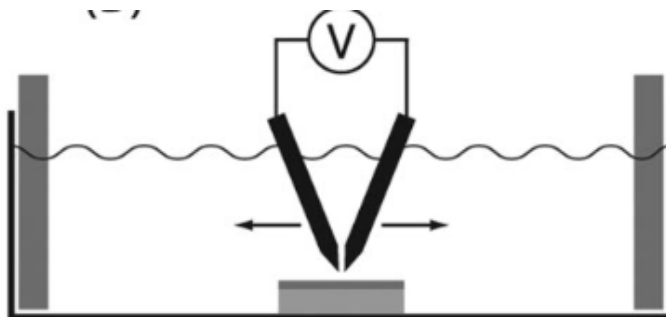
Figure 1. 4 Experimental setup for measuring current density in the cell [9]

(Reprinted with permission from Ref.9. Copyright © 2008, Angewandte chemie)

5
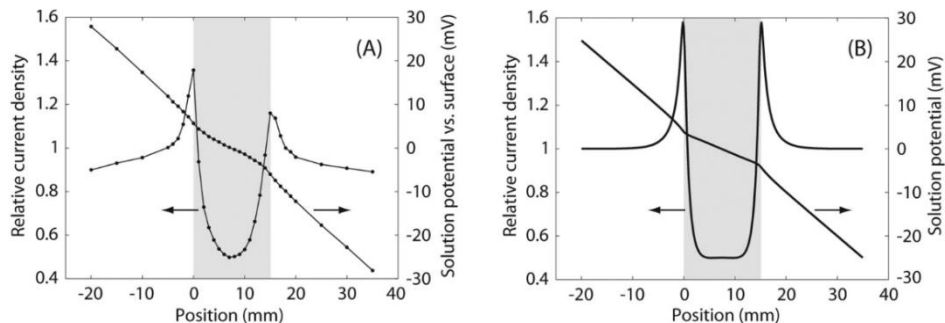
Figure 1. 5 (A) Experimental and (B) Theoretical results for measuring the current density [9]

(Reprinted with permission from Ref.9. Copyright © 2008, Angewandte chemie)

Here, in the figure 2 (A), the difference in height of the current density in the anodic pole and cathodic pole of the bipolar electrode was considered to be due to variation in ionic strength closer to the surface [9]

The potential difference between the cathodic pole and anodic pole of a bipolar electrode was measured by using two 100 µm wide bipolar electrode separated by a distance 1.00 µm. In the extended part of the microbands, a voltmeter was connected to measure the potential between the anodic and cathodic pole of the bipolar electrode.
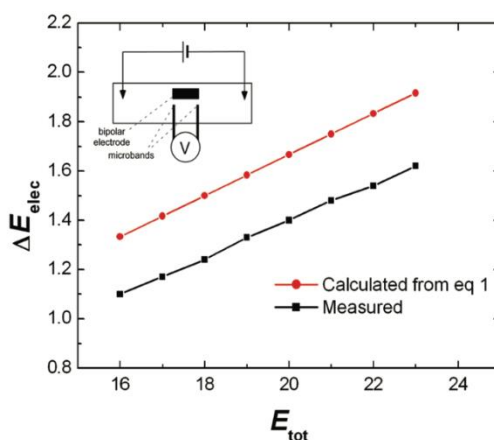
Figure 1. 6 Plot of the variation in the potential induced compared to the applied external potential[4]

(Reprinted with permission from Ref.4. Copyright © 2009, Analytical Chemistry)

E_{tot} was also measured based on the equation, $\Delta E_{elec} = (E_{tot}/l_{channel}) \times l_{elec}$ [4]

The difference in the theoretical and experimental value of the E_{tot} was assumed to be due the voltage drops at the interface of driving electrode and solution.

The current produced across the bipolar electrode during the ECL experiment was also measured by using two split electrodes and putting ammeter between the two electrodes and another ammeter was placed between the power supply and driving electrode. And it was found that the current produced by applying a 20V from external power supply caused 65 μA current in the entire microchannel and 54 nA current was passed through the bipolar electrode. So, a total of ~1% of faradic current was produced in the bipolar electrode system[4]. Both current and ECL was measured and compared and it was observed that a linear relationship exists between ECL and the current measured, which proved the fact that ECL can be used to report the current produced in a bipolar electrode system.
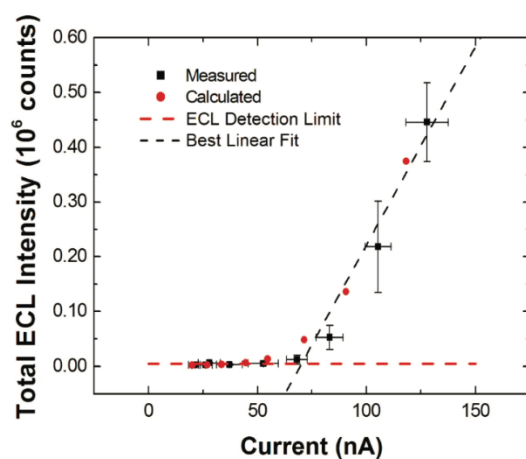
Figure 1. 7 Relationship of ECL and the current produced in a split bipolar electrode[4]
(Reprinted with permission from Ref.4. Copyright © 2009, Analytical Chemistry)

It is also possible to have faradic reactions to occur at the bipolar electrode without applying the external voltage. Simply by applying pressure, it is possible to have an ionic flow

which creates enough potential difference at the interfaces of the bipolar electrode and the electrolyte solution for the oxidation and reduction reactions to occur. By having external connections to two types of electrodes, in which one of the part was cathodic Au electrode and the anodic part was Au with a coating of 5 nm Cr and 20 nm Ag, it was possible to have faradic reactions occurring in the solution of DI water and 1.0 mM BQ/HQ in DI water by applying pressure[11]. In the cell having DI water, O_2 was reduced with Ag dissolution and in case of cell having BQ/HQ, BQ was reduced. It was found that, current which was measured from the rate of Ag dissolution increased with the increase of flow of the solution and the potential difference was also increased with the increase of applying solution pressure with time.[11]
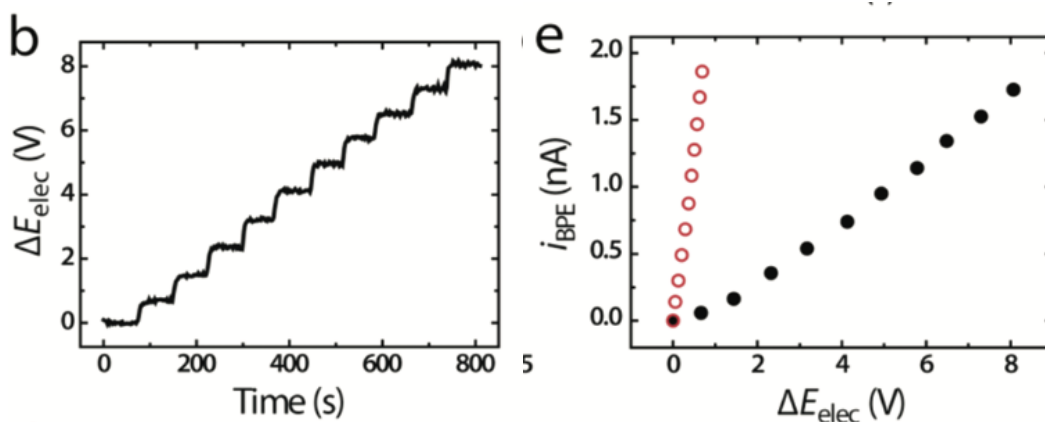
Figure 1. 8 b) Change of onset potential upon changing ionic flow rate with time in the cell having DI water, e) Relationship between current produced upon change of applied potential with flow rate for the cell having DI water (Red circle) also for the cell having HQ/BQ with water (Black circle) [11]

In a bipolar electrode cell, to reduce the background signal, the driving electrode should have higher resistance and the driving electrodes should be placed well separated from the bipolar electrode. When voltage is applied, the driving electrode accepts the electron from the power

supply [12]. BPE-ECL has the advantage over conventional fluorescence as it does not suffer from the scattered light coming out of sample. In case of the open bipolar electrode system, current not only pass through BPE but also pass through the whole cell. The division of the current formed into two parts is known as faradic depolarization and the ratio of this part of current which is passing through bipolar electrode is known as the degree of depolarization[13]. Now, as solution has a much lower resistance than bipolar electrode, the potential difference across the bipolar electrode is mainly due to the BPE's length and electric field throughout the whole cell. But in closed bipolar system, the sensing and reporting solutions exist at the different compartment and most of the current passes through the bipolar electrode as the voltage drop across the bipolar electrode is higher compared to the open bipolar system. This is due to the fact that, solution resistance is higher and the bipolar electrode is highly conductive[14].
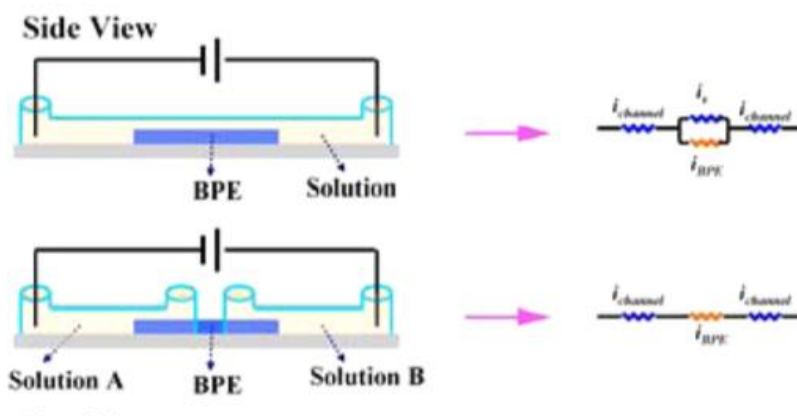
Figure 1. 9 Comparison between closed bipolar and open bipolar electrode[14]

(Reprinted with permission from Ref.14. Copyright © 2015, Analytical Chemistry)

The distribution of external voltage applied in an open bipolar cell is[14]:

$E_{tot} = iR_{channel} + iR + iR_{channel} + E_{sys}(1/R = 1/R_s + 1/R_{BPE})$

And the distribution of external voltage applied in a closed bipolar cell is[14]:

$E_{tot} = iR_{channel} + iR_{BPE} + iR_{channel} + E_{sys}$

It was found that the external voltage needed to get ECL in the bipolar electrode system is much higher than that of three electrode system. This is possibly due to the difference in size of BPE, conductivity of the solution used for measuring ECL also depends on how the BPE is modified. There is similar potential difference all over the surface in case of three electrode system. On the other hand, the potential difference varies throughout the length of the bipolar electrode. As the ratio of length to area in a bipolar electrode increases, electrolyte solution experiences higher resistance in bipolar electrode compared to that of three electrode system.

$R_s = \rho\ l/A$ [14]

1.2 Application of Bipolar electrode:

1.2.1 Bipolar electrode as cancer biomarkers:

Closed bipolar electrode was used to detect cancer biomarkers[14]. In that case, the cathodic part of the ITO bipolar electrode was modified with Au films and then the capture DNA and the Th@SiO$_2$ was added as an electrochemical tag to the bipolar cathode. In the anodic part of the bipolar electrode 0.1 M PBS buffer with 10 mM Ru(bpy)$_3{}^{2+}$ and 50 mM TPA was added as the ECL solution. With the increase of concentration of AFP and PSA in the target analyte solution ECL was found to increase when voltage was applied.
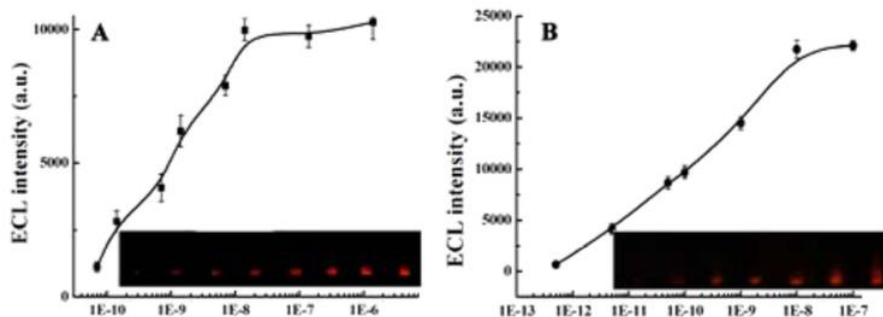
Figure 1. 10 Calibration curve for the detection of A) AFP, B) PSA by closed bipolar electrode [14]

(Reprinted with permission from Ref.14. Copyright © 2015, Analytical Chemistry)

This paper described a novel electrochemiluminescence (ECL) imaging platform for simultaneous detection of cancer biomarkers based on a closed bipolar electrode (BPE) array. It consisted of two separated channel arrays: detection channel array and sensing channel array, which were connected by a group of parallel ITO BPEs on a glass substrate[14]. Besides, two parallel ITO strips were fabricated at the two sides of BPE array and employed as driving electrodes. After Au films were electrochemically deposited on the cathodes of the BPE array, nanobioprobes including biorecognition elements (aptamer or antibody) and a novel electrochemical tag, which was synthesized by doping thionine in silica nanoparticles (Th@SiO$_2$ NPs), were introduced into the cathodes by immunoreaction or DNA hybridization. The Th@SiO$_2$ coupled nanobioprobes as both recognition probes and signal amplification indicators could mediate the ECL signals of Ru(bpy)$_3^{2+}$/tripropylamine (TPA) on the anodes of BPE array through faradaic reaction due to the charge neutrality of BPE[14]. Thus, multiplex detection of cancer biomarkers (adenosine triphosphate (ATP), prostate-specific antigen (PSA), α-fetoprotein (AFP) and thrombin) was realized by forming specific sensing interfaces onto the cathodic poles of BPEs in different sensing channels and reported by the ECL images of the Ru(bpy)$_3^{2+}$/TPA system on the anodic poles of BPEs in detection channels[14]. The results demonstrated that this visual ECL platform enabled sensitive detection with excellent reproducibility, which might open a new door toward the development of simple, sensitive, cost-effective, and high throughput detection methods on.[14]

1.2.2 Bipolar electrode in electrodeposition:

Bipolar electrode can be used to cause electrodeposition[15]. In an electrolyte solution, if there are multiple species with different potential exists, then the species having more positive potential deposits closer to the center of the bipolar anode and the component which has more negative electrochemical potential tends to deposit closer to the terminals of the poles. For

example, gradient deposition of CdS was done on Au bipolar electrode by applying voltage from DC power supply through the solution contained 10 mL 0.10 M KNO_3, 0.02 M Cd^{2+}, 0.05 M $S_2O_3^{2}$. Glassy carbon electrode worked as the driving electrodes because of the lower probability of hydrogen evolution compared to that of the metallic electrodes. For not having unequal interfaces between the solution and the electrode surface, Au wire was used as a bipolar electrode. Upon applying sufficient voltage, there were three zones created on the cathode of the bipolar electrode. The zone toward the cathodic terminal was found to be gray as Cd along with CdS were found to be deposited, the middle zone was found to be orange as CdS was found to be deposited and the zone closer to the center of the bipolar electrode was found to be yellow due to the deposition of S.[15]
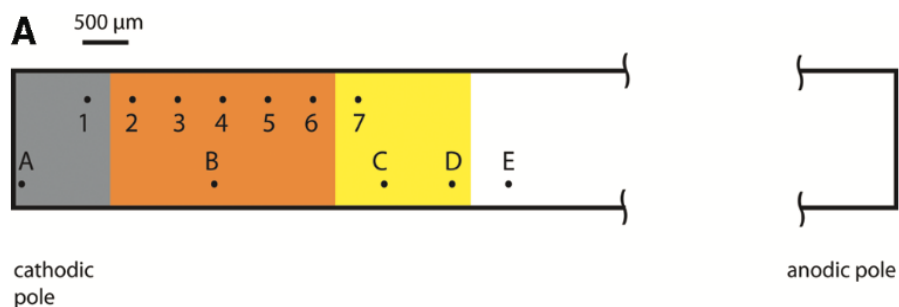
Figure 1. 11 Electrodeposition of CdS solution on bipolar [15]

(Reprinted with permission from Ref.15. Copyright © 2010, Langmuir)

1.3 Current measurement process in bipolar electrode:

1.3.1 Ag electrodissolution to measure the current generated in bipolar electrode system:

In the bipolar electrode system, there is no direct electrical contact of the bipolar electrodes with the external power supply. So, to measure current produced by applying voltage, ECL or the rate of Ag dissolution is quantified. ECL can easily be detected by CCD or photomultiplier tube.[16]

Ag electrodissolution system can be used to measure the current through the bipolar electrode system. As the overpotential between the electrode and solution is maximum at the outer terminal, anodic Ag dissolution starts from the outer terminal and moves to the center of the bipolar electrode gradually. Two split electrodes connected with ammeter used as the bipolar electrode. The reduction of p-benzoquinone was equal to Ag dissolution on the anodic part of BPE and the current was measured by the ammeter connected, which proved that Ag dissolution can also quantify the current produced in the bipolar electrode system apart from ECL.[16]By Ag electrodissolution process, target DNA was detected by modifying cathodic part of the bipolar anode with complementary target DNA when voltage was applied through the electrolyte solution of 0.10 M acetate buffer. The sensor system was not found to be sensitive to target DNA when the cathodic part of the bipolar electrode was modified with 6 mercaptohexanol.[16]
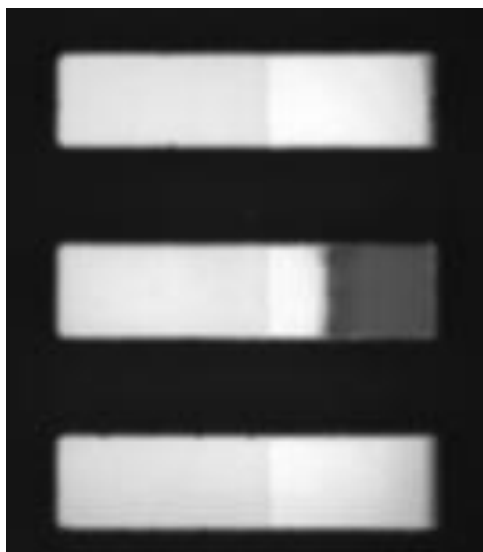
Figure 1. 12 Ag dissolution process. The first and third electrode was unaffected as it was not modified with DNA and the middle electrode was affected as it was modified with DNA[16] (Reprinted with permission from Ref.16. Copyright © 2010, American Chemical Society)

Ag dissolution mechanism was also used to measure the catalytic activity for the oxygen reduction reaction. Three different ITO bipolar electrode was analyzed. The cathodic part of the first electrode was modified with Pt dendrimer-encapsulated nanoparticles, the middle electrode was just the ITO electrode and the cathodic part of the third electrode was modified with Au dendrimer-encapsulated nanoparticles. The anodic part of the bipolar electrode had parallel Ag microbands. When voltage was applied, Ag dissolution occurred at the first and third type of electrodes with the surface oxide reduced at the cathodic part, measuring the electrocatalytic activity of the Pt and Au modified electrode. No light emission was observed here.
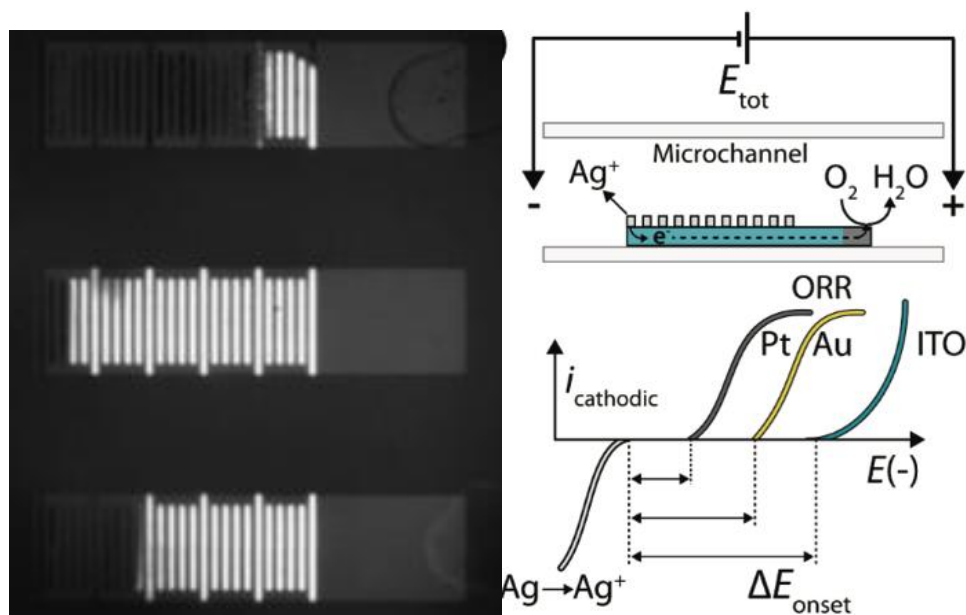
Figure 1. 13 Difference in oxygen reduction reaction at Pt modified (top electrode), ITO electrode (middle electrode), Au electrode (lower electrode)[17]

(Reprinted with permission from Ref.17. Copyright © 2001, Physical Chemistry)

1.3.2: ECL process to analyze the current produced in the bipolar electrode system:

ECL (Electrochemiluminescence) is the process of conversion of electrical energy into light energy. The intermediate formed at the electrode surface reacts to produce the

excited state, from where light is emitted as it relaxes to the ground state in the ECL process. ECL is different from chemiluminescence as chemiluminescence is associated with the production of excited state upon mixing of the solution whether in ECL, production of the excited state is controlled by the application of applied voltage. To be a stable compound which has the potency to show ECL, the solution of the compound should show a reversible peak in cyclic voltammetry. Reversibility can be achieved when oxidation peak current equals the reduction peak current in the CV. The ECL producing compound should have sufficient energy to produce the excited state. The compound $Ru(bpy)_3^{2+}$ work as one of the most promising ECL agent as it shows highly efficient luminescence, it has high solubility in different aqueous and non-aqueous medium and it shows reversible behavior in the CV. The other common co-reactants used for producing ECL are oxalate, H_2O_2, perdisulfate ion etc. Compared to chemiluminescence in the electrochemiluminescence system, place and timing of the reaction producing light can be easily controlled.

The mechanism to produce ECL from the solution of $Ru(bpy)_3Cl_2$ with Tripropyl amine (TPrA) acted as a coreactant and when sufficient potential is applied for the formation of excited state in the aqueous system is as follows.

When homogeneous oxidation of $Ru(bpy)_3Cl_2$ and TPrA occurs [18]-

$Ru(bpy)_3^{2+}$ -e → $Ru(bpy)_3^{3+}$

$Ru(bpy)_3^{3+}$ + Pr_3N → $Ru(bpy)_3^{2+}$ + $Pr_3N^{.+}$

$Pr_3N^{.+}$ → $Pr_2N^{.}CHEt$ + H^+

$Ru(bpy)_3^{3+}$ + $Pr_2NC^{.}HEt$ → $Ru(bpy)_3^{2+\,*}$ + $Pr_2N^+{=}CHEt$

$Ru(bpy)_3^{2+\,*}$ → $Ru(bpy)_3^{2+}$ + hv
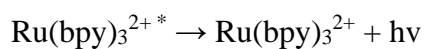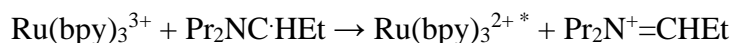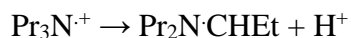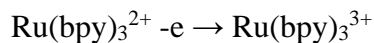
(here Pr= $CH_3CH_2CH_2$- and Et= CH_3CH_2-)

and when direct oxidation of TPrA at the electrode occurs the mechanism is as follows[18]-

$Pr_3N - e \rightarrow Pr_3N^{\cdot+}$

$Pr_3N^{\cdot+} \rightarrow Pr_2N^{\cdot}CHEt + H^+$

$Pr_2N^{\cdot}CHEt - e \rightarrow Pr_2N^+=CHEt$
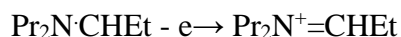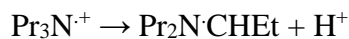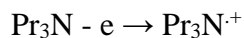
In both routes the following reaction can also occur [18]-

$Ru(bpy)_3^{2+} + Pr_2N^{\cdot}CHEt \rightarrow Ru(bpy)^{3+} + Pr_2N^+=CHEt$

$Ru(bpy)^{3+} + Ru(bpy)_3^{3+} \rightarrow Ru(bpy)_3^{2+\,*} + Ru(bpy)_3^{2+}$
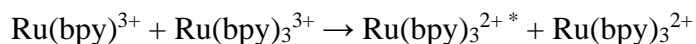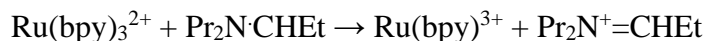
Here, the rate limiting step is the formation of TPrA radical [17]. Here, as when TPrA oxidized directly to the electrode surface, forms TPrA$^{\cdot}$ which reacts with $Ru(bpy)_3^{2+}$ to form $Ru(bpy)_3^+$. $Ru(bpy)_3^+$ also has the ability to be oxidized at the electrode surface to form $Ru(bpy)_3^{2+}$ but in that case ECL will be quenched [18].

When the concentration of $Ru(bpy)_3^{2+}$ was higher compared to that of the TPrA, then reversible behavior in the CV was observed as $Ru(bpy)_3^{2+}$ and TPrA oxidized directly to the glassy carbon electrode surface which started at 0.6 V, the oxidation peak was found to increase and the reduction peak was found to be disappeared [19].
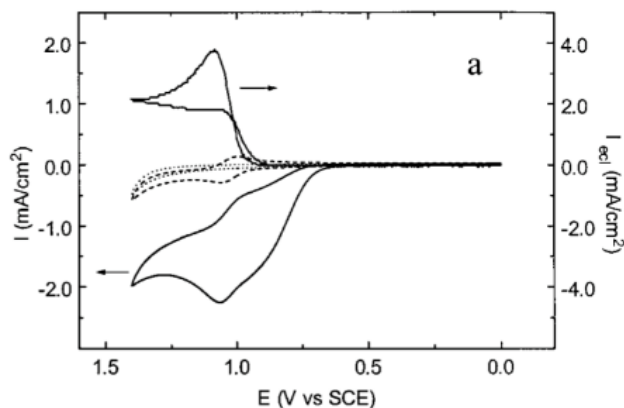
Figure 1. 14 CV and ECL curve of 1 mM Ru(bpy)$_3^{2+}$ in 0.15 M PBS buffer at glassy carbon electrode when there was no TPrA (represented by dashed line) and when there was 10 mM TPrA (represented by solid line) and when there was no Ru(bpy)$_3^{2+}$ nor TPrA (dotted line) [19]

(Reprinted with permission from Ref.19. Copyright © 2002, American Chemical Society)

However, when Ru(bpy)$_3^{2+}$ concentration was lower compared to the concentration of TPrA, the first peak appeared at 0.6 V was due to the fact that TPrA oxidized directly to the electrode surface and the second peak at 1.1 V was due to the oxidation of Ru(bpy)$_3^{2+}$. This happened because when Ru(bpy)$_3^{2+}$ was in excess, ECL increased with increasing concentration of the TPrA but as soon as TPrA radical was produced due to the oxidation of TPrA by the reaction, their concentration exceeded that of the concentration of Ru(bpy)$_3^{2+}$, the current was seemed to be proportional to the concentration of Ru(bpy)$_3^{2+}$ [19]
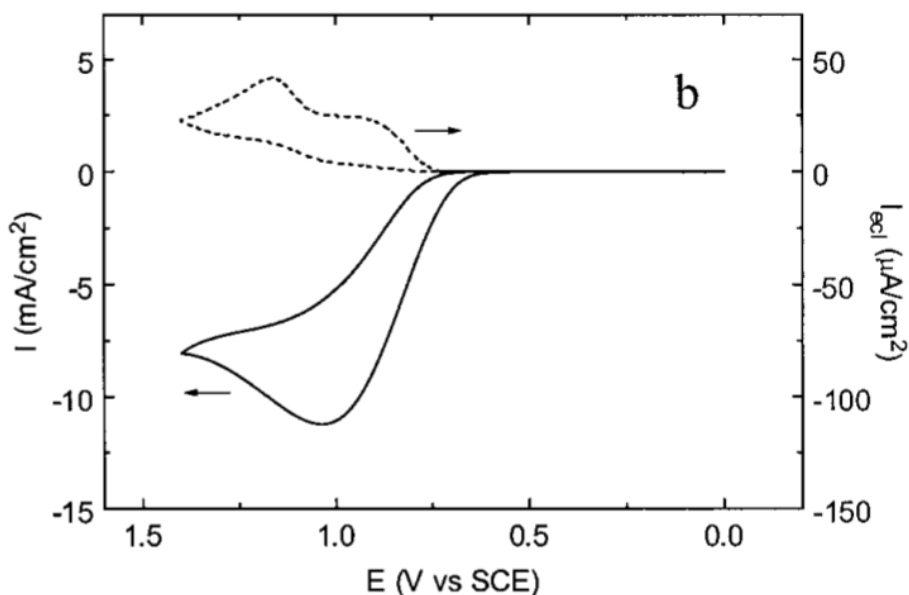
Figure 1. 15 CV and ECL spectrum of 1 µM Ru(bpy)$_3^{2+}$ and 100 mM TPrA in PBS buffer at glassy carbon electrode [19]

(Reprinted with permission from Ref.19. Copyright © 2002, American Chemical Society)

It was observed that with the increase of concentration of Ru(bpy)$_3^{2+}$ second peak of the ECL curve became larger. From this observation, it was concluded that at a higher concentration of Ru(bpy)$_3^{2+}$ the reaction mechanism followed homogenous oxidation of TPrA and Ru(bpy)$_3^{2+}$ [18].
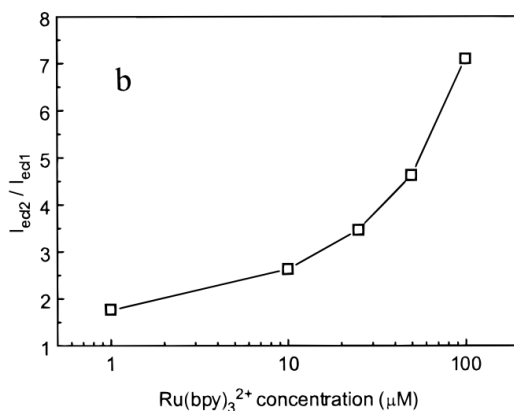
Figure 1. 16 Dependence of the ECL intensity upon changing the concentration of Ru(bpy)$_3^{2+}$ [18] (Reprinted with permission from Ref.18. Copyright © 2000, Analytical Chemistry)

Glassy carbon electrode shows 10 times and 100 times higher ECL intensity in case of Ru(bpy)$_3^{2+}$, TPrA system compared to that of gold and Pt electrode respectively. As Pt has good catalytic activity, it facilitates the decomposition of water in the aqueous system forming O$_2$ which is an effective quencher also formation of H$_2$ causes the pH to reduce so ECL reduces further.[18]

The addition of halide can increase the ECL 4-5 times as it absorbs to the surface of Pt or Au which inhibits oxide formation. It was found that Iodide most strongly absorbs to the electrode whether chloride least strongly absorbs to the electrode. However, at a much higher concentration, halides tend to oxidize which is harmful for the TPrA radical (TPrA·) [18].
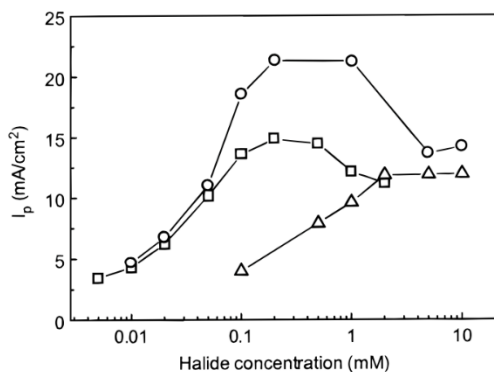
Figure 1. 17 Dependence of the ECL by changing the halide concentration [18]

(Reprinted with permission from Ref.18. Copyright © 2000, Analytical Chemistry)

The coreactant is a compound that can undergo bond cleavage to produce oxidized or reduced product that reacts with the ECL producing compound from where excited state is produced. In the coreactant system, the excited state is produced by a single potential step, whether in the annihilation ECL system, the excited state is produced by double potential step. In the aqueous system, the potential range of water is too low to produce excited state of the ECL. So coreactant is used in the aqueous system which can produce the excited state. It was found that only 3.6% TPrA causes the ECL to be produced from the $Ru(bpy)_3^{2+}$ complex in aqueous solution.[18]

At higher concentration of TPrA with the increase of pH ECL increases upto a pH of 7.5 and after that it decreased due to the production of a quenching agent O_2 by the reaction between hydroxide ion and $Ru(bpy)_3Cl_2$

$$Ru(bpy)_3^{3+}+OH^- \rightarrow Ru(bpy)_3^{2+}+¼ O_2 + ½H_2O \quad [20]$$
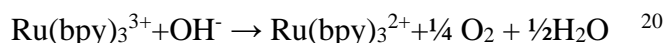
and also the $TPrA^{·+}$ is not stable in this higher pH region due to dissociation and there is a lower solubility of the TPrA at higher pH [21], and at lower pH lack of deprotonation of the TPA can cause reduction of ECL [21].
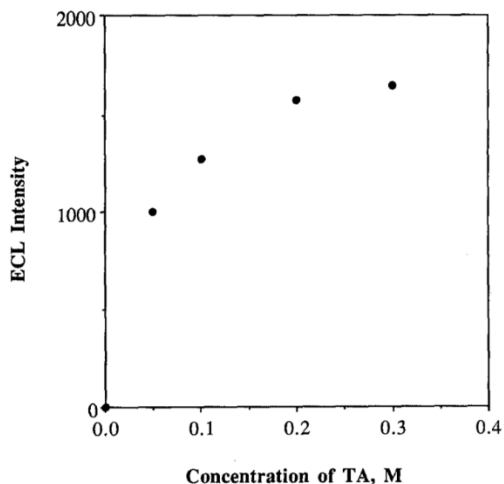
Figure 1. 18 Change of ECL intensity with the change of pH [21]

(Reprinted with permission from Ref.21. Copyright © 1990, Electrochemical Society)

As the pH changes, the oxidation potential of a co-reactant also changes. For example, the oxidation potential of oxalate decreases with an increase of solution pH [17].
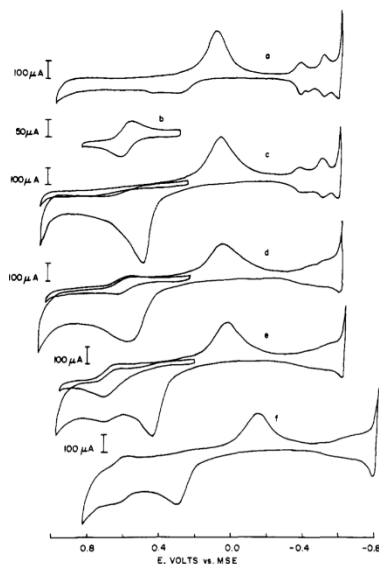
Figure 1. 19 CV at a Pt electrode for a) 1.19 1.0 M H_2SO_4, b) 1.0 mM Ru(bpy)$_3$(ClO$_4$)$_2$ and 1.0 M H_2SO_4, c) 1.0 M H_2SO_4 and 3.0 mM $H_2C_2O_4$, 1.0 M H_2SO_4, d)3.0 mM $H_2C_2O_4$ and 1.0 M H_2SO_4 and 1.0 mM Ru(bpy)$_3$(ClO$_4$)$_2$, e) 3.0 mM $H_2C_2O_4$ and 0.1 M H_2SO_4 and 1.0 mM Ru(bpy)$_3$(ClO$_4$)$_2$, f) 3.0 mM $H_2C_2O_4$ and 1.0 M H_2SO_4 and 1.0 mM Ru(bpy)$_3$(ClO$_4$)$_2$ (adjusted to pH 4.5)[17]

(Reprinted with permission from Ref.17. Copyright © 2001, Physical Chemistry)

The quantum efficiency of an ECL system can be calculated by comparing the intensity of the ECL system to that of the ECL of the $Ru(bpy)_3^{3+}/Ru(bpy)_3^+$ ECL system [17].

Viscosity of the solution reduces ECL, whereas bimetallic ruthenium complexes showed higher ECL than monometallic ruthenium complexes [22]. ECL intensity was seen to be increased when there is a substitution in the bipyridyl ligand. For example, $Ru(dp\text{-}bpy)_3^{2+}$ showed 14 times more enhanced ECL and $Ru(phen)_3^{2+}$ showed 24 times higher ECL emission compared to that of $Ru(bpy)_3^{2+}$ [23].

Based on bipolar electrode sensing system, Zhan et.al detected benzyl viologen in $Ru(bpy)_3^{2+}$-TPA ECL solution [6]. Here in the cathodic pole both proton (H^+) and benyl viologen (BV^{2+}) was found to be reduced.

$$2H^+ + 2e^- = H_2 \qquad (1)$$

$$BV^{2+} + e^- = BV^+ \qquad (2)$$
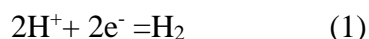
Now at a negative potential in a voltammogram, reaction 1 occurred at -1.08 v and after that at potential -0.52 V reaction 2 occurred on the ITO working electrode, when Ag/AgCl was used as a reference electrode[6]. Now, the anodic process in both the cases are the same, so the potential window reduces from 1.8 V to 1.38 V from reaction (1) to reaction (2). Now, for the ECL analysis upon applying voltage, when $\Delta Eappl = 1.4$ V then ECL was observed for the BV^{2+} when $\Delta Eappl$ was increased to 1.8 V, ECL intensity was enhanced due to the reduction of proton based on equation 1. For example, when 100 μM BV^{2+} was present with 5 mM $Ru(bpy)_3^{2+}$ and 25 mM TPA, ECL intensity was found to increase 40 times when voltage was applied such that $\Delta Eapp$ was 1.8 V compared to the solution without having BV^{2+} [6].
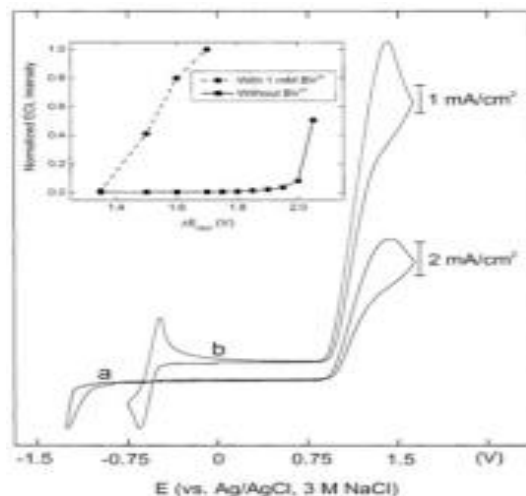
Figure 1. 20 Detection of Benzyl viologen by ECL intensity enhancement [6]

(Reprinted with permission from Ref.6. Copyright © 2002, American Chemical Society)

Bipolar electrode based biosensor can detect individual analyte from a mixture of analytes by carefully controlling applied potential. For example, Zhan *et al.* detected $K_3Fe(CN)_6$, $Ru(NH_3)_6Cl_3$, BV^{2+} from the mixture of all of these in the ECL solution of 5 mM $Ru(bpy)_3^{2+}$ and 0.1 M Na_2SO_4 solution [24]. From the voltammogram data, potential window for the redox processes was found to be 0.69 V for $K_3Fe(CN)_6$, 1.12 V for $Ru(NH_3)_6Cl_3$ and 1.47 V for BV^{2+} [24] which was calculated from the difference between the onset potential of the $Ru(bpy)_3^{2+}$ and formal potential of each of the substance. Here, the formal potential was calculated from the average of cathodic and anodic peak.
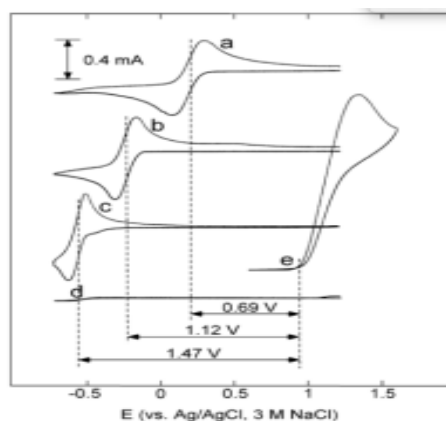
Figure 1. 21 CV of a) 5.00 mM $K_3Fe(CN)_6$, b) 5.00 mM $Ru(NH_3)_6Cl_3$, c) 5.00 mM BV^{2+}, d)0.1 M Na_2SO_4, e)5.00 mM $Ru(bpy)_3Cl_2$ and 25 mM TPA [24]

(Reprinted with permission from Ref.24. Copyright © 2003, Analytical Chemistry)

When ECL analysis was done, upon applying voltage, onset potential for $K_3Fe(CN)_6$ was found to be 0.75 V and for $Ru(NH_3)_6Cl_3$ and for BV^{2+} onset potential were found to be 1.15 V and 1.40 V respectively which were close to the value found in the CV experiment. [24]
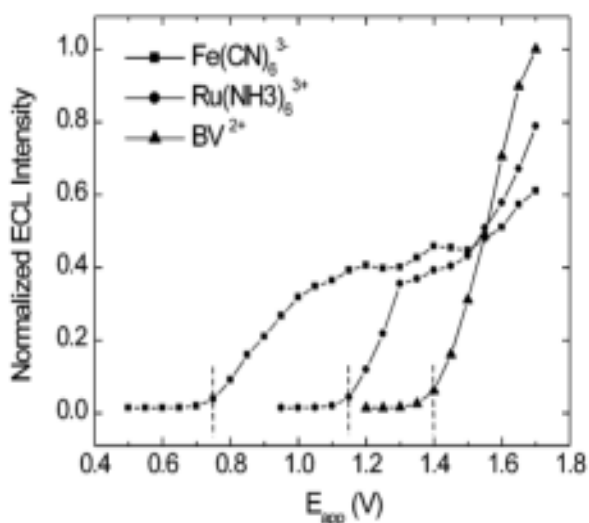
Figure 1. 22 ECL data for the detection of $K_3Fe(CN)_6$, $Ru(NH_3)_6Cl_3$, BV^{2+} [24]
(Reprinted with permission from Ref. 24. Copyright © 2002, American Chemical Society)

1.4 Basic Principle of Surface Plasmon Resonance:

When light propagates from a prism of refractive index n_p to air of refractive index n_o and if $n_p > n_o$, then for a incidence angle of light, it passes through the prism and air interface. That angle is known as the critical angle. Now, if the light is incident at an angle larger than the critical angle, then the light is reflected. Angle of incidence light is varied to get an SPR curve and relected light angle is monitored. A minimum in the SPR curve is associated

with the displacement of electron cloud with the interaction of electric vector of incident light. This creates an oscillation of electrons which balances the coloumbic forces between electrons and nucleus. If the frequency of incident light matches with the frequency of electrons oscillating in the conduction band of metals surface plasmon resonance occurs. Associated with the surface plasmon resonance wave, there is an evanescent wave, which spreads in the outer medium, upto 200 nm from the metal surface. With the absorption of an organic film, refractive index increases, so angle of incidence light also increases to match with that of resonance condition.
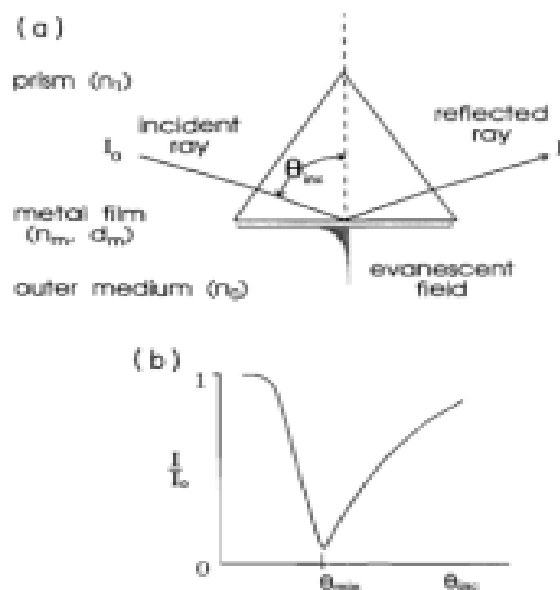
Figure 1. 23 a) Surface plasmon resonance measurement system, b) SPR curve for the change of reactivity with incidence angle [25]

(Reprinted with permission from Ref.25. Copyright © 1996, Canadian Journal of Chemistry)

When a sample is present, SPR curve changes its minimum angle of reflectivity, thickness of the metal film and differential reflectivity. The dielectric function also changes in presence of a sample because the electron cloud of the metal changes. For the resonance to

24

occur, dielectric function of both the surface and medium should be the same and dielectric constant of the surrounding medium can influence the frequency of surface plasmon band. The change of angle minima with the change of film thickness was studied by Gryczynski,I *et.al* by varying thickness of polyvinyl alcohol layer on glass substrate [26].
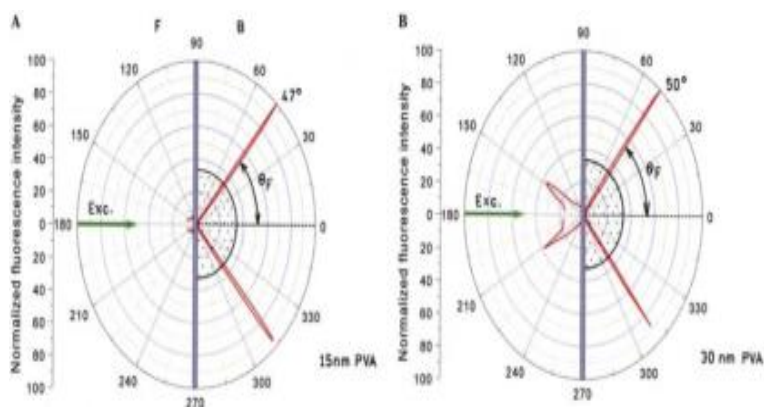
Figure 1. 24 Change of minimum angle based on film thickness [26]

(Reprinted with permission from Ref.26. Copyright © 2004, Analytical Biochemistry)

Surface plasmon of a metal can be excited when light incidents on a specific angle which causes minimum reflectivity[27,28] or when directional light from excited luminophore hits a metallic surface at a specific angle which causes minimum reflectivity[26,29].

Only in case of p-polarized light surface plasmon resonance can be observed [26]. For a parallel electric vector of the incident light with respect to the plane of incidence we can get p-polarized light. However, for a perpendicular electric vector of the incident light with respect to the plane of incidence, we can get s-polarized light. The s-polarized light does not show surface plasmon resonance [26]. Gryczynski *et al.* showed that maximum emission intensity was observed in the case of light emitted horizontally with the plane of glass slides coated with polyvinyl alcohol independent of the fact that whether the light was excited horizontally or

25

vertically with respect to the plane.
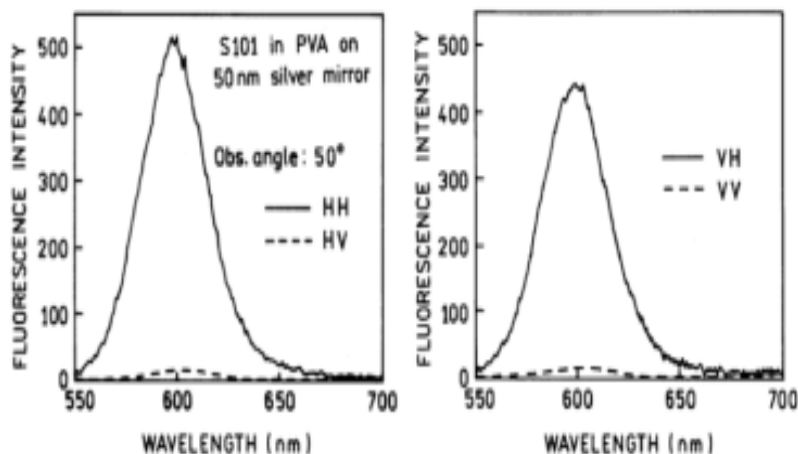
Figure 1. 25 Effect of polarization of light on fluorescence intensity for a glass slide coated with 30 nm thick PVA [26]

(Reprinted with permission from Ref.26. Copyright © 2004, Analytical Biochemistry)

The average path a free electron moves in a metal is about 50 nm. So, a particle for smaller than 50 nm no scattering is observed. When the particle is smaller than the Bohr radius electron tend to confine within the surface of the material. Now, when light of wavelength larger than the size of the particle incidents on the surface of the nanomaterial, the free electrons tend to oscillate according to the frequency of the incident light which causes surface plasmon resonance[30].

Based on the Mie theory, the extinction cross section, σ of a spherical nanoparticle is given by

$\sigma_{ext} = \varepsilon_2 / ([\varepsilon_1 + 2\varepsilon_m]^2 + \varepsilon_2^2)$ [31]

The dielectric function has a real and imaginary part. Here, ε_1 is the real part which is basically permittivity or polarizability or refractive index of a material with respect to light. It has a negative value for a large number of materials and the condition for surface plasmon resonance

is observed when $\varepsilon_1 = -2\varepsilon_m$ [31]. The negative value of the dielectric function is due to the tendency of the free electrons in a metal not to accept the incoming electromagnetic radiation. ε_2 is the imaginary part which is the tendency of a material to absorb photon.
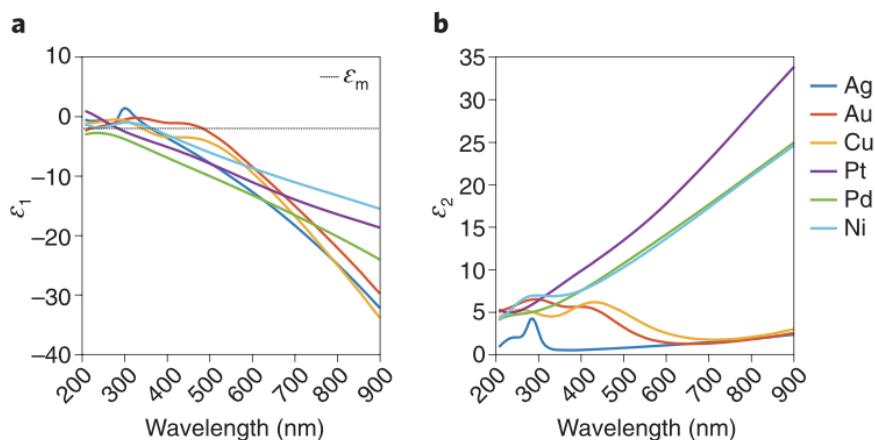
Figure 1. 26 Variation of real part (a) and imaginary part (b) with wavelength for different materials [31]

(Reprinted with permission from Ref.31. Copyright © 2018, Analytical Biochemistry)

There are two types of electronic transitions possible in a material. The intraband transition causes due to the electronic transition from s orbital which is filled and situated below a fermi level to a s orbital which is full and situated above a fermi level. This transition occurs in the visible region. As the transition occurs between two s orbitals the transition is energetically forbidden. So, the energy from plasmons or lattice phonons is needed to drive this electronic transition.[31] The rate constant for this transition is $10^3 s^{-1}$. [32]

The interband transition occurs due to the electronic transition from d orbital which is filled and situated below a fermi level to a s orbital which is empty and situated above the fermi level. Based on the position of the d orbital interband transition occurs. For example, in Ag the d orbital is far below the fermi level. So, in the visible light, d to s transition does not occur in Ag. In Au or

27

Cu, the d band lies closer to the fermi level compared to Ag, so interband transition can occur in the visible light when the light has an excess energy compared to a minimum threshold energy. [31] As d to s electronic transition is energetically favorable so the rate constant is higher for interband transition compared to that of the intraband transition which is 10^{15} s^{-1}. [32] Due to this higher rate constant, plasmon mostly decay by interband transition but for Ag as interband transition does not occur in the visible light, plasmon mostly decays by intraband transition.
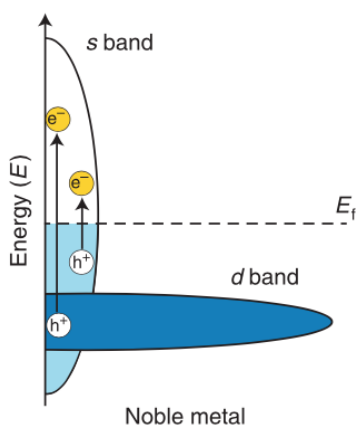
Figure 1. 27 Interband and intraband transition in noble metals [31]

(Reprinted with permission from Ref.31. Copyright © 2018, Analytical Biochemistry)

In case of non-noble metals, the d orbital is not totally full, and it overlaps with the fermi level, so interband transition easily occurs in the visible region. So, the non-noble metals have higher value of ε_2. So, the noble metals have lower ε_2 value and $\varepsilon_1 = -2\varepsilon_m$ shows the plasmonic behavior in the visible region [31]. Materials such as aluminum, palladium, platinum tends to absorb light very strongly so they do not show surface plasmon resonance behavior. [32]
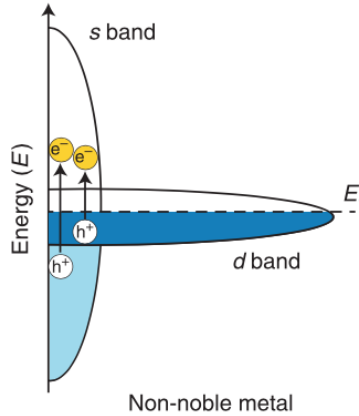
Figure 1. 28 Interband and intraband transitions in non-noble metals [31]

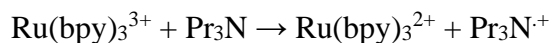(Reprinted with permission from Ref.31. Copyright © 2018, Analytical Biochemistry)

After the plasmonic material is excited by absorbing light the plasmon tends to decay which is proportional to the plasmon line width. The propagation of the electronic oscillation along the interface decay into both the metallic surface and the adsorbate.

The equation for the propagation length is [33]-

$$L_{sp} = 1/2k_{sp} = c/\omega = \{(\varepsilon'_m + \varepsilon_d)/(\varepsilon_m'\varepsilon_d)\}^{3/2} (\varepsilon'_m)^2/ \varepsilon_m$$

Here, ε_m' is the dielectric function of light in metal and ε_d is the dielectric function of light in dielectric substance. [33]

The length of the surface plasmon propagating along the metal surface, can be determined by photon scanning tunneling microscopy. [33]

The propagation constant has a real part, $\Delta\beta$ which is changed as the refractive index changes. The propagation constant increases with the increase of refractive index based on the following equation

$$Re\{\Delta\beta\} = k\Delta n \quad [34]$$

The plasmon can decay by four processes termed as bulk damping, radiation damping, electron surface scattering and chemical interface damping (CID). The equation for plasmon damping, Γ is as follows

$\Gamma = \Gamma_b + \Gamma_{rad} + \Gamma_{surf} + \Gamma_{CID}$ [35]

Due to the bulk damping, Γ_b the plasmonic energy is converted to heat energy. Due to the radiation damping, Γ_{rad} plasmon energy is converted to light emission, due to the electron surface scattering, Γ_{surf} electron used to scatter out of the surface and due to CID, Γ_{CID} charge transfer to the substance absorb to the material occurs. [38]

Chemical interface damping is dependent on Fermi velocity, v_F which is the probability of an electron from the nanoparticle to transfer its energy to the molecule attached and CID is also dependent on the effective path length, l_{eff} which is the distance travelled by the electron before it can transfer its energy to the absorbed material. Here, $l_{eff} = 4V/S$ [36]. So, the chemical interface damping is,

$\Delta\Gamma = A_{CID} \cdot v_F/l_{eff}$ [36]

Chemical interface damping is inversely proportional to l_{eff}. So, for larger nanoparticles CID and scattering is negligible, but for smaller nanoparticles CID is much higher[35]
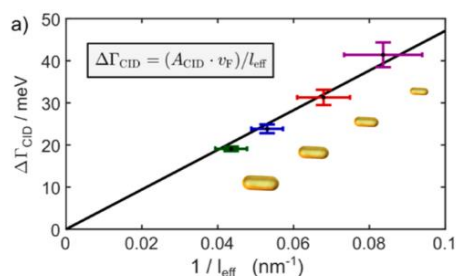
Figure 1. 29 Variation of chemical interface damping with the variation of the inverse of effective path length due to the attachment of thiol to the surface of gold nanoparticle [35]

From the linear regression co-efficient of this curve, it was calculated that the probability of electron scattering at the interface of thiol-nanorod was 34%.
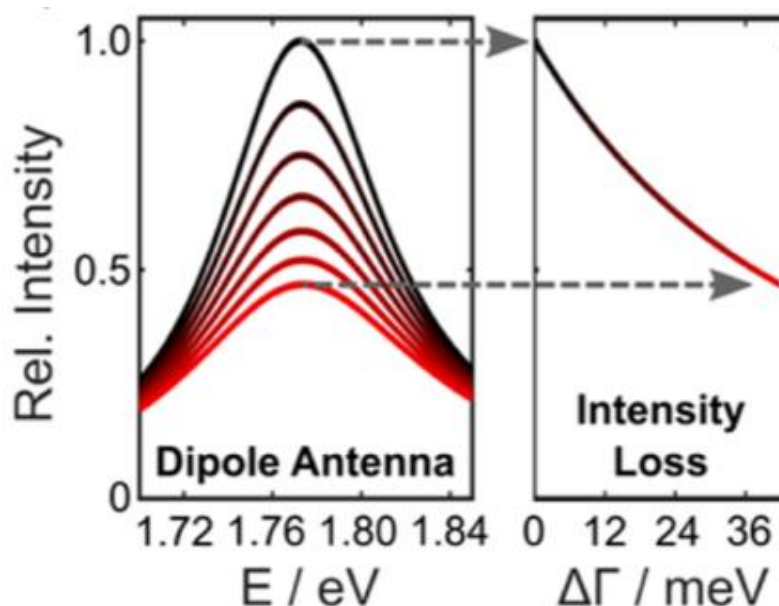
Figure 1. 30 Decay of plasmonic band of gold nanorod by attaching DDT [35]

(Reprinted with permission from Ref.35. Copyright © 2017, ACS Nano)

1.5 Principle of Fluoroscence enhancement:

There are two terms to characterize the emission from a fluorophore, quantum yield, Q_0 and lifetime, τ.

Here, $Q_0 = k_r / k_r + k_{nr}$

And $\tau = 1 / k_r + k_{nr}$

Where, k_r is the radiative decay rate and k_{nr} is the nonradiative decay rate

The excited state of the fluorophores relaxation process involves relaxation from higher to lower vibration excited state followed by radiative decay to ground state.

The fluorescence from a fluorophore depends on the following equation,

$F = QP_0(1-10^{-\varepsilon bc}) = QP_0\varepsilon bc$, [36] where P_0 is the power of excitation, b is the length of the cell, c is the concentration of the fluorophore, Q is the quantum yield, ε is the molar absorptivity. Sensitivity of a fluorometer is measured by the term $P_0\varepsilon bc$ [36]

The incident light is basically an electromagnetic radiation which interacts with the nano material surface. Due to this interaction, the free electron moving in the nano material tends to get separated from the nucleus of the material. The coloumic repulsion force amongst the electrons tends to push the electrons in the opposite direction which causes an oscillation of the conduction electrons. Due to this occurrence, nanomaterials absorbs light strongly. [37]

The mechanism of the surface plasmon resonance enhancement is that, if the incident light couples with the absorption band of the plasmonic material there is an enhancement of the incident light and it also scatters from the surface of the plasmonic material and if this scattered light matches or closer to the emission band of the fluorophore absorbed on the material then there is again an enhancement of the scattered light. In case of plasmon enhanced fluorescence, only scattered light is enhanced and the enhancement is represented by E^2. [36]

The emission due to fluorescence is due to two reasons.

1. The excitation of electron to the excited state from ground state,

2. The electronic relaxation from excited state to ground state causing production of light [38]

1.6 Gold nanorod and surface plasmon resonance enhancement:

The longitudinal band of the gold nanorod can enhance the electromagnetic field and to excite the longitudinal band, the excitation light has to be parallel to the length axis and the scattering of light from the gold nanorod is also parallel to the length axis of the gold nanorod [38]. So, the fluorescence can be turned on and off by changing the angle of excitation light [38].
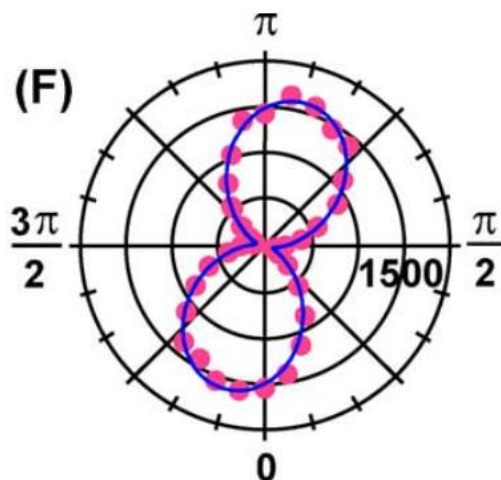
Figure 1. 31 Change of fluorescence intensity with the variation of excitation light angle [38]

(Reprinted with permission from Ref.38. Copyright © 2010, Nano Today)

1.6.1 Structure of gold nanorods:

Gold nanoparticles not only absorb light but also scatters light and the summation of both of the light absorbed and scattered causes the extinction spectra. Color of this light scattered from the nanoparticle changes with change in the refractive index. To monitor the nanoparticles darkfield microscopy is used [39]. The advantage of gold is that it does not oxidize, stronger light absorption or scattering is possible for gold nanorods compared to gold nanospheres and the gold nanorods absorption band is tunable based on the aspect ratio. [40] The synthesized gold nanorod have end where there are five {111} faces on the ends and on the sides where there are {100} and {110} crystal faces due to the reagents used for the formation of the nanorods. Both gold nanorods and gold nanoparticles have {111} and {100} facets but in addition to these gold nanorod have {110} facet which is useful to bind any molecules more strongly compared to the other two facets, so gold nanorods show higher Raman enhancement compared to gold nanoparticles. [41] For example, the use of Ag(I) was responsible for slowing down the synthesis, as it was reduced by ascorbic acid to metallic Ag and blocked the more energetically favorable {110} crystal face on

33

the side so the crystal of gold nanorod grew at the {100} crystal face direction. The surfactant used also covered the side of the nanorod, so reaction used to take place at the end of the nanorods. [39]

For example, thiols tend to bind at the end of the nanorod [42], mercaptopropanoic acid also used to bind to the {111} crystal face [43]. However, the polyelectrolyte can cover up the whole nanorod by electrostatic interaction [44]
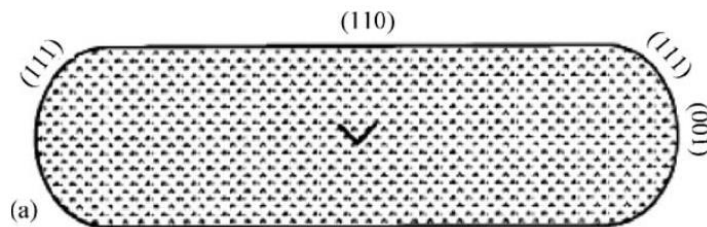
Figure 1. 32 Gold nanorod showing different crystal facets [45]

(Reprinted with permission from Ref.45. Copyright © 2005, Coorrdination Chemistry Review)

Gold nanorod has a transverse band which can be excited specifically if the excitation light is parallel to the short axis of the nanorod, conversely in order to excite the longitudinal band then the excitation light has to be parallel to that of the long axis of gold nanorods and for excitation in any other angle, both the transverse and longitudinal band can be excited. [45]
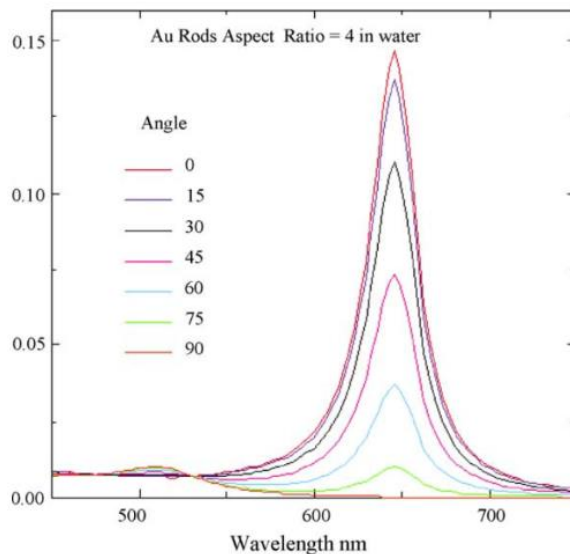
Figure 1. 33 UV-Visible spectrum of gold nanorod with respect to the change of angle of the excitation light correspond to the longitudinal band [45]

(Reprinted with permission from Ref.45. Copyright © 2005, Coordination Chemistry Review)

The stability of the gold nanorod decreases when the salt content is high, CTAB concentration is low and when organic solvent is added. [37]

To measure the surface area of gold nanorod, following equation can be used-

Surface area= $2\pi r^2 + 2\pi r l$ [46]

With the increase of the aspect ratio, the intensity of the longitudinal absorption band increases also it shifts to higher wavelength. [47]
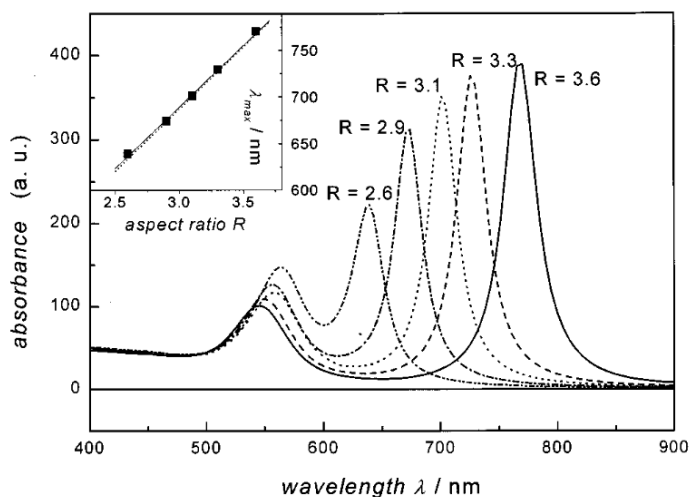
Figure 1. 34 UV-Visible spectrum of gold nanorods showing the variation of absorption band with the change of aspect ratio [47]

(Reprinted with permission from Ref.47. Copyright © 1999, Physical Chemistry)

With the increase of the concentration of gold ions, gold nanorods of higher aspect ratio are produced but upto a certain concentration aspect ratio decreases as a Au-Br-surfactant forms.

The conversion of Au^{3+} to Au^+ can be done by the ascorbic acid, the seed particles can be converted from Au+ to Au^0. Au^+ can be stabilized by forming CTA-X-AuX$_2^-$ complex [48]. Silver ions can form AgBr which can be absorbed at the surface of gold nanorods. To form AgCl, the chloride needs to come not only from HAuCl$_4$ but also from HCL[49]. Ag ions between the headgroups of the CTAB molecule reduces the charge density of Br$^-$ which can cause repulsion of CTAB surfactants [50].
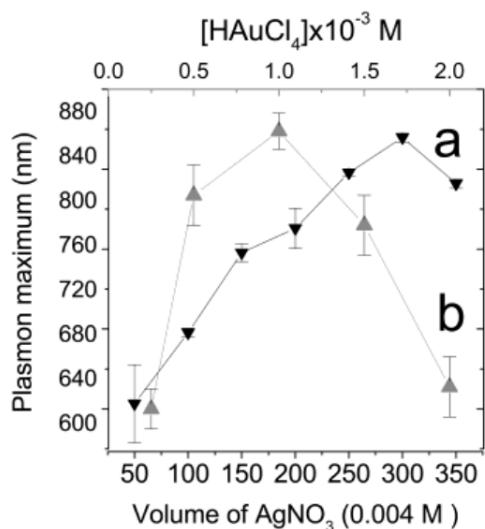
Figure 1. 35 Variation of aspect ratio of gold nanorods with the change of gold ion concentration[50]

(Reprinted with permission from Ref.50. Copyright © 2010, Chemistry of materials)

As with increasing temperature, number of surfactants associated with the gold nanorods decrease, aspect ratio decreases with increasing concentration. With the increase of the seed concentration, aspect ratio also decreases [51]. Larger seeds cause polydispersity with a lower surface energy [52].

Halides decrease reduction potential of gold, they decrease the stability of the silver layer on gold nanorods[53]. Amongst the halides, bromide produces the gold nanorod, whereas chloride only produces spheres and iodide produces nanoparticles of different shapes [52].

The thickness of the CTAB layer was found to be 32 ± 2 A^o which was measured by small angle neutron scattering experiment. The number of ligand molecules attached to the gold nanorods can be measured by digesting the CTAB coated gold nanorods in aqua regia or in KCN, then analyze the solution by mass spectrometer, ^{1}H NMR or by thermogravimetric method and then from the concentration and surface area of the nanorods the density of the ligand can be measured [54]. CTAB can produce bilayer in the gold nanorod, in which the first layer has their headgroup bonded to the gold surface and the headgroup of the second layer faces the aqueous solution. [52]

Surface free energy is measured by the strength and number of the bonds associated with a surface. It is calculated by the following equation-

$\gamma = \frac{1}{2} N_B \varepsilon \rho_A$ [55]

Where N_B belongs to the number of broken bonds, ε belongs to the bond strength, number of atoms in the surface was represented by ρ_A.[55] The number of atoms in {111} was found to be 2.31($1/a_0^2$), in {100} was found to be 2($1/a_0^2$) and in {110} was found to be 1.41($1/a_0^2$). The trend in surface energy of different indices are such as $\gamma_{\{111\}} < \gamma_{\{100\}} < \gamma_{\{110\}}$ [55]

The nanoparticles have the lowest surface energy because of their spherical shape [55].

Compared to gold nanorods, due to having more sharp corners and edges gold nanobipyramids show higher PL quantum yield. This effect is known as the lightening rod effect.[56]

When the images of photoluminescence and image of DF scattering for gold nanobipyramids were compared, it was observed that the brighter spots in the DF image and in the photoluminescence were different. This was due to the fact that, the scattering is not dependent on the direction of light, but the photoluminescence is dependent on the direction of light. So, the

brighter spots observed in the DF scattering image was not brighter in the photoluminescence image [56]

1.7 Condition for surface plasmon resonance:

The interaction of nanoparticles and dyes can cause fluorescence enhancement or fluorescence quenching. This interaction is dependent on the composition of the nanoparticle, the distance between the dye and nanomaterial, the orientation of the dipole, the extent to which the plasmonic band of the nanomaterial can overlap with the absorption or emission band of the dye [40]. When the fluorophore is within 5 nm to the surface of nanomaterial, fluorescence quenches, as the fluorophore then tend to donate its excited electron to the metal. However, as the distance from the metallic surface is within 10-20 nm then the fluorescence increases. [30] The gold nanoparticle of a diameter of 10-20 nm causes less scattering of light due to their small size and so it can show enhancement due to surface plasmon resonance [57].
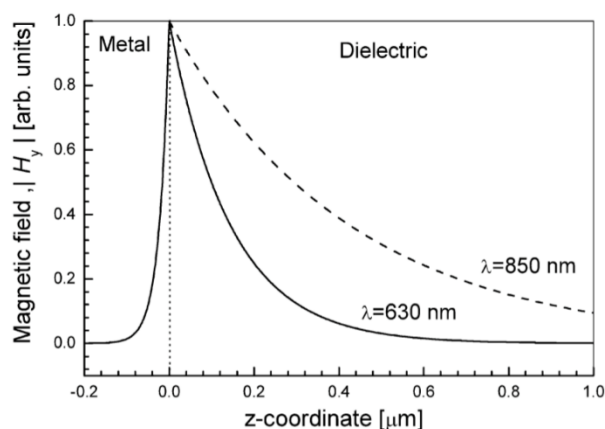
Figure 1. 36 Variation of magnetic field in the interface of gold and a dielectic material [57]

(Reprinted with permission from Ref.57. Copyright © 2013, ACS Nano)

For example, about 10 times enhancement was observed when IR dye was coated with a silica thickness of 17 nm and when the dye was excited by a wavelength of 779 nm. The

maximum enhancement was observed when the IR dye was bonded with a gold nanorod which has the plasmon band at 776 nm [40] Here, the silica shell thickness was varied by adding different concentrations.
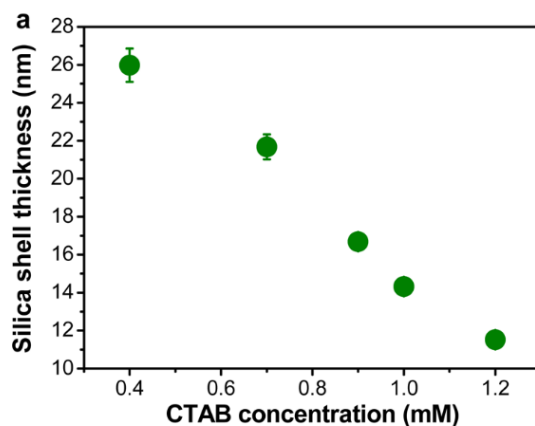
Figure 1. 37 Change of silica shell thickness by changing the concentration of CTAB [40]

(Reprinted with permission from Ref.40. Copyright © 2014, ACS Nano)

Here, the IR dye loading per nanorod was calculated by taking the fluorescence spectrum of the supernatant and comparing the fluorescence peak observed with that of the calibration curve formed by measuring the fluorescence peak intensity with concentration. From this calculation dye to dye separation was found to be 9 nm or higher and it was found that at a dye-dye separation less than 9 nm, quenching occurred due to increased dye to dye interaction. This phenomena is known as Forster resonance energy transfer [40].
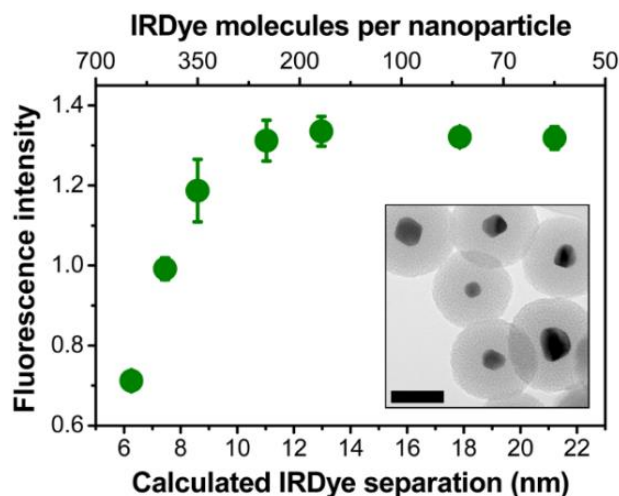
Figure 1. 38 Variation of fluorescence intensity with the change of dye to dye separation distance[40]

(Reprinted with permission from Ref.40. Copyright © 2014, ACS Nano)

1.8 Effect of nanomaterial-dye interaction:

Due to the resonance coupling between dye and gold nanorod, splitting in the plasmonic band of the gold nanorod occurs. This coupling causes hybridized states. For example, Au@PSS which showed a characteristic absorption band at 740 nm, this plasmonic band shifted due to the introduction of HITC and this splitting peak changed with the change in concentration of HITC [58].
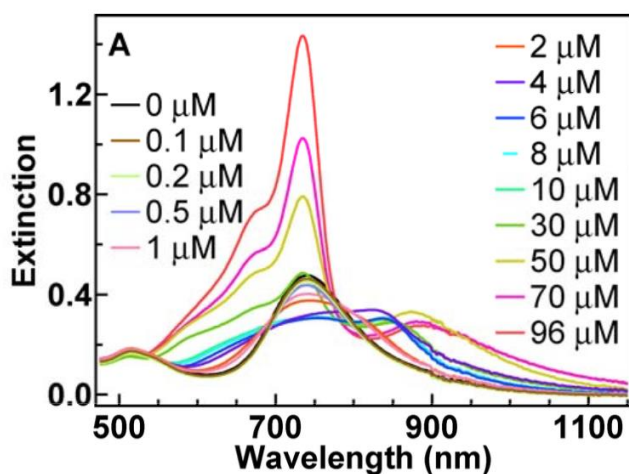
Figure 1. 39 Change of splitting of the plasmonic band at 740 nm for Au@PSS as the concentration of HITC increased [58]

(Reprinted with permission from Ref.. 58Copyright © 2008, American Chemical Society)

In this experiment, the number of dyes attached to each gold nanorods was measured to be 44000. This measurement was done by comparing the UV-Visible absorption spectrum of 10 µM HITC solution and the UV-Visible spectrum of the supernatant solution found after centrifugation of the mixture of HITC and Au@PSS [58]. It was found that 21% of the HITC molecule was there in the supernatant solution.
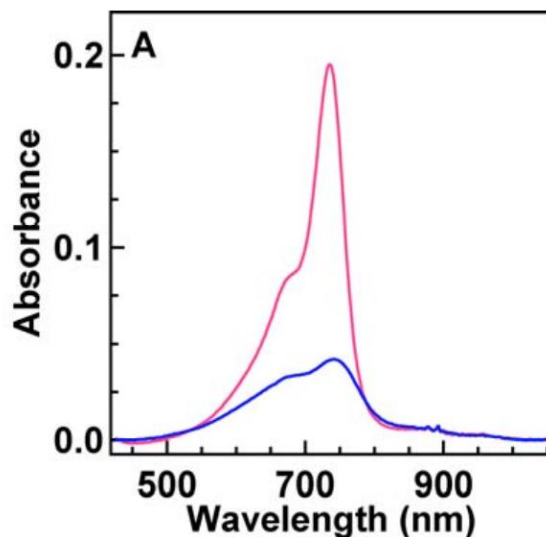
Figure 1. 40 UV-Visible spectrum of 10 µM HITC (red) and supernatant solution after the centrifugation of the mixture of 10 µM HITC and Au@PSS [58]

(Reprinted with permission from Ref.58. Copyright © 2008, American Chemical Society)

The shift of the plasmon band of the Au@PSS is also dependent on the change of the concentration of HITC.
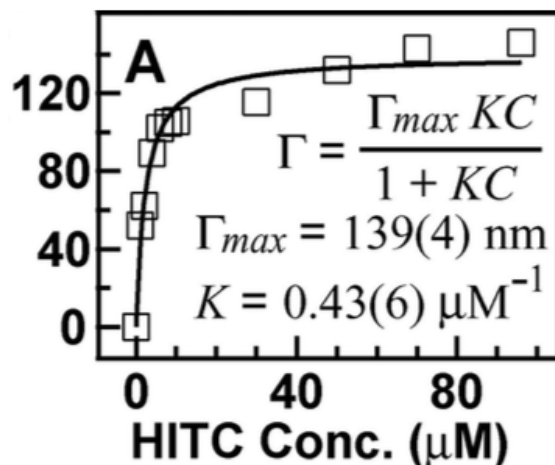
Figure 1. 41 Change of the shift of the plasmon band of Au@PSS with the change of the concentration of HITC [58]

(Reprinted with permission from Ref.58. Copyright © 2008, American Chemical Society)

This plasmonic shift followed the Langmuir equation.

$\Gamma = \Gamma_{max}KC/ 1+KC$

Where Γ, Γ_{max}, K, C are represented by the change of plasmonic shift, the highest plasmonic shift, binding constant of the Langmuir equation and the concentration of the dye respectively [59].

The resonance coupling is also dependent on the pH of the solution. At pH below 12, a peak at 835 nm was observed due to the resonance coupling between the dye and the gold nanorod. At a pH higher than 12, due to the breaking of conjugated double bonds there was a drop in the plasmonic band shift. The change of red color of the PSS coated gold nanorods to the green color due to the addition of HITC again turned red at pH higher than 12 [59].
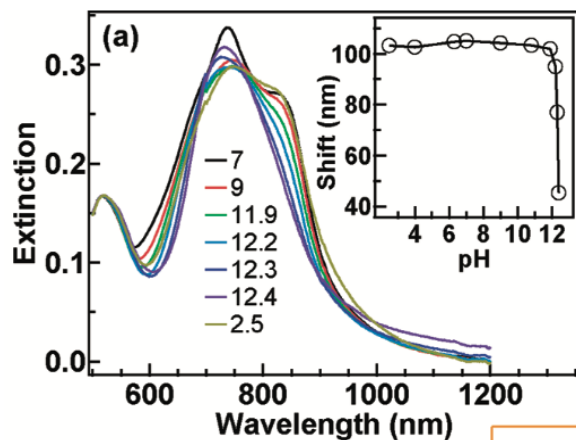
Figure 1. 42 Plasmonic band shift of the HITC-gold nanorod complex upon changing the pH of the solution [59]

(Reprinted with permission from Ref.59. Copyright © 2010, American Chemical Society)

1.9 Properties of nanomaterials:

Nanoparticles exhibit incredible power and ductility compared to that of the bulk metals. Due to the electronic transition, noble bulk materials exhibit little fluorescence[60], however in the case of nanorods, cross sectional area of the band for the electronic transition was increased by their longitudinal plasmon band [61,62], so ECL intensity increases with a different wavelength of light which depends upon the extent of overlap. El-Sayed *et. al* proved that reactivity of nanomaterials is higher in case of nanomaterial having higher number of corners and edges[63].

Nanoparticles can increase ECL of a luminophore as [64]-

1.Nanoparticles helps to fix the incident light into the evanescent field, so rate of absorption of light increases.

2.Nanoparticles can change fluorescence lifetime, quantum yield, radiative process and

nonradiative process of a fluorophore.

3.Nanomaterials absorption band can overlap with the emission band of the luminophore showing surface plasmon resonance.

During the ECL enhancement process, energy of the surface plasmon is transferred to the nanoparticle surface.

Gold nanorods has two absorption band on its UV visible spectrum. The first band corresponds to the transverse band which represents the smaller axis and the longitudinal band represents the longer axis. When the longitudinal band of the gold nanorod, can overlap with the emission band of the $Ru(bpy)_3^{2+}$ and if the distance between the center of the $Ru(bpy)_3^{2+}$ and gold nanorods is within a particular distance, then we can get an enhancement of the ECL signal due to surface plasmon resonance effect. The coupling between the gold nanorods and the center of the $Ru(bpy)_3^{2+}$ depends on composition of the nanoparticles, distance and degree of overlap between them, orientation of the dipole moment. The degree of coupling depends on the distance between the center of the luminophore and the metallic surface which was examined by Gryczynski,I. *et al* [26]
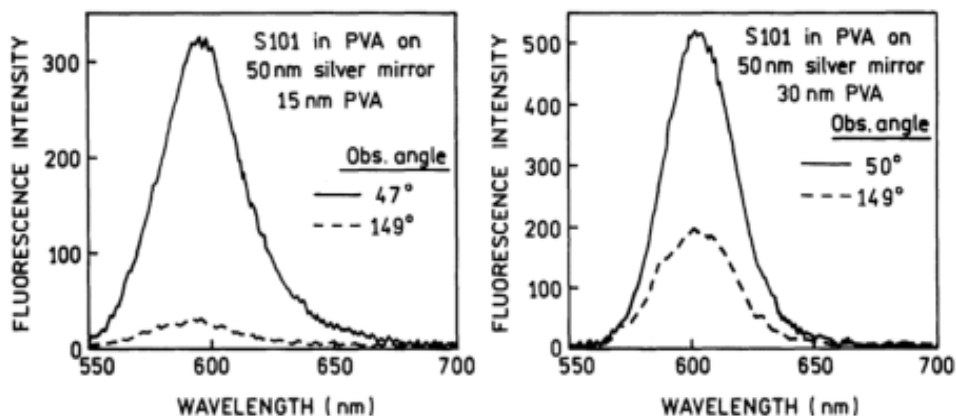
Figure 1. 43 Fluorescence emission intensity based on spectral overlap (-) representing emission from absorbed light and (- - -) representing emission from reflected light [26]

(Reprinted with permission from Ref.26. Copyright © 2004, Analytical Biochemistry)

The bipolar sensor based on gold nanorods can act by

1.Aggregation or disaggregation of the target analyte to the surface of gold nanorods,

2.Change of refractive index of the surface of gold nanorods.

Gold nanorods or gold nanoparticles can be attached with the electrode due to electrostatic attraction or covalent binding. Gold nanorods have additional advantage compared to the fluorescent dyes is that they do not show photobleaching. [39]

1.10 Distance dependent ECL enhancement:

Wang et.al[1] showed 5 times electrochemiluminescence signal enhancement of $Ru(bpy)_3^{2+}$ compared to that of the bare gold electrode by functionalizing gold electrode with SiO_2 capped gold nanoparticles. In case of SiO_2 thickness of 6 nm in the $Au@SiO_2$ coated gold electrode, the ECL intensity increased 5 times compared to that of the bare gold electrode. However, when SiO_2 thickness was 30 nm, ECL intensity decreased as the electric field decreased with distance from the electrode. They investigated the ECL results by modifying the gold electrode with PDDA, PDDA & SiO_2, PDDA & AuNPs, PDDA & Au capped with SiO_2. They found that even though gold electrode modified with PDDA and SiO_2 and gold electrode modified with PDDA and $Au@SiO_2$ showed similar electrochemical behavior due to similarity in their sizes, ECL behavior of these two types of electrodes were vastly different. PDDA and $Au@SiO_2$ modified electrode showed much higher ECL intensity due to surface plasmon resonance [1].
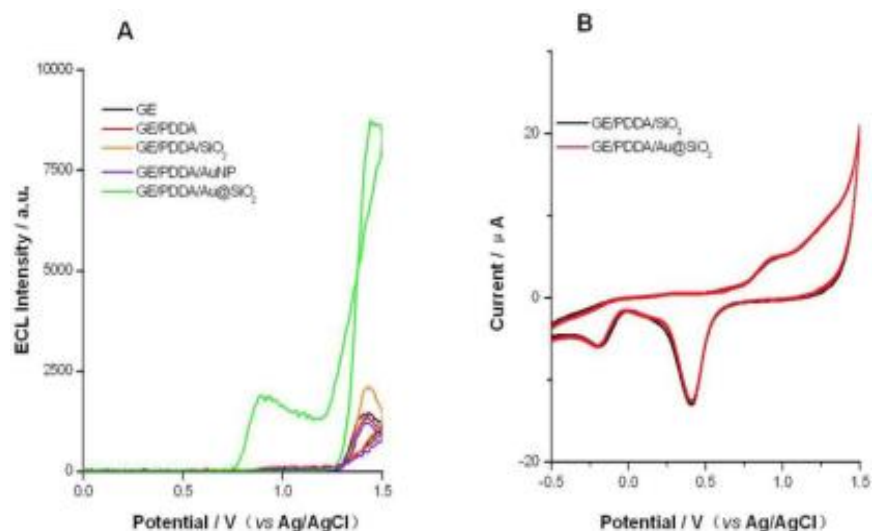
Figure 1. 44 A)ECL intensity against applied potential spectrum of different modified gold electrodes, B) CV of PDDA,SiO_2 modified and PDDA,Au@SiO_2 modified gold electrode [1]

(Reprinted with permission from Ref.1. Copyright © 2015, Scientific reports)

However, the surface plasmon resonance effect was dependent on thickness of SiO_2. When the thickness was 6 nm then ECL intensity was reduced due to transfer of energy of Ru(bpy)$_3^{2+}$ to the nanoparticle surface which is known as Fourier Resonance Energy Transfer (FRET). ECL intensity was found to be maximum for the shell thickness of 6 nm when the spectral overlap was maximum for the resonance to occur. However, when the thickness of SiO_2 increased further as ECL intensity was found to be decreased with the distance from the electrode surface, surface plasmon resonance intensity decreases exponentially. At 30 nm thickness of SiO_2, the ECL intensity was found to be the same as that of the PDDA, SiO_2 modified gold electrode, which signified the fact that at a distance of 30 nm from the surface, surface plasmon resonance enhancement effect was just vanished [1].

46
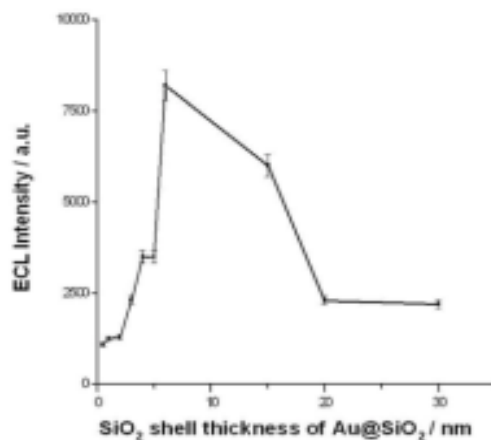
Figure 1. 45 Dependence on ECL intensity on SiO$_2$ shell thickness [1]

(Reprinted with permission from Ref.1. Copyright © 2015, Scientific reports)

1.11 Detection of Hg^{2+} by surface plasmon resonance enhancement of gold nanorods [65]:

Wang et.al detected Hg^{2+} by the surface plasmon resonance of gold nanorods[65]. They functionalized gold electrode with mercaptopropanoic acid, which can bind gold nanorods by forming covalent bonding with their terminal sulfer. The system was further modified with ss-DNA and in the presence of Hg^{2+} the system was taken the shape of a hairpin. Ru(bpy)$_3^{2+}$ was bound with the channel of the ss-DNA to show the ECL signal. This ECL signal was intensified due to the presence of Hg^{2+} [65]. They showed that although gold electrode modified with DNA and gold electrode modified with DNA, AuNRs in the presence of Hg^{2+} and Ru(bpy)$_3^{2+}$ showed similar electrochemical behavior, their ECL characteristics were vastly different [65]. Due to the surface plasmon resonance of gold nanorods, ECL response of the electrode surface modified with AuNRs was much higher [65].
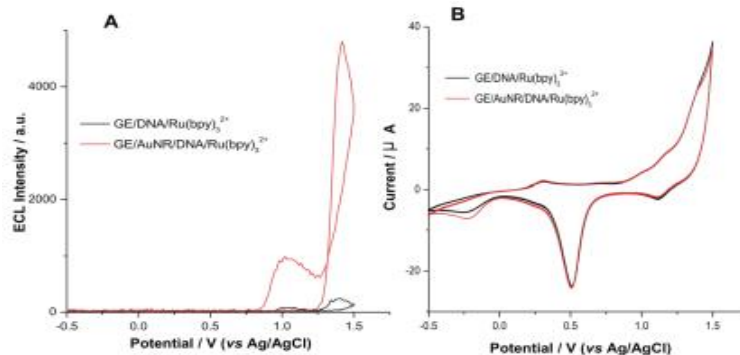
Figure 1. 46 A) ECL intensity vs applied potential spectrum for Hg^{2+} detection by DNA modified and DNA@AuNR modified gold electrode in the presence of $Ru(bpy)_3^{2+}$, B) CV curve of DNA modified and DNA@AuNR modified gold electrode in the presence of $Ru(bpy)_3^{2+}$ [65]

(Reprinted with permission from Ref.65. Copyright © 2014, Electrochimica Acta)

They tested the sensor system, by trying three different types of gold nanorods having longitudinal plasmon bands at 607 nm, 632 nm and 673 nm and found that gold nanorods having longitudinal plasmon band at 632 nm showed maximum ECL intensity.

Wang *et.al* also investigated the biosensor sensitivity taking three different sized ss-DNA sequence [65].

54
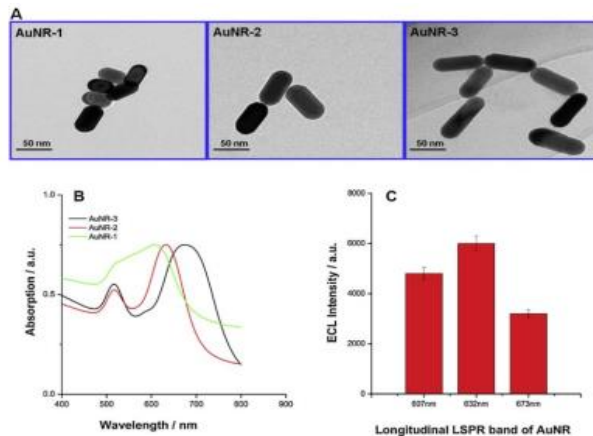
Figure 1. 47 A) TEM images, B)UV-Visible spectrum and C) ECL intensity based on longitudinal

plasmon bands for three different sizes of gold nanorods for detecting Hg^{2+} [65]

(Reprinted with permission from Ref.65. Copyright © 2014, Electrochimica Acta)

Wang *et.al* also investigated the biosensor sensitivity taking three different

sized ss-DNA sequence [65].

Table 1. 1 Three different types of DNA sequence for testing the sensor system for detecting Hg^{2+}

DNA name	Sequence
DNA 1	5'-SH-C6-CCCTTTTTTTTTCCCCCCTTTTTTTTT-3'
DNA 2	5'-SH-C6-CCCCCCCCCTTTTTTTTTCCCCCCTTTTTTTTT-3'
DNA 3	5'-SH-C6-CCCCCCCCCCCCCCCCTTTTTTTTTCCCCCCTTTTTTTTT-3'

It was found that although the three different types of DNA modified electrode

showed the   similar electrochemical responses, ECL intensity was higher in case of the

electrode modified with the DNA-2.
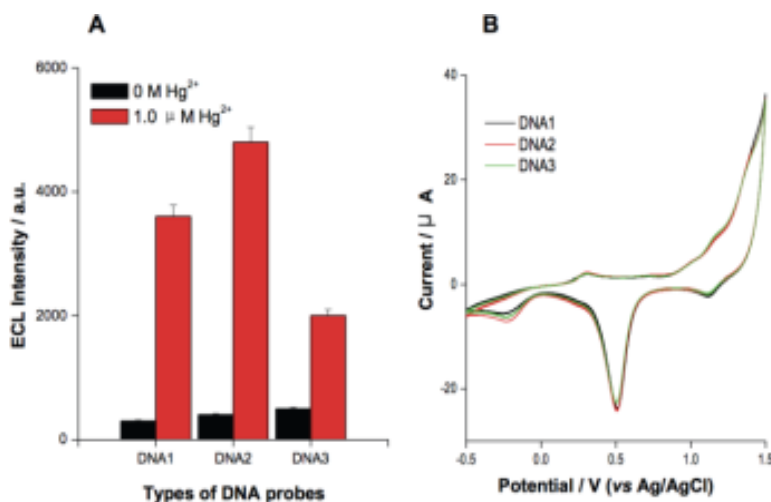
Figure 1. 48 A) ECL characteristics and B) Electrochemical behavior of electrode modified with different DNA sequences [65]

(Reprinted with permission from Ref.65. Copyright © 2014, Electrochimica Acta)

To test sensitivity of the system, they checked the sensor system with different concentration of Hg^{2+} and it was found that ECL intensity increased with increasing concentration of Hg^{2+} and there was a linear relationship between ECL and log of concentraton of Hg^{2+} [65].
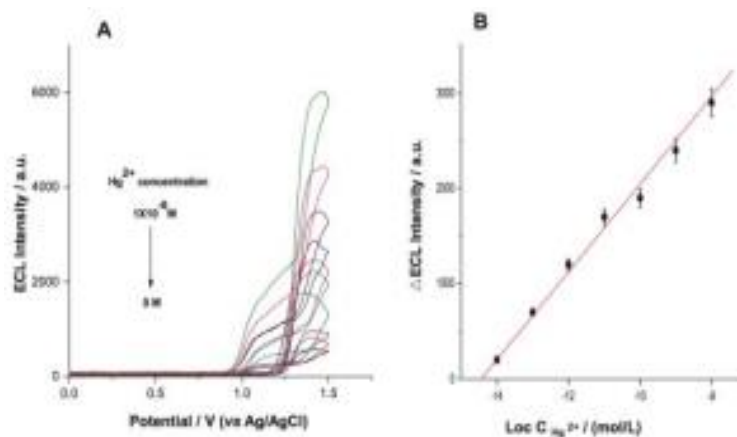
Figure 1. 49 Sensitivity of the sensor for detecting Hg^{2+} [65]

(Reprinted with permission from Ref.65. Copyright © 2014, Electrochimica Acta)

1.12 Activity of the Biopolar electrical sensor:

The sensor system based on nanoparticles work with two basic principles.

a) Due to the change in refractive index, plasmon band of the nanoparticle changes,

b) Due to the nanoparticle's aggregation plasmon band of the nanoparticle changes.

The sensitivity of the longitudinal band is higher towards the change in surrounding medium compared to the transverse band and it was found that there is a linear

relationship between square of the change of longitudinal band and with the square of the refractive index change of the medium.[66] There is a term known as dielectric sensitivity, which belongs to the determination of the system's sensitivity toward the change in refractive index. The unit of dielectric sensitivity is eV/RIU [67].

The longitudinal band of gold nanorod is more sensitive to the change in refractive index of the medium [66].

This dependence is showed by the equation-

$$\lambda_{LSPR}= \lambda_p(2n_m^2+1)$$

where the wavelength of plasmonic band is represented by λ_p [36]

The random distribution of the electromagnetic field causes higher field intensity in the dielectric compared to that of the metal. So, the optical parameters of the dielectric changes the refractive index surrounding the plasmonic material. [68]

Refractive index sensitivity of the nanomaterial changes with shapes in the trend nanorods>nanotriangles>spheres [69]

The sensitivity of the gold nanorod based sensor depends on the refractivity which is the probability of the free electrons to be displaced relative to the nucleus in a nanomaterial. As the electron density changes by binding a molecule to the metallic surface, plasmonic band of the molecule changes.

For example, when gold nanorod is transferred from a medium of water to a medium of toluene, then the shift of longitudinal plasmon band was much higher compared to the shift of the transverse band. [66]
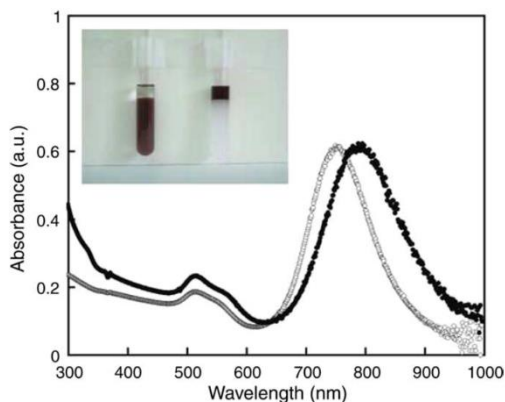
Figure 1. 50 Change of absorption band of gold nanorod by changing the solvent from water to toluene [66]

(Reprinted with permission from Ref.66. Copyright © 2005, Chemical Physics Letters)

The change in plasmonic wavelength due to the change in refractive index is also represented by-

$$\Delta\lambda= m\Delta n \ [1-\exp(-2d/l_d)]$$

here, m is the sensitivity of the nanomaterial to the change in refractive index, d is the thickness of the molecule absorb to the nanomaterial, l_d is the length of electromagnetic decay [37].

Metallic nanorods have many advantages to be useful as a sensor.

1.It is plasmon band can match with the excitation light sources,

2.There is less probability to get background fluorescence from near IR light and plasmon band of the nanorods can be tuned to the region of near IR light,

3.This near IR light can penetrate much deeper into tissues,

4.There can be different sensitivity achieved in the same nanorod as the ends and the sides of a nanorod react differently.

5.Photobleaching is not a problem in case of nanorods. [39]

1.13 Gold nanorods as photoimagers:

Nanorods can absorb light in the infrared region and can radiate this light as heat or light emission. In this way, nanorod can be used as photoimagers and also can be used as photothermal destroyers [39]. For example, by using gold nanorod, cancer cell was imaged 3 times brighter compared to two photon imaging technique and it was detected upto a cell depth of 75µm, whether in two photon imaging technique cancer cell was detected upto a depth of 40 µm.[70] Collagen matrix set was used to embed EGFR-overexpressing A431 skin cancer cell and it was mixed in a 1:1 ratio with the targeted or non-targeted nanorods. The system was excited by Ti:sapphire laser at the wavelength of 760 nm light and the system was imaged by GaAsP photomultiplier tube. It was found that, much higher excitation light source of 9.00 mW was needed to detect the cell when no gold nanorods was attached to the cell. On the other hand, when specific gold nanorod was attached with the cell, much lower excitation power was needed to visualize the cell again. When non-specific target was added with the cell, there was a coagulation of the gold nanorods and only limited portion of the cell was shown to be attached [70].
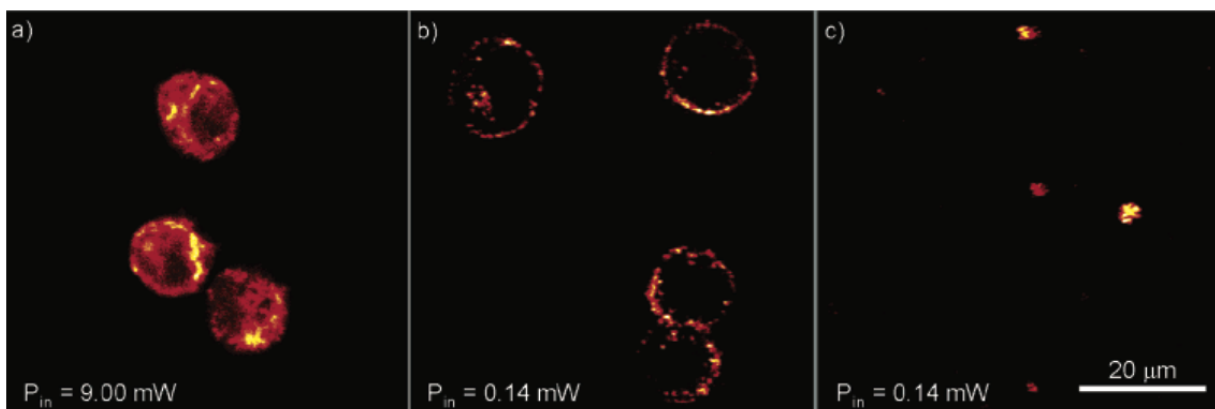
Figure 1. 51 a) Images of cancer cell without any gold nanorod present, b) Image of cancer cell in the presence of target specific gold nanorods, c) Image of cancer cell in the presence of nonspecific gold nanorods [70]

(Reprinted with permission from Ref.70. Copyright © 2007, Nano Letters)

Again, when the cell images in different depth of tissue was compared, it was observed that for imaging a cell for each 20 µm depth, 26% power was necessary to increase to maintain the same intensity of the images. This resulted 625 times more imaging capabilities of the cell in the presence of gold nanorod compared to imaging the cell without the presence of gold nanorods.
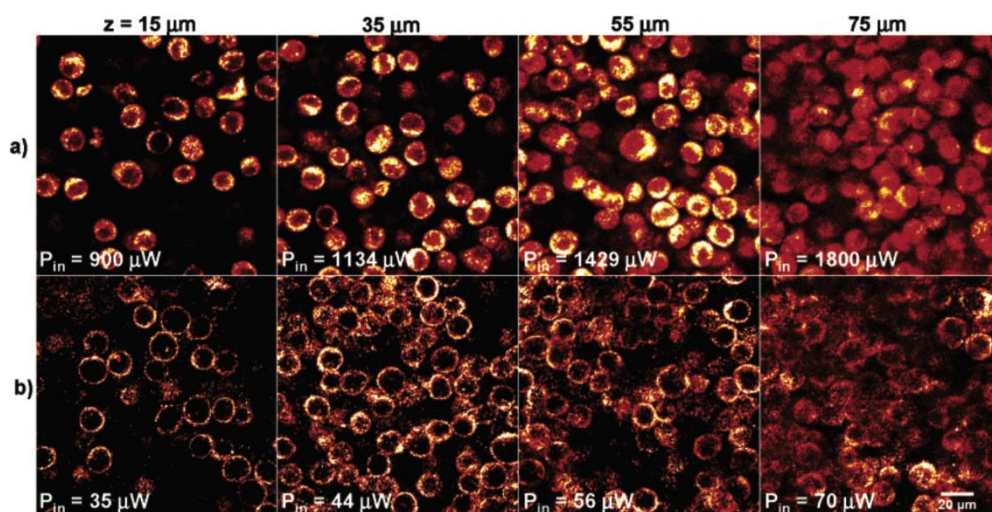
Figure 1. 52 a) Imaging of the cancer cell at different depth of the tissue when bonded to gold nanorods, b) Imaging of the cancer cell at different depth of the tissue without the presence of gold nanorods [70]

(Reprinted with permission from Ref.70. Copyright © 2007, Nano Letters)

1.14 Gold nanorods as photodamagers:

Gold nanorods can absorb infrared radiation and they radiate the radiation back causing heat energy to produce, which can damage target cells. For example, phosphatidylcholine protected gold nanorods was mixed with cultured media consisted of Hela Cells which was stained by Trypan Blue, were irradiated by the Nd:YAG laser at a wavelength of 1064 nm. It was found that in the absence of Trypan Blue staining or in the absence of gold nanorods, no cell damage was observed upon irradiation with laser light. However, in the presence of PC coated gold nanorod, when the cancer cell was stained, cell death was observed by the laser irradiation. This is how, gold nanorod can be used to kill cancer cells. [71]
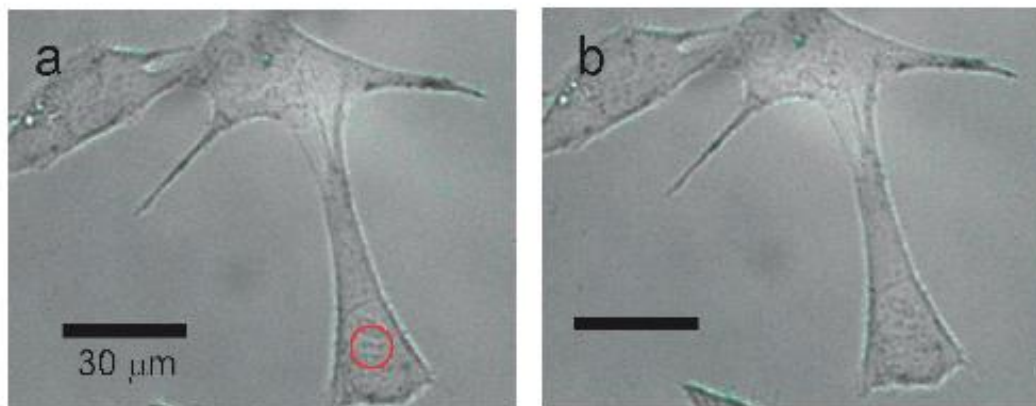
Figure 1. 53 Laser irradiation of cancer cell in the absence of gold nanorods [71]

(Reprinted with permission from Ref.71. Copyright © 2006, Chemical Letters)
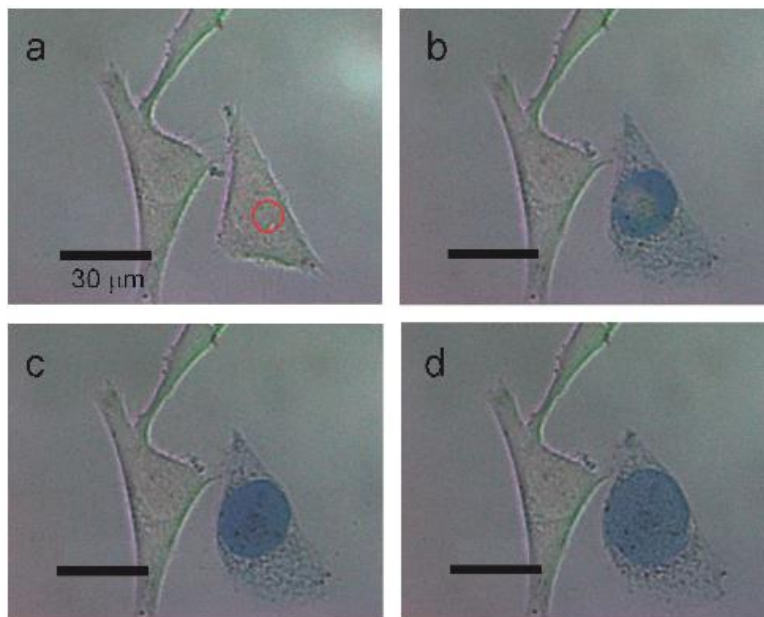
Figure 1. 54 a) Hela cell in presence of PC coated gold nanorod and stained by Trypan blue before laser irradiation, b) few seconds after laser irradiation, c) 1 min after laser irradiation, d) 2 min after laser irradiation [71]

(Reprinted with permission from Ref.71. Copyright © 2006, Chemical Letters)

1.15 Use of Gold nanorods to detect streptavidin[72] :

Gold nanorod was used to detect streptavidin both in plasma and in PBS buffer, when gold nanorod was bonded to biotin [72]. The binding characteristics of the streptavidin to the sensor was measured by the change of plasmonic band of the gold nanorod due to the variation of the concentration of streptavidin. The sensitivity of the gold nanorod was tested by varying the reaction medium from water to ethanol to 3:1 mixture of ethanol:toluene to 1:1 mixture of ethanol:toluene to 1:3 mixture of ethanol:toluene and toluene and it was found that the longitudinal band of the gold nanorod was more sensitive to the change of medium compared to the transverse band of the gold nanorod [72].
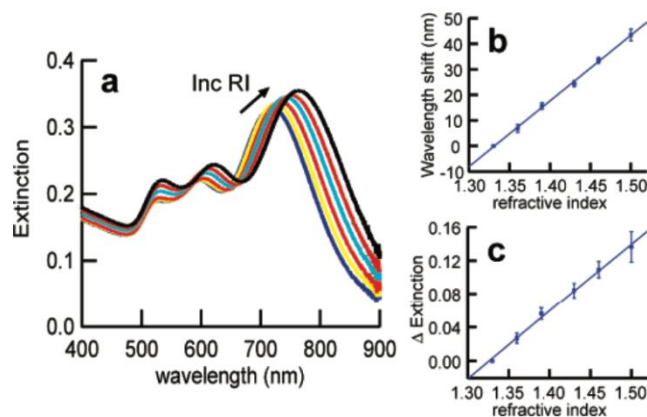
Figure 1. 55 a) UV-Visible spectrum of gold nanorod showing changes in gold nanorods absorption band in different medium, b) Relationship of plasmon band shift with change of reaction medium, c) Change of extinction absorption band upon changing reaction medium [72]

(Reprinted with permission from Ref.72. Copyright © 2007, Analytical Chemistry)

Streptavidin when bonded to the sensor gradually changed the longitudinal absorption band of the gold nanorod with time and upon increasing the concentration of the streptavidin, the absorption band red shifted proving sensitivity of the gold nanorod based sensor. The detection limit of this gold nanorod based sensor was 94 pM in PBS buffer medium and 19 nM in serum medium [72].
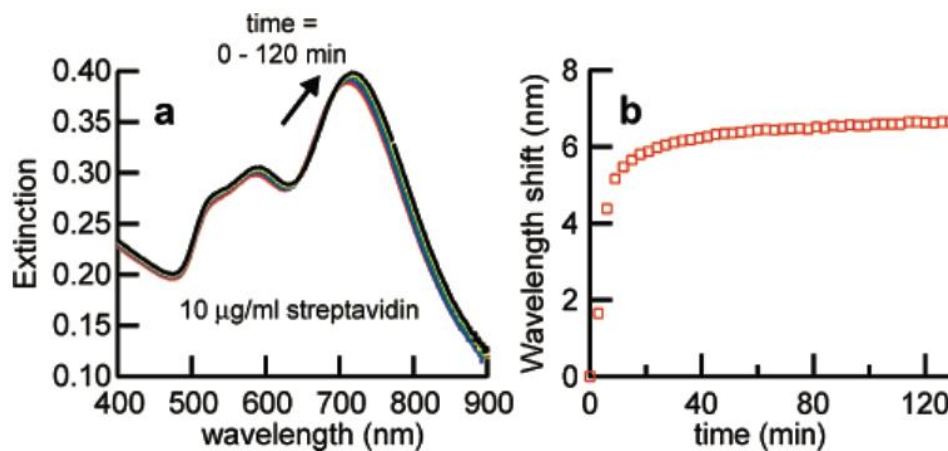
Figure 1. 56 a) change in the plasmon band of the gold nanorod with time upon binding to streptavidin, b) plasmon band shift with time upon binding to streptavidin [72]

(Reprinted with permission from Ref.72. Copyright © 2007, Analytical Chemistry)
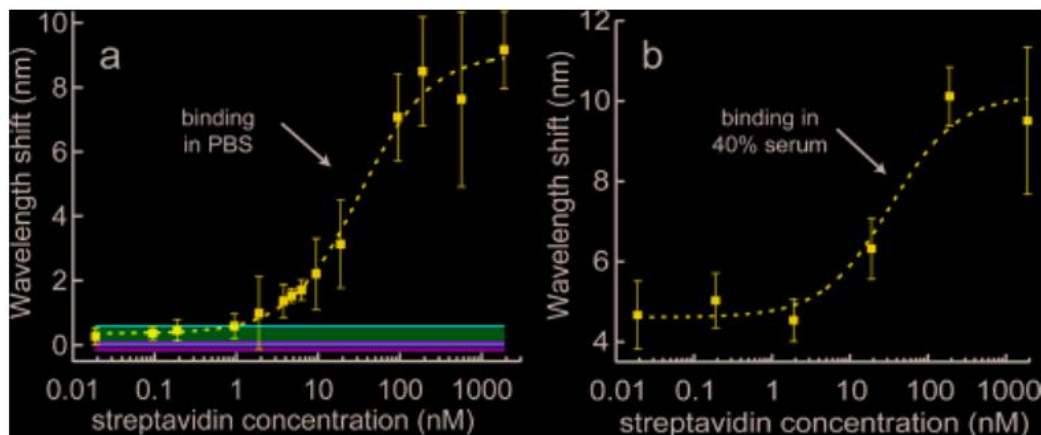
Figure 1. 57 a) Gold nanorod's plasmon band shift with increasing the concentration of streptavidin in PBS buffer, b) Gold nanorod's plasmon band shift with increasing the concentration of streptavidin in 40% serum [72]

(Reprinted with permission from Ref.72. Copyright © 2007, Analytical Chemistry)

1.16 Use of gold nanorods to detect Lithium:

Lithium was detected by forming a 2:1 complex of ligand-metal due to the aggregation of the Au nanoparticle functionalized 1,10 phenanthroline causing color change [73]. Here, front end of the ligand was bonded with Li^+ and back end of the ligand was bonded with 4 nm Au nanoparticle. The Li^+ caused ligands to bind, formed aggregation of the ligand by making a color change of the solution from orange color to gray color and there was no cloudiness observed in the solution [73].
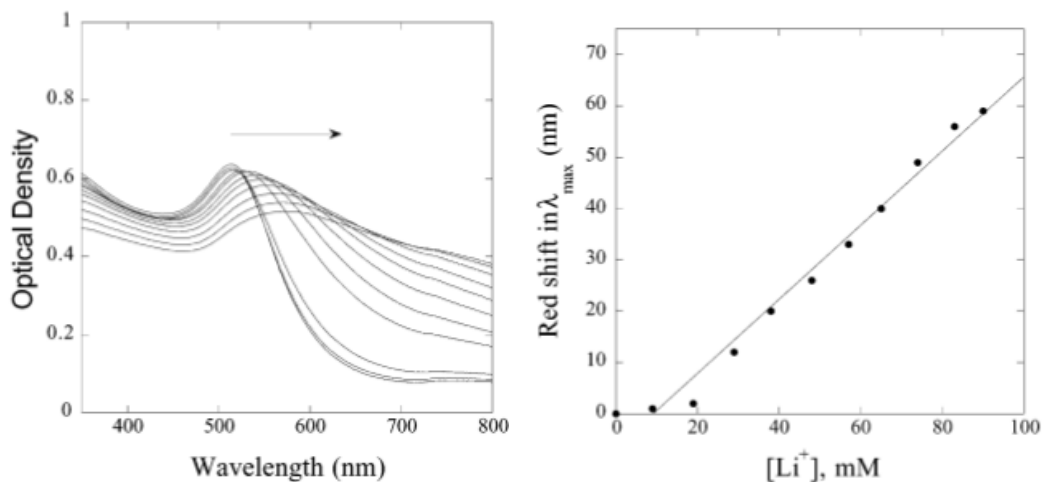
Figure 1. 58 Plasmon band shift of Au nanoparticles with increasing concentration of Li^+ [73]

(Reprinted with permission from Ref.73. Copyright © 2002, Langmuir)

Refractive index based sensitivity of the gold nanorods was also tested to detect the goat antirabbit IgG protein [74]. For that, the surface of gold nanoparticles was modified with SAM of mercaptohexadecanoic acid and mercaptoundecanol and this gold nanoparticle was then exposed to the capture protein of rabbit IgG which caused a red shift in the plasmonic band of gold nanoparticles. After that the sensor was washed so that some physically absorbed IgG was removed caused a blue shift of the plasmonic band, after that 30 nM of target protein which was goat antirabbit IgG was introduced which caused a red shift of the plasmon band and again washing of the sensor removed some target protein which caused a further blue shift of the plasmonic band. Sensors specificity was also tested by goat antimouse IgG protein as the target compound, only little change of the plasmonic band observed which proved the specificity of the sensor to goat antirabbit IgG protein. [74].

Reference 1:

(1)   Wang, D.; Guo, L.; Huang, R.; Qiu, B.; Lin, Z.; Chen, G. Surface Enhanced Electrochemiluminescence of Ru(Bpy)32+. *Sci. Rep.* **2015**, *5* (1), 7954. https://doi.org/10.1038/srep07954.

(2)   Wallace, W. L.; Bard, A. J. Electrogenerated Chemiluminescence. 35. Temperature Dependence of the ECL Efficiency of Tris(2,2'-Bipyridine)Rubidium(2+) in Acetonitrile and Evidence for Very High Excited State Yields from Electron Transfer Reactions. *J. Phys. Chem.* **1979**, *83* (10), 1350–1357. https://doi.org/10.1021/j100473a022.

(3)   Ulrich, C.; Andersson, O.; Nyholm, L.; Björefors, F. Potential and Current Density Distributions at Electrodes Intended for Bipolar Patterning. *Anal. Chem.* **2009**, *81* (1), 453–459. https://doi.org/10.1021/ac801871c.

(4)   Mavré, F.; Chow, K.-F.; Sheridan, E.; Chang, B.-Y.; Crooks, J. A.; Crooks, R. M. A Theoretical and Experimental Framework for Understanding Electrogenerated Chemiluminescence (ECL) Emission at Bipolar Electrodes. *Anal. Chem.* **2009**, *81* (15), 6218–6225. https://doi.org/10.1021/ac900744p.

(5)   Mavré, F.; Anand, R. K.; Laws, D. R.; Chow, K.-F.; Chang, B.-Y.; Crooks, J. A.; Crooks, R. M. Bipolar Electrodes: A Useful Tool for Concentration, Separation, and Detection of Analytes in Microelectrochemical Systems. *Anal. Chem.* **2010**, *82* (21), 8766–8774. https://doi.org/10.1021/ac101262v.

(6)   Zhan, W.; Alvarez, J.; Crooks, R. M. Electrochemical Sensing in Microfluidic Systems Using Electrogenerated Chemiluminescence as a Photonic Reporter of Redox Reactions. *J. Am. Chem. Soc.* **2002**, *124* (44), 13265–13270. https://doi.org/10.1021/ja020907s.

(7)   Chow, K.-F.; Mavré, F.; Crooks, J. A.; Chang, B.-Y.; Crooks, R. M. A Large-Scale, Wireless Electrochemical Bipolar Electrode Microarray. *J. Am. Chem. Soc.* **2009**, *131* (24), 8364–8365. https://doi.org/10.1021/ja902683f.

(8)   Loget, G.; Kuhn, A. Shaping and Exploring the Micro- and Nanoworld Using Bipolar Electrochemistry. *Anal. Bioanal. Chem.* **2011**, *400* (6), 1691–1704. https://doi.org/10.1007/s00216-011-4862-1.

(9)   Ulrich, C.; Andersson, O.; Nyholm, L.; Björefors, F. Formation of Molecular Gradients on Bipolar Electrodes. *Angew. Chem. Int. Ed.* **2008**, *47* (16), 3034–3036. https://doi.org/10.1002/anie.200705824.

(10)   Perdue, R. K.; Laws, D. R.; Hlushkou, D.; Tallarek, U.; Crooks, R. M. Bipolar Electrode Focusing: The Effect of Current and Electric Field on Concentration Enrichment. *Anal. Chem.* **2009**, *81* (24), 10149–10155. https://doi.org/10.1021/ac901913r.

(11) Dumitrescu, I.; Anand, R. K.; Fosdick, S. E.; Crooks, R. M. Pressure-Driven Bipolar Electrochemistry. *J. Am. Chem. Soc.* **2011**, *133* (13), 4687–4689. https://doi.org/10.1021/ja111050h.

(12) Zhang, X.; Chen, C.; Li, J.; Zhang, L.; Wang, E. New Insight into a Microfluidic-Based Bipolar System for an Electrochemiluminescence Sensing Platform. *Anal. Chem.* **2013**, *85* (11), 5335–5339. https://doi.org/10.1021/ac400805f.

(13) Duval, J.; Kleijn, J. M.; van Leeuwen, H. P. Bipolar Electrode Behaviour of the Aluminium Surface in a Lateral Electric Field. *J. Electroanal. Chem.* **2001**, *505* (1–2), 1–11. https://doi.org/10.1016/S0022-0728(01)00461-2.

(14) Wu, M.-S.; Liu, Z.; Shi, H.-W.; Chen, H.-Y.; Xu, J.-J. Visual Electrochemiluminescence Detection of Cancer Biomarkers on a Closed Bipolar Electrode Array Chip. *Anal. Chem.* **2015**, *87* (1), 530–537. https://doi.org/10.1021/ac502989f.

(15) Ramakrishnan, S.; Shannon, C. Display of Solid-State Materials Using Bipolar Electrochemistry. *Langmuir* **2010**, *26* (7), 4602–4606. https://doi.org/10.1021/la100292u.

(16) Chow, K.-F.; Chang, B.-Y.; Zaccheo, B. A.; Mavré, F.; Crooks, R. M. A Sensing Platform Based on Electrodissolution of a Ag Bipolar Electrode. *J. Am. Chem. Soc.* **2010**, *132* (27), 9228–9229. https://doi.org/10.1021/ja103715u.

(17) Gross, E. M.; Pastore, P.; Wightman, R. M. High-Frequency Electrochemiluminescent Investigation of the Reaction Pathway between Tris(2,2'-Bipyridyl)Ruthenium(II) and Tripropylamine Using Carbon Fiber Microelectrodes [†]. *J. Phys. Chem. B* **2001**, *105* (37), 8732–8738. https://doi.org/10.1021/jp011434z.

(18) Zu, Y.; Bard, A. J. Electrogenerated Chemiluminescence. 66. The Role of Direct Coreactant Oxidation in the Ruthenium Tris(2,2')Bipyridyl/Tripropylamine System and the Effect of Halide Ions on the Emission Intensity. *Anal. Chem.* **2000**, *72* (14), 3223–3232. https://doi.org/10.1021/ac000199y.

(19) Miao, W.; Choi, J.-P.; Bard, A. J. Electrogenerated Chemiluminescence 69: The Tris(2,2'-Bipyridine)Ruthenium(II), (Ru(Bpy)$_3^{2+}$)/Tri-n-Propylamine (TPrA) System Revisited─A New Route Involving TPrA$^{•+}$ Cation Radicals. *J. Am. Chem. Soc.* **2002**, *124* (48), 14478–14485. https://doi.org/10.1021/ja027532v.

(20) Creutz, C.; Sutin, N. Reaction of Tris(Bipyridine)Ruthenium(III) with Hydroxide and Its Application in a Solar Energy Storage System. *Proc. Natl. Acad. Sci.* **1975**, *72* (8), 2858–2862. https://doi.org/10.1073/pnas.72.8.2858.

(21) Leland, J. K. Electrogenerated Chemiluminescence: An Oxidative-Reduction Type ECL Reaction Sequence Using Tripropyl Amine. *J. Electrochem. Soc.* **1990**, *137* (10), 3127. https://doi.org/10.1149/1.2086171.

(22)   Richter, M. M. Electrochemiluminescence (ECL). *Chem. Rev.* **2004**, *104* (6), 3003–3036. https://doi.org/10.1021/cr020373d.

(23)   McCord, P.; Bard, A. J. Electrogenerated Chemiluminescence: Part 54. Electrogenerated Chemiluminescence of Ruthenium(II) 4,4'-Diphenyl-2,2'-Bipyridine and Ruthenium(II) 4,7-Diphenyl-1,10-Phenanthroline Systems in Aqueous and Acetonitrile Solutions. *J. Electroanal. Chem. Interfacial Electrochem.* **1991**, *318* (1), 91–99. https://doi.org/10.1016/0022-0728(91)85296-2.

(24)   Zhan, W.; Alvarez, J.; Crooks, R. M. A Two-Channel Microfluidic Sensor That Uses Anodic Electrogenerated Chemiluminescence as a Photonic Reporter of Cathodic Redox Reactions. *Anal. Chem.* **2003**, *75* (2), 313–318. https://doi.org/10.1021/ac020488h.

(25)   Debono, R. F.; Loucks, G. D.; Manna, D. D.; Krull, U. J. Self-Assembly of Short and Long-Chain *n* -Alkyl Thiols onto Gold Surfaces: A Real-Time Study Using Surface Plasmon Resonance Techniques. *Can. J. Chem.* **1996**, *74* (5), 677–688. https://doi.org/10.1139/v96-073.

(26)   Gryczynski, I.; Malicka, J.; Gryczynski, Z.; Lakowicz, J. R. Radiative Decay Engineering 4. Experimental Studies of Surface Plasmon-Coupled Directional Emission. *Anal. Biochem.* **2004**, *324* (2), 170–182. https://doi.org/10.1016/j.ab.2003.09.036.

(27)   Vossen, J. L.; Choudhari, P.; Raether, H. *Physics of Thin Films*; Academic Press: Newyork, San Fransisco, London, 1977.

(28)   Boardman, A. D. *Electromagnetic Surface Modes*; Wiley, 1982.

(29)   Lakowicz, J. R. Radiative Decay Engineering 3. Surface Plasmon-Coupled Directional Emission. *Anal. Biochem.* **2004**, *324* (2), 153–169. https://doi.org/10.1016/j.ab.2003.09.039.

(30)   Eustis, S.; El-Sayed, M. A. Why Gold Nanoparticles Are More Precious than Pretty Gold: Noble Metal Surface Plasmon Resonance and Its Enhancement of the Radiative and Nonradiative Properties of Nanocrystals of Different Shapes. *Chem Soc Rev* **2006**, *35* (3), 209–217. https://doi.org/10.1039/B514191E.

(31)   Aslam, U.; Rao, V. G.; Chavez, S.; Linic, S. Catalytic Conversion of Solar to Chemical Energy on Plasmonic Metal Nanostructures. *Nat. Catal.* **2018**, *1* (9), 656–665. https://doi.org/10.1038/s41929-018-0138-x.

(32)   Ru, E. C. L.; Etchegoin, P. G. *Principles of Surface-Enhanced Raman Spectroscopy*; 2009.

(33)   Hutter, E.; Fendler, J. H. Exploitation of Localized Surface Plasmon Resonance. *Adv. Mater.* **2004**, *16* (19), 1685–1706. https://doi.org/10.1002/adma.200400271.

(34)   Homola, J. Present and Future of Surface Plasmon Resonance Biosensors. *Anal. Bioanal. Chem.* **2003**, *377* (3), 528–539. https://doi.org/10.1007/s00216-003-2101-0.

(35)   Foerster, B.; Joplin, A.; Kaefer, K.; Celiksoy, S.; Link, S.; Sönnichsen, C. Chemical Interface Damping Depends on Electrons Reaching the Surface. *ACS Nano* **2017**, *11* (3), 2886–2893. https://doi.org/10.1021/acsnano.6b08010.

(36)   Li, J.-F.; Li, C.-Y.; Aroca, R. F. Plasmon-Enhanced Fluorescence Spectroscopy. *Chem. Soc. Rev.* **2017**, *46* (13), 3962–3979. https://doi.org/10.1039/C7CS00169J.

(37)   Cao, J.; Sun, T.; Grattan, K. T. V. Gold Nanorod-Based Localized Surface Plasmon Resonance Biosensors: A Review. *Sens. Actuators B Chem.* **2014**, *195*, 332–351. https://doi.org/10.1016/j.snb.2014.01.056.

(38)   Chen, H.; Ming, T.; Zhao, L.; Wang, F.; Sun, L.-D.; Wang, J.; Yan, C.-H. Plasmon–Molecule Interactions. *Nano Today* **2010**, *5* (5), 494–505. https://doi.org/10.1016/j.nantod.2010.08.009.

(39)   Murphy, C. J.; Gole, A. M.; Hunyadi, S. E.; Stone, J. W.; Sisco, P. N.; Alkilany, A.; Kinard, B. E.; Hankins, P. Chemical Sensing and Imaging with Metallic Nanorods. *Chem Commun* **2008**, No. 5, 544–557. https://doi.org/10.1039/B711069C.

(40)   Abadeer, N. S.; Brennan, M. R.; Wilson, W. L.; Murphy, C. J. Distance and Plasmon Wavelength Dependent Fluorescence of Molecules Bound to Silica-Coated Gold Nanorods. *ACS Nano* **2014**, *8* (8), 8392–8406. https://doi.org/10.1021/nn502887j.

(41)   Nikoobakht, B.; El-Sayed, M. A. Surface-Enhanced Raman Scattering Studies on Aggregated Gold Nanorods. 7.

(42)   Caswell, K. K.; Wilson, J. N.; Bunz, U. H. F.; Murphy, C. J. Preferential End-to-End Assembly of Gold Nanorods by Biotin−Streptavidin Connectors. *J. Am. Chem. Soc.* **2003**, *125* (46), 13914–13915. https://doi.org/10.1021/ja037969i.

(43)   Thomas, K. G.; Barazzouk, S.; Ipe, B. I.; Joseph, S. T. S.; Kamat, P. V. Uniaxial Plasmon Coupling through Longitudinal Self-Assembly of Gold Nanorods. *J. Phys. Chem. B* **2004**, *108* (35), 13066–13068. https://doi.org/10.1021/jp049167v.

(44)   Gole, A.; Murphy, C. J. Polyelectrolyte-Coated Gold Nanorods: Synthesis, Characterization and Immobilization. *Chem. Mater.* **2005**, *17* (6), 1325–1330. https://doi.org/10.1021/cm048297d.

(45)   Perezjuste, J.; Pastorizasantos, I.; Lizmarzan, L.; Mulvaney, P. Gold Nanorods: Synthesis, Characterization and Applications. *Coord. Chem. Rev.* **2005**, *249* (17–18), 1870–1901. https://doi.org/10.1016/j.ccr.2005.01.030.

(46) Hill, H. D.; Millstone, J. E.; Banholzer, M. J.; Mirkin, C. A. The Role Radius of Curvature Plays in Thiolated Oligonucleotide Loading on Gold Nanoparticles. *ACS Nano* **2009**, *3* (2), 418–424. https://doi.org/10.1021/nn800726e.

(47) Link, S.; Mohamed, M. B.; El-Sayed, M. A. Simulation of the Optical Absorption Spectra of Gold Nanorods as a Function of Their Aspect Ratio and the Effect of the Medium Dielectric Constant. *J. Phys. Chem. B* **1999**, *103* (16), 3073–3077. https://doi.org/10.1021/jp990183f.

(48) Pérez-Juste, J.; Liz-Marzán, L. M.; Carnie, S.; Chan, D. Y. C.; Mulvaney, P. Electric-Field-Directed Growth of Gold Nanorods in Aqueous Surfactant Solutions. *Adv. Funct. Mater.* **2004**, *14* (6), 571–579. https://doi.org/10.1002/adfm.200305068.

(49) Chang, H.-H.; Murphy, C. J. Mini Gold Nanorods with Tunable Plasmonic Peaks beyond 1000 Nm. *Chem. Mater.* **2018**, *30* (4), 1427–1435. https://doi.org/10.1021/acs.chemmater.7b05310.

(50) Nikoobakht, B.; El-Sayed, M. A. Preparation and Growth Mechanism of Gold Nanorods (NRs) Using Seed-Mediated Growth Method. *Chem. Mater.* **2003**, *15* (10), 1957–1962. https://doi.org/10.1021/cm020732l.

(51) Ward, C. J.; Tronndorf, R.; Eustes, A. S.; Auad, M. L.; Davis, E. W. Seed-Mediated Growth of Gold Nanorods: Limits of Length to Diameter Ratio Control. *J. Nanomater.* **2014**, *2014*, 1–7. https://doi.org/10.1155/2014/765618.

(52) Murphy, C. J.; Sau, T. K.; Gole, A. M.; Orendorff, C. J.; Gao, J.; Gou, L.; Hunyadi, S. E.; Li, T. Anisotropic Metal Nanoparticles: Synthesis, Assembly, and Optical Applications. *J. Phys. Chem. B* **2005**, *109* (29), 13857–13870. https://doi.org/10.1021/jp0516846.

(53) Langille, M. R.; Personick, M. L.; Zhang, J.; Mirkin, C. A. Defining Rules for the Shape Evolution of Gold Nanoparticles. *J. Am. Chem. Soc.* **2012**, *134* (35), 14542–14554. https://doi.org/10.1021/ja305245g.

(54) Burrows, N. D.; Vartanian, A. M.; Abadeer, N. S.; Grzincic, E. M.; Jacob, L. M.; Lin, W.; Li, J.; Dennison, J. M.; Hinman, J. G.; Murphy, C. J. Anisotropic Nanoparticles and Anisotropic Surface Chemistry. *J. Phys. Chem. Lett.* **2016**, *7* (4), 632–641. https://doi.org/10.1021/acs.jpclett.5b02205.

(55) Xia, Y.; Xia, X.; Peng, H.-C. Shape-Controlled Synthesis of Colloidal Metal Nanocrystals: Thermodynamic versus Kinetic Products. *J. Am. Chem. Soc.* **2015**, *137* (25), 7947–7966. https://doi.org/10.1021/jacs.5b04641.

(56) Rao, W.; Li, Q.; Wang, Y.; Li, T.; Wu, L. Comparison of Photoluminescence Quantum Yield of Single Gold Nanobipyramids and Gold Nanorods. *ACS Nano* **2015**, *9* (3), 2783–2791. https://doi.org/10.1021/nn506689b.

(57)   Reineck, P.; Gómez, D.; Ng, S. H.; Karg, M.; Bell, T.; Mulvaney, P.; Bach, U. Distance and Wavelength Dependent Quenching of Molecular Fluorescence by Au@SiO $_2$ Core–Shell Nanoparticles. *ACS Nano* **2013**, *7* (8), 6636–6648. https://doi.org/10.1021/nn401775e.

(58)   Ni, W.; Yang, Z.; Chen, H.; Li, L.; Wang, J. Coupling between Molecular and Plasmonic Resonances in Freestanding Dye−Gold Nanorod Hybrid Nanostructures. *J. Am. Chem. Soc.* **2008**, *130* (21), 6692–6693. https://doi.org/10.1021/ja8012374.

(59)   Ni, W.; Chen, H.; Su, J.; Sun, Z.; Wang, J.; Wu, H. Effects of Dyes, Gold Nanocrystals, PH, and Metal Ions on Plasmonic and Molecular Resonance Coupling. *J. Am. Chem. Soc.* **2010**, *132* (13), 4806–4814. https://doi.org/10.1021/ja910239b.

(60)   Mooradian, A. Photoluminescence of Metals. *Phys. Rev. Lett.* **1969**, *22* (5), 185–187. https://doi.org/10.1103/PhysRevLett.22.185.

(61)   Eustis, S.; El-Sayed, M. Aspect Ratio Dependence of the Enhanced Fluorescence Intensity of Gold Nanorods: Experimental and Simulation Study. *J. Phys. Chem. B* **2005**, *109* (34), 16350–16356. https://doi.org/10.1021/jp052951a.

(62)   Mohamed, M. B.; Volkov, V.; Link, S.; El-Sayed, M. A. The `lightning' Gold Nanorods: Fluorescence Enhancement of over a Million Compared to the Gold Metal. *Chem. Phys. Lett.* **2000**, *317* (6), 517–523. https://doi.org/10.1016/S0009-2614(99)01414-1.

(63)   Narayanan, R.; El-Sayed, M. A. Catalysis with Transition Metal Nanoparticles in Colloidal Solution: Nanoparticle Shape Dependence and Stability. *J. Phys. Chem. B* **2005**, *109* (26), 12663–12676. https://doi.org/10.1021/jp051066p.

(64)   Shan, Y.; Xu, J.-J.; Chen, H.-Y. Distance-Dependent Quenching and Enhancing of Electrochemiluminescence from a CdS:Mn Nanocrystal Film by Au Nanoparticles for Highly Sensitive Detection of DNA. *Chem. Commun.* **2009**, No. 8, 905. https://doi.org/10.1039/b821049g.

(65)   Wang, D.; Guo, L.; Huang, R.; Qiu, B.; Lin, Z.; Chen, G. Surface Enhanced Electrochemiluminescence for Ultrasensitive Detection of Hg2+. *Electrochimica Acta* **2014**, *150*, 123–128. https://doi.org/10.1016/j.electacta.2014.10.121.

(66)   Yang, J.; Wu, J.-C.; Wu, Y.-C.; Wang, J.-K.; Chen, C.-C. Organic Solvent Dependence of Plasma Resonance of Gold Nanorods: A Simple Relationship. *Chem. Phys. Lett.* **2005**, *416* (4–6), 215–219. https://doi.org/10.1016/j.cplett.2005.09.093.

(67)   Nehl, C. L.; Liao, H.; Hafner, J. H. Optical Properties of Star-Shaped Gold Nanoparticles. *Nano Lett.* **2006**, *6* (4), 683–688. https://doi.org/10.1021/nl052409y.

(68)   Guo, X. Surface Plasmon Resonance Based Biosensor Technique: A Review. *J. Biophotonics* **2012**, *5* (7), 483–501. https://doi.org/10.1002/jbio.201200015.

(69)   Willets, K. A.; Van Duyne, R. P. Localized Surface Plasmon Resonance Spectroscopy and Sensing. *Annu. Rev. Phys. Chem.* **2007**, *58* (1), 267–297. https://doi.org/10.1146/annurev.physchem.58.032806.104607.

(70)   Durr, N. J.; Larson, T.; Smith, D. K.; Korgel, B. A.; Sokolov, K.; Ben-Yakar, A. Two-Photon Luminescence Imaging of Cancer Cells Using Molecularly Targeted Gold Nanorods. *Nano Lett.* **2007**, *7* (4), 941–945. https://doi.org/10.1021/nl062962v.

(71)   Takahashi, H.; Niidome, T.; Nariai, A.; Niidome, Y.; Yamada, S. Gold Nanorod-Sensitized Cell Death: Microscopic Observation of Single Living Cells Irradiated by Pulsed Near-Infrared Laser Light in the Presence of Gold Nanorods. *Chem. Lett.* **2006**, *35* (5), 500–501. https://doi.org/10.1246/cl.2006.500.

(72)   Marinakos, S. M.; Chen, S.; Chilkoti, A. Plasmonic Detection of a Model Analyte in Serum by a Gold Nanorod Sensor. *Anal. Chem.* **2007**, *79* (14), 5278–5283. https://doi.org/10.1021/ac0706527.

(73)   Obare, S. O.; Hollowell, R. E.; Murphy, C. J. Sensing Strategy for Lithium Ion Based on Gold Nanoparticles. *Langmuir* **2002**, *18* (26), 10407–10410. https://doi.org/10.1021/la0260335.

(74)   Mayer, K. M.; Lee, S.; Liao, H.; Rostro, B. C.; Fuentes, A.; Scully, P. T.; Nehl, C. L.; Hafner, J. H. A Label-Free Immunoassay Based Upon Localized Surface Plasmon Resonance of Gold Nanorods. *ACS Nano* **2008**, *2* (4), 687–692. https://doi.org/10.1021/nn7003734.

<div align="center">

Chapter Two

Results and Discussion

</div>

2.1 Research Summary

The preferred reagent for producing ECL is $Ru(bpy)_3^{2+}$ and its derivatives as they are highly soluble in water, highly stable electrochemically and can be repeatedly regenerated in multiple cycles of ECL reaction [1]. However, the efficiency of ECL solution made of $Ru(bpy)_3^{2+}$ is very low, 3.5-6% [2]. The target of improving sensitivity of the bipolar electrochemical sensor was achieved by increasing bipolar electrochemical sensitivity based on plasmonic enhancement of ECL also as ECL reaction rate increases with increasing surface area of the gold electrode by the employment of gold nanorods which eventually increases the ECL intensity. [3]

For this purpose gold nanorod of aspect ratio 2.6 was synthesized which shows its longitudinal band at 650 nm that can overlap with the emission of $Ru(bpy)_3Cl_2$, 620 nm [4] to show the plasmonic enhancement of ECL from $Ru(bpy)_3Cl_2$ and gold nanoparticles was also synthesized. The ECL experiment was done in a closed bipolar cell having 5 mM $Ru(bpy)_3^{2+}$, 25 mM TPA and 0.1 M phosphate buffer solution in the reporting compartment and 5 mM $K_3Fe(CN)_6$, 0.1 M KNO_3 in the sensing compartment [2]. The efficiency of the ECL solution of $Ru(bpy)_3^{2+}$ was tested in bare gold electrode and also by modifying the electrodes with PDDA-CTAB coated gold nanoparticles modified gold electrode, PDDA-CTAB coated gold nanorods modified gold electrode, PDDA, CTAB etc. In the cases of gold electrode modified with PDDA-CTAB coated gold nanorods, PDDA-CTAB coated gold nanoparticles, CTAB coated gold nanorods ECL was found to be increased compared with the bare gold electrode mainly due to the surface plasmon resonance effect also as ECL reaction rate increases with increasing surface area by the employment of gold nanorods or gold nanoparticles on the gold electrode which eventually increases the ECL intensity [3]. However, for the gold electrode modified with PDDA, CTAB the

<div align="center">

73

</div>

ECL signal was also found to be decreased mainly due to reduction of surface area by the PDDA surfactant.

To analyze the increase of surface area upon applying PDDA-CTAB coated gold nanorods, cyclic voltammetric analysis were done on the bare gold and PDDA-CTAB coated gold nanorod modified gold electrode and fluorescence experiments were done in the presence and absence of CTAB coated gold nanorods to get to know about the plasmonic enhancement.

For the surface area measurement, cyclic voltammetric experiments were done on bare gold electrode and gold electrode modified with PDDA, CTAB coated gold nanorod in 1.0 mM $K_3Fe(CN)_6$ mixed with 0.5 M KCl in water. For both bare gold and PDDA-CTAB coated gold nanorod modified gold electrode CV measurements were done by measuring current at different scan rate for the potential range of 0 to 500 mV. From the slope of the graph, oxidation peak current vs √Scan rate, electrochemically active surface area of the electrode was calculated based on the equation

$I_p = 0.4463nF(nF/RT)^{1/2} AD^{1/2}v^{1/2}C$ [5]

From the comparison of the surface area of the bare gold electrode (13 cm^2) and surface area of the PDDA-gold nanorod modified gold electrode (26 cm^2) it was found that due to the gold nanorods the electrode has two times higher surface area compared to the bare gold electrode. This explained the fact that, due to the enhancement of the surface area, rate of ECL reaction increases as the number of active sites increases which also increases the probability of collisions to happen between the reactants. [3]This enhancement in the surface area and the plasmonic enhancement by gold nanorods explains the 12 to 18 times ECL enhancement in case of PDDA, CTAB coated gold nanorod modified gold electrode compared to bare gold electrode in the later part of this discussion.

In the fluorescence experiments, fluorescence intensity was found to be increased 2.8-7.4 times in case of $Ru(bpy)_3Cl_2$ solution in the presence of CTAB coated gold nanorods compared to the $Ru(bpy)_3Cl_2$ solution without gold nanorods. Fluorescence experiments were done for solutions of different concentrations of $Ru(bpy)_3Cl_2$ and it was found that enhancement factor decreases with increasing the concentration of $Ru(bpy)_3Cl_2$ due to the FRET effect [6]. The maximum enhancement was observed for a solution of $Ru(bpy)_3Cl_2$ concentration 2.6×10^{-12} M and 7.4 times fluorescence enhancement was observed for a solution containing $Ru(bpy)_3Cl_2$ and PSS,CTAB coated gold nanorods compared to the fluorescence emission observed for a solution of $Ru(bpy)_3Cl_2$ only. On the other hand, minimum enhancement was observed for a solution of $Ru(bpy)_3Cl_2$ concentration 1×10^{-10} M and 1.6 times fluorescence enhancement was observed for a solution containing $Ru(bpy)_3Cl_2$ and PSS,CTAB coated gold nanorods compared to the fluorescence emission observed for a solution of $Ru(bpy)_3Cl_2$ only. These fluorescence experiments proved the plasmonic enhancement of gold nanorods to increase the ECL efficiency of $Ru(bpy)_3Cl_2$. [7]

2.2 Photolithographic process of cell preparation [8] :

2.2.1 Materials:

1″x3″x1.1 mm gold coated microscopic glass slides were purchased from Deposition research laboratory. The slides were coated with 100 nm thick layer of gold and 5 nm thick layer of chromium. The chemicals used were Sodium carbonate (Na_2CO_3) (ACS reagent $\geq$99.5%, Aldrich Chemical Co.), potassium iodide (KI) (ACS reagent $\geq$99%, Aldrich Chemical Co.), Iodine (I_2) (ACS reagent $\geq$99.8%, Aldrich Chemical Co.), sodium hydroxide (NaOH) (BioXtra $\geq$98%, Aldrich Chemical Co.), Hydrogen per oxide (H_2O_2) (30% stabilized ACS, VWR

Chemicals BDH), Sulphuric acid (H_2SO_4) (Sulphuric acid 95-98% ACS, FCC, VWR Chemicals BDH), Chromium etchant (Aldrich Chemical Co.).

2.2.2 Substrate preparation:

For all ECL experiments, an electrochemical cell was constructed by attaching gold coated glass slide with a glass block. The gold electrode was formed by spin coating a photoresist film on the gold coated glass slide and the photoresist film was exposed to UV irradiation through a mask for 1-2 minutes. Afterwards the gold coated glass slide was immersed in a photographic developing solution of 0.1 M Na_2CO_3. After that, the gold coated glass slides were immersed in gold etching solution which was made by dissolving 4 g KI and 1 g I_2 in 40 mL of deionized water. The chromium adhered to the gold electrode was removed by immersing the slides to chromium etching solution. After that, the gold coated glass slide was immersed in the photoresist removal solution of 0.25 M NaOH. Finally, the electrodes were washed with distilled water, cleaned with Piranha solution [1:3 molar ratio of H_2O_2 and H_2SO_4] to remove all the attached organic materials and dried with nitrogen gas before being used as an electrode in the ECL experiments [8].

2.3 ECL experimental setup:

The ECL experiments were done in a closed bipolar electrochemical circuit. The closed bipolar cell was formed by attaching a glass block with the gold coated glass slide which formed a 3D frame to hold the solution. The bottom part of the glass block was cleaned, and it was bonded to the gold coated glass slides by epoxy. The electrode was cleaned by taking 0.1 M H_2SO_4 and scanning in the cyclic voltammetry from -0.2 to +1.5 V for 30 cycles at the rate of 0.1 V/s. The cell was covered with black tape to prevent any light leaking from the cell. The compartment

of the electrical cell was large enough to minimize ohmic loss and to ensure enough solution for the ECL reaction [9].

2.3.1 Chemicals:

Tris (2,2'-bipyridyl) dichlororuthenium (II) hexahydrate ($Ru(bpy)_3Cl_2$) (99.95% trace metals basis, Aldrich Chemical Co.), Tripropyl amine (≥98%, Aldrich Chemical Co.), sodium phosphate monobasic (NaH_2PO_4) (BioXtra ≥99%, Aldrich Chemical Co.), sodium phosphate dibasic (Na_2HPO_4) (99.95%, Aldrich Chemical Co.), potassium ferricyanide ($K_3Fe(CN)_6$) (ACS reagent ≥99%, Aldrich Chemical Co.), potassium nitrate (KNO_3) (ACS reagent ≥ 99%, Aldrich Chemical Co.), sodium perchlorate ($NaClO_4$) (ACS reagent ≥ 98%, Aldrich Chemical Co.), ethanol (absolute ≥99.5%, GR ACS), acetonitrile (low water content ≥99.5% ACS, VWR Chemicals BDH), tetrabutyl ammonium perchlorate (≥99%, Aldrich Chemical Co.), Ferrocenemethanol (≥99%, Stream Chemicals Inc.) etc.

2.3.2 Procedure:

The ECL experiment was done in a closed bipolar cell having 5 mM $Ru(bpy)_3^{2+}$, 25 mM TPA and 0.1 M phosphate buffer solution in the reporting compartment [9] and 5 mM $K_3Fe(CN)_6$, 0.1 M KNO_3 in the sensing compartment [2]. When the bipolar electrode is open, current can pass through both the solution and the electrode as both the driving and bipolar electrodes are immersed in the same solution in the open bipolar electrode system. On the other hand, in closed bipolar electrode the cathode and anode of the cell are immersed in two different solutions and the current can pass through the bipolar electrode while the ions pass through the solution.[10] The ECL was observed at the anodic part of the bipolar electrode when potential was applied from the power supply. The power supply was connected to the regular electrode which formed cathode and anode at the regular electrode and oppositely charged bipolar electrode system.

77
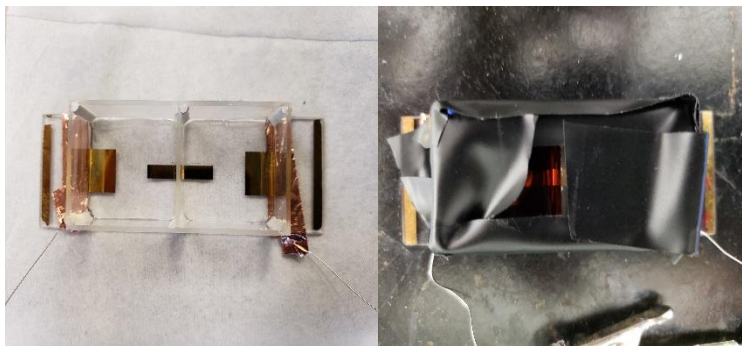
Figure 2. 1 Closed bipolar electrode system for ECL measurement

Figure 2. 2 ECL observed at closed bipolar electrode system

The ECL produced by bare gold electrode and modified gold electrode were compared. The ECL was detected by a Nikon charge coupled device (CCD) camera at a focal length of 11, ISO 3200 and the exposure time was 5 seconds. The operation of the CCD camera was based on averaging intensities coming from each point of the image that was focused. To reduce any background current the pictures were taken 10 seconds after switching on the current.[11] The ECL intensity was analyzed by Image J software from the images taken at different applied voltages. The data were processed by Microsoft excel, Graphpad Prism and Origin 2020 software.

2.3.3 ECL experiment with non-aqueous solution:

In most of the ECL system, aqueous solution has been used. In this aqueous solution based ECL system, oxygen has been produced by the following reaction

$Ru(bpy)_3^{3+} + OH^- \rightarrow Ru(bpy)_3^{2+} + \frac{1}{4} O_2 + \frac{1}{2}H_2O$ [12]
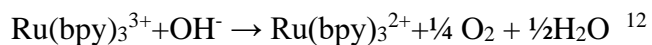
Oxygen has the tendency to quench the ECL system, so lower ECL efficiency was found from the aqueous ECL system [12]. So, as an alternative to aqueous ECL system, which is non-aqueous ECL system was tried to get a higher efficiency of the ECL using tripropyl amine as a coreactant.

$Ru(bpy)_3Cl_2$ does not dissolve in organic solvent. So, to work with non-aqueous solvent $Ru(bpy)_3(ClO_4)_2$ was synthesized. In 1:1 mixture of ethanol and water, by the metathesis reaction of $Ru(bpy)_3Cl_2$ with excess $NaClO_4$, $Ru(bpy)_3(ClO_4)_2$ was formed. Recrystallization of the formed product was done four times in a 1:1 mixture of ethanol: water to purify the $Ru(bpy)_3(ClO_4)_2$. [2]

For working with the aqueous solution 10 mM $K_4Fe(CN)_6$ and 0.1 M KNO_3 aqueous solution was used in the sensing compartment and 5 mM $Ru(bpy)_3Cl_2$, 25 mM Tripropyl amine and 0.1 M PBS buffer was used in the reporting compartment. ECL found from this aqueous solution based closed bipolar cell was compared with that of non-aqueous ECL solution based closed bipolar cell where 10 mM Ferrocene-methanol, 0.1 M Tetrabutyl ammonium perchlorate dissolved in acetonitrile was used in the reporting compartment and 5 mM $Ru(bpy)_3(ClO_4)_2$, 25 mM Tripropyl amine and 0.1 M Tetra butyl ammonium perchlorate dissolved in acetonitrile was used in the sensing compartment.

Comparison of ECL in the aqueous and non aqueous ECL system
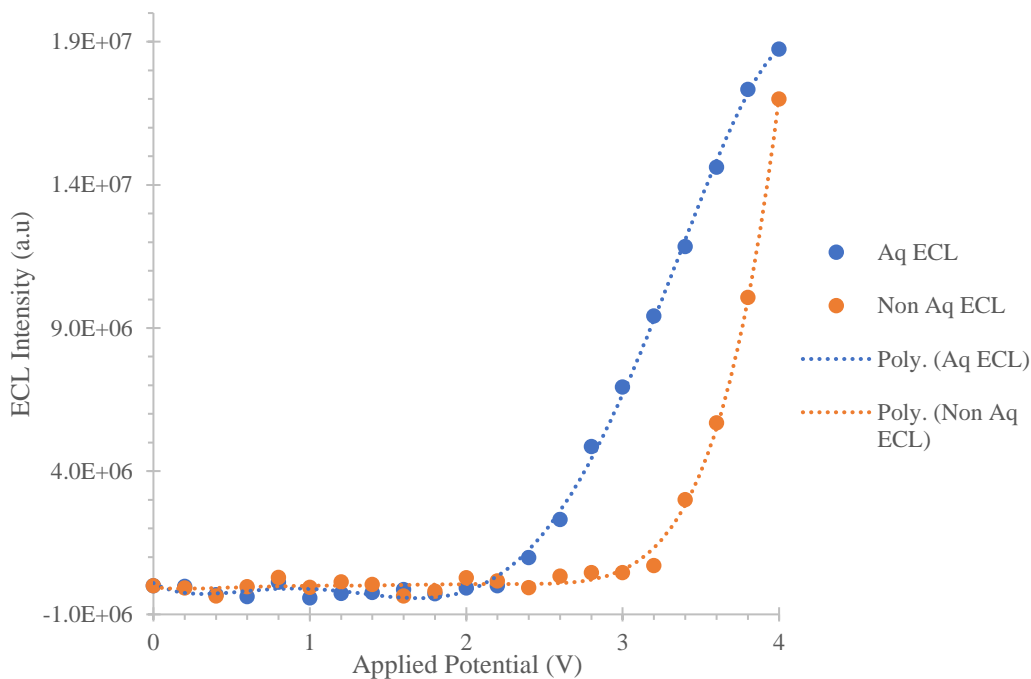
Figure 2. 3 Comparison of ECL curves from aqueous solution of $Ru(bpy)_3Cl_2$ and non-aqueous solution of $Ru(bpy)_3(ClO_4)_2$ in closed bipolar cell

In the figure 2.3 from the comparison of onset potential and slope of the curves it can be found that at least two times enhancement of ECL was found from non-aqueous ECL solution of $Ru(bpy)_3(ClO_4)_2$ in acetonitrile relative to aqueous ECL solution of $Ru(bpy)_3Cl_2$ in water.

Due to the difference in diffusion co-efficient in different solvents [13], onset potential was different in case of aqueous and non-aqueous ECL solutions. Again, with the decrease of dielectric constant from water (78.54) [14] to acetonitrile (36.64) [14], the reorganization energy decreased which facilitated rate of electron transfer causing ECL to increase in case of non-aqueous ECL solution compared to aqueous ECL solution. [13]

2.4 ECL enhancement of Ru(bpy)₃Cl₂ by the surface plasmon resonance effect of gold nanorods:

To increase the ECL efficiency of Ru(bpy)₃Cl₂, the gold electrode was modified with CTAB coated gold nanorods by different types of self-assembled monolayer system [4]. Gold nanorods has emission band which can overlap effectively with the absorption band of $Ru(bpy)_3^{2+}$, which is the condition for showing surface plasmon resonance [4]. So, gold nanorod of aspect ratio 2.6 was synthesized based on the work of Catherine J.Murphy *et.al* [15]. For the synthesis of gold nanorod a concentration of 0.1 M CTAB was used. This concentration is much higher than the critical micelle concentration of gold nanorod which is 1 mM in water, so centrifugation was done three times to reduce the concentration of CTAB to 0.01 mM [6] and a concentration of CTAB higher than 1 mM causes aggregation [16].

2.4.1 Gold nanorod synthesis:

2.4.1.1 Chemicals:

Chloroauric acid (HAuCl₄) (99.995% trace metal basis, Aldrich Chemical Co.), sodium borohydride (NaBH₄) (≥98%, Across Organics MS), hexadecyltrimethylammonium bromide (CH₃(CH₂)₁₅N(Br)(CH₃)₃) (≥98%, Aldrich Chemical Co.), silver nitrate (AgNO₃) (ACS reagent ≥99.8%, Aldrich Chemical Co.), ascorbic acid (99%, Aldrich Chemical Co.), hydrochloric acid (36.5-38.0% ACS, VWR Chemicals BDH). The solutions were prepared by Millipure-Q deionized water.

2.4.1.2 Apparatus used:

The gold nanorods formed was centrifuged out of the solution by Eppendorf centrifuge 5424 which has a maximum capacity of 24x2 mL, and which can rotate at a maximum speed of 21130 x g or 15000 rpm. Temperature range of the centrifuge machine was -10⁰C to 40⁰C.

The synthesized gold nanorod was characterized by Agilent Cary 8454 UV-Vis Diode Array UV-Visible spectrophotometer which has deuterium discharge lamp as a source to produce spectrum at the UV range and tungsten lamp as a source to produce spectrum at the visible range. The spectrophotometer had a wavelength range of 190-1100 nm with the sample interval of 0.9 nm.

2.4.1.3 Precautions:

For the synthesis of gold nanorods, each of the apparatus was cleaned by soap and then with water. After that the apparatus was put in the aqua regia solution. Again, the apparatus was washed with water, after that with nanopure water and dried at room temperature. Vials having metallic caps was not used to avoid contamination. The solutions were prepared in dark beaker to avoid light. Plastic spatula was used to take the silver salt, to avoid contamination from the metal. The hygroscopic $NaBH_4$ and $HAuCl_4$ was weighed as fast as possible to avoid contamination by moisture of the air. The vials of the samples were covered with aluminum foil and the samples were kept in the dark so that photooxidation of the sample could not occur [17].

2.4.1.4 Procedure:

For synthesizing gold nanorods, 0.01 M 0.25 mL $HAuCl_4.3H_2O$ solution was added to 0.10 M 9.75 mL CTAB solution, 0.01 M 0.60 mL $NaBH_4$ solution was prepared freshly by ice-cold water and was stirred so fast. The solution was converted from yellow to yellowish brown. The solution was kept unmoved for 1.5 hr. at 27^0C after stirring rapidly for 10 minutes, seed solution was formed. [15]

0.01M 0.030 mL of $AgNO_3$, 0.01 M 0.50 mL of $HAuCl_4.3H_2O$, 0.10 M 8.0 mL of CTAB solutions were mixed. 0.2 mL 1.0 M HCL, 80 µL 0.1 M ascorbic acid, 2.0 mL seed solution were added to the mixture. The mixture was kept unmoved for 16-20 hours at 27^0C temperature. After that, the mixture was centrifuged three times in a centrifugation machine at a

rotating speed of 16000 g for 35 minutes. After each centrifugation step, precipitate was

collected, and ultrapure water was added to the precipitate to remove any excess CTAB in the

gold nanorods. After the centrifugation steps were done, gold nanorods precipitates were

collected and dispersed in 3.0 mL ultrapure water [7].

2.4 Characterization of gold nanorods
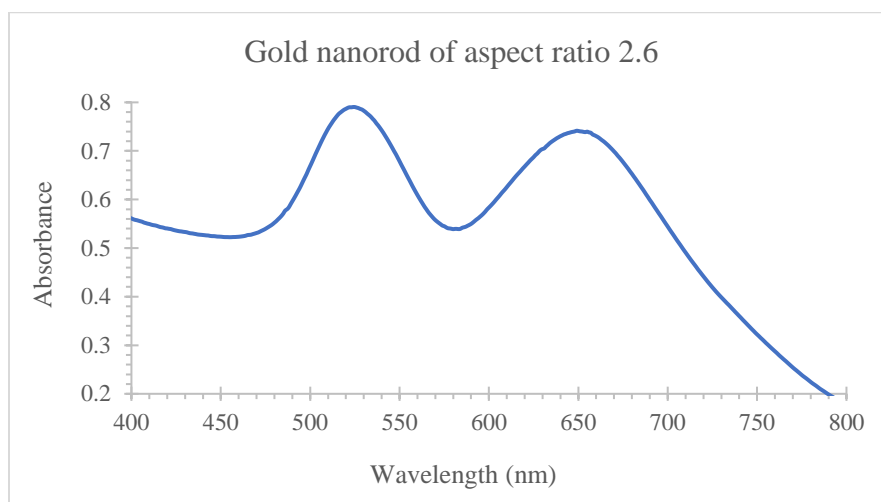
Figure 2. 4 Gold nanorods having longitudinal plasmon band at 650 nm

Based on the TEM experiment, it was also found that the synthesized gold nanorod

had an aspect ratio of 2.6 by measuring the length and width of the nanorod of the TEM image by

using ImageJ software. The concentration of the gold nanorod formed was 4.1×10^{-9} M which was

calculated from the width, length and the number of gold nanorods formed in the growth solution

used. For practical uses, gold nanorod solution was diluted 10^8 times during cleaning of the gold

nanorod by centrifugation.
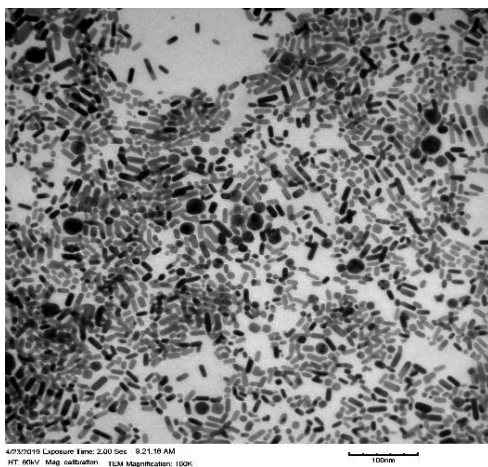
Figure 2. 5 TEM image of gold nanorods
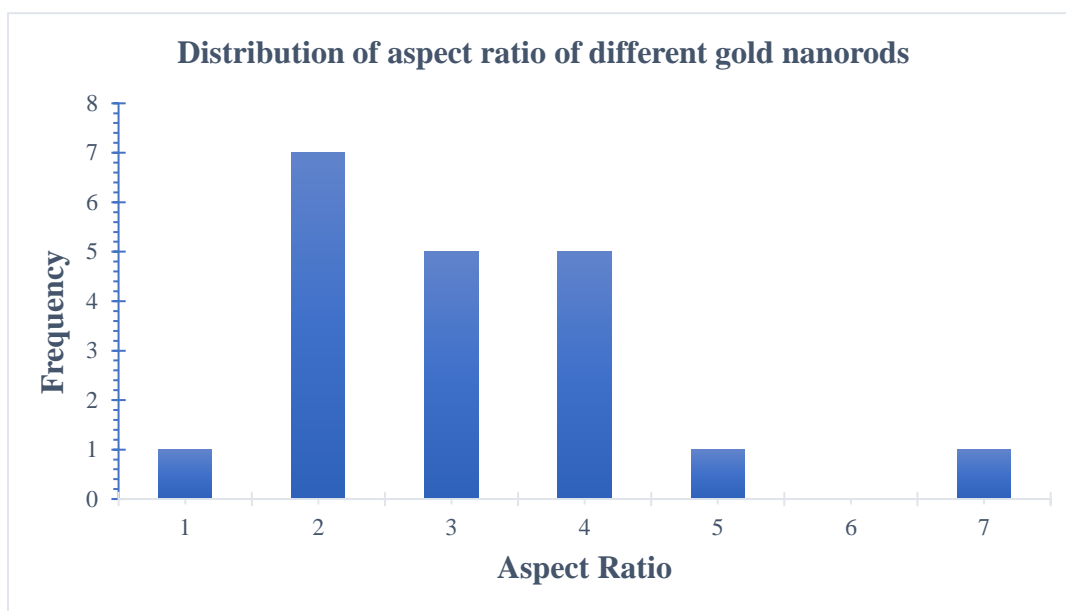
Figure 2. 6 Histogram showing distribution of aspect ratios of different gold nanorods

2.5 Gold nanoparticle synthesis:

Gold nanoparticles were also synthesized based on the procedure described in Catherine J.Murphy *et al.*[15]. Since the concentration of $AgNO_3$ was the key factor which determined the aspect ratio of gold nanorods, it was not added in the synthesis of gold

nanoparticles. The produced gold nanoparticles showed its characteristic transverse mode peak

near at 520 nm which proved that the synthesis was successfully completed.

Gold nanoparticles
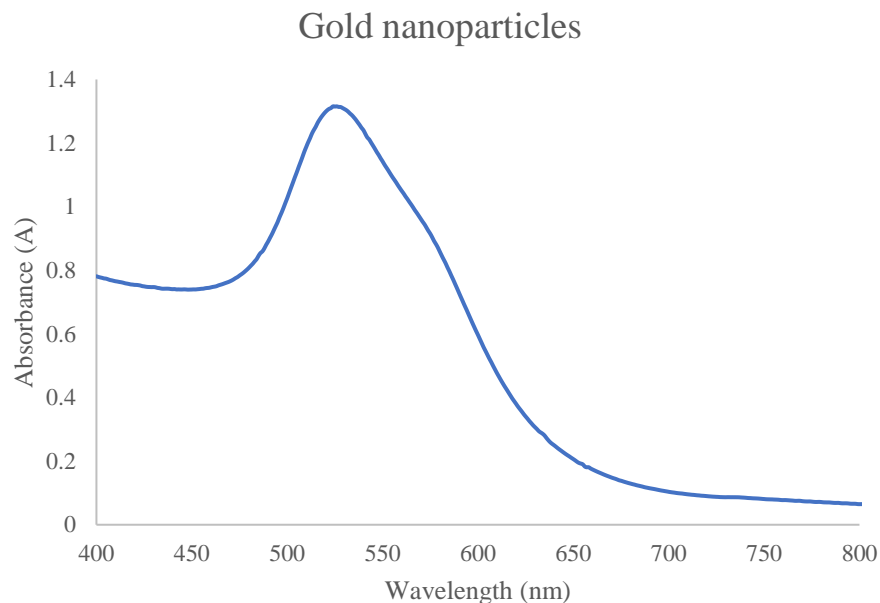
Figure 2. 7 UV-Visible spectrum of gold nanoparticles

2.6 Measurement of surface area:

2.6.1 Chemicals used:

Potassium ferricyanide ($K_3Fe(CN)_6$) (ACS reagent $\geq$99%, Aldrich Chemical

Co.), Potassium chloride (KCl) (ACS reagent, 99-100.5%, Aldrich Chemical Co.), Poly

(diallyldimethylammonium chloride) (20 wt.% in H_2O, Aldrich Chemical Co.). All the solutions

were prepared by nanopure water.

2.6.2 Procedure:

The solution used for doing the CV was 1.0 mM $K_3Fe(CN)_6$ and 0.5 M KCl in

water. For both bare gold and PDDA-gold nanorod modified gold electrode CV measurements

were done by measuring current at different scan rate for the potential range of 0 to 500 mV. In

85

these analysis, bipolar electrode was used as the working electrode, Ag/AgCl was used as the reference electrode and platinum electrode was used as the counter electrode.

From the slope of the graph, oxidation peak current vs √Scan rate, electrochemically active surface area of the electrode was calculated based on the equation

$I_p = 0.4463nF(nF/RT)^{1/2} AD^{1/2}v^{1/2}C$ [5]

From the comparison of the surface area of the bare gold electrode (13 cm^2) and surface area of the PDDA-gold nanorod modified gold electrode (26 cm^2) it was found that due to the gold nanorods the electrode has two times higher surface area compared to the bare gold electrode.

2.6.2.1 Cyclic voltammetric analysis for a bare gold electrode:

Cyclic voltammetric analysis was done on the electrochemical cell containing the bare gold electrode. The oxidation peak current were analyzed for different scan rates in the solution of 1.0 mM K$_3$Fe(CN)$_6$ mixed with 0.5 M KCl in water.
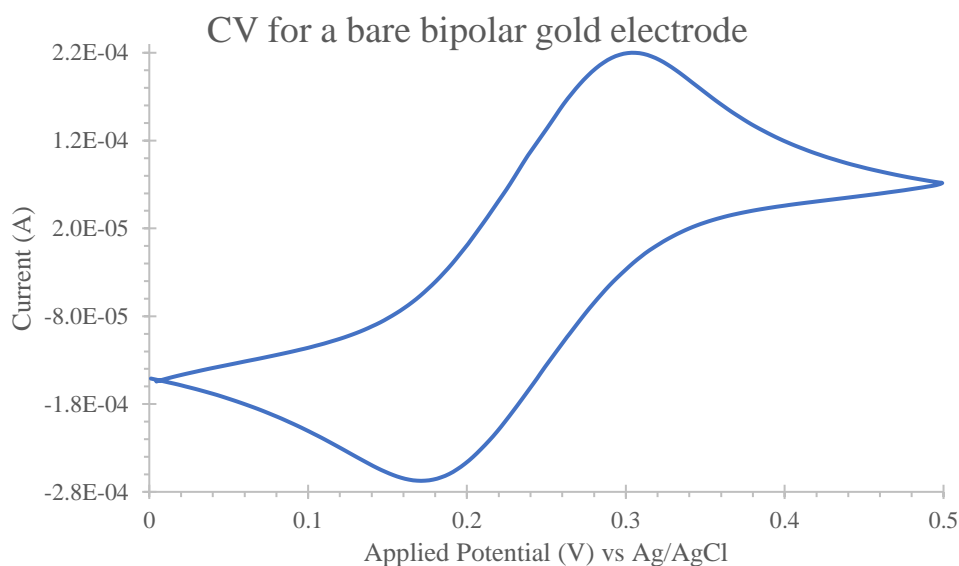
Figure 2. 8 Cyclic voltammogram for a bare bipolar gold electrode at a scan rate of 50 mV/s for a solution of K$_3$Fe(CN)$_6$ and KCl in water

Here, in the graph 2.8, the large separation of the oxidation and reduction peak was possibly due to uncompensated resistance which is known as the ohmic drop. [18]. The oxidative peak current produced due to the cyclic voltammetric analysis by changing scan rates were plotted. From the slope of the graph, oxidation peak current vs √Scan rate, electrochemically active surface area of the electrode was calculated based on the equation

$I_p = 0.4463nF(nF/RT)^{1/2} AD^{1/2}v^{1/2}C$ ……..(1)   [5]
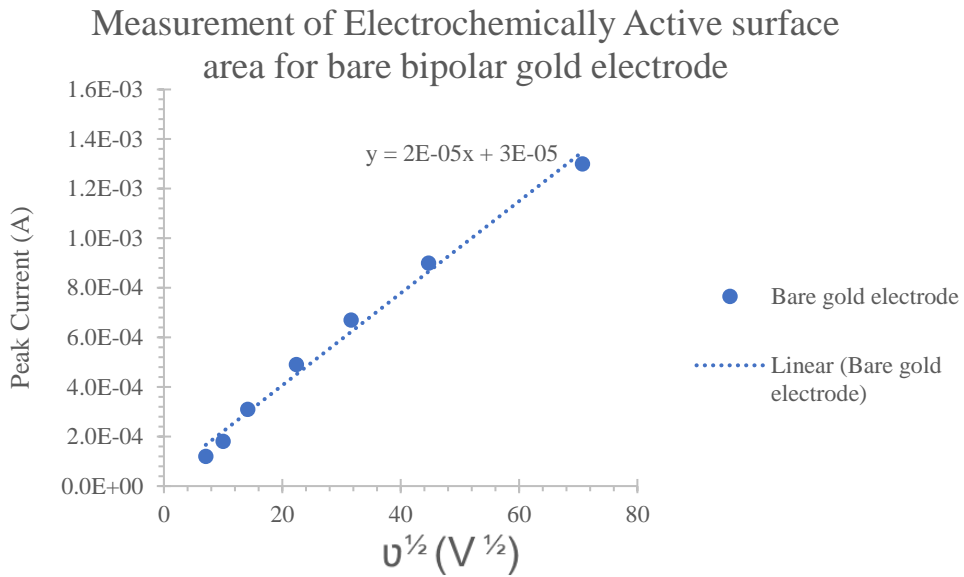
Figure 2. 9 Measurement of surface area for a bare bipolar gold electrode

From the slope of this graph, the electrochemically active surface area of the bare gold electrode was calculated as here D has a value of 7.6×10^{-6} cm^2s^{-1} [19] which is for the diffusion co-efficient of $K_3Fe(CN)_6$, C is the concentration (mol cm^{-3}) of $K_3Fe(CN)_6$ and the rest of the symbols have meaning of their own. This gave the value for the electrochemically active surface area of the bare gold electrode, which is 0.13 cm^2, whether the geometric surface area of bare gold electrode was 0.27 cm^2. Due to the ohmic drop, there is large difference between the geometric surface area and electrochemically active surface area. [18]

2.6.2.2 Cyclic voltammetric analysis for a modified gold electrode:

Cyclic voltametric analysis was also done on the electrochemical cell containing the PDDA, CTAB coated gold nanorods modified gold electrode. The oxidation peak current was analyzed for different scan rates in the solution of 1.0 mM $K_3Fe(CN)_6$ mixed with 0.5 M KCl in water.
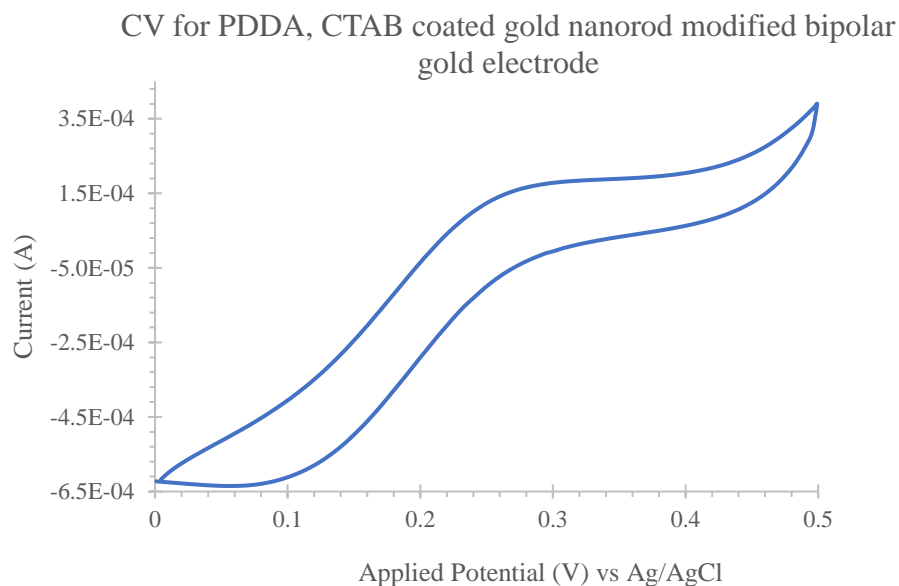
Figure 2. 10 Cyclic voltammogram of PDDA, CTAB coated gold nanorod modified bipolar gold electrode at a scan rate of 50 mV/s for a solution of $K_3Fe(CN)_6$ and KCl in water

For PDDA, CTAB gold nanorod coated modified gold electrode the oxidative peak current produced due to the cyclic voltammetric analysis by changing scan rates were plotted. Here, due to the increase of resistivity by applying PDDA, CTAB coated gold nanorods separation of the oxidation, reduction peak increased further compared to the bare gold electrode as it was difficult now for $Fe(CN)_6^{3-}$ to penetrate the PDDA, CTAB coated gold nanorod layer and reach the bare gold electrode surface. [20] From the slope of the graph, oxidation peak current vs √Scan rate, electrochemically active surface area of the electrode was calculated based on the equation

$I_p = 0.4463nF(nF/RT)^{1/2} AD^{1/2}v^{1/2}C$ ……..(1) [5]

Here, due to some surface blocking effect of the PDDA, CTAB irreversibility was

observed in the CV. [18]

Measurement of electrochemically active surface area for PDDA, CTAB coated gold nanorod modified bipolar gold electrode
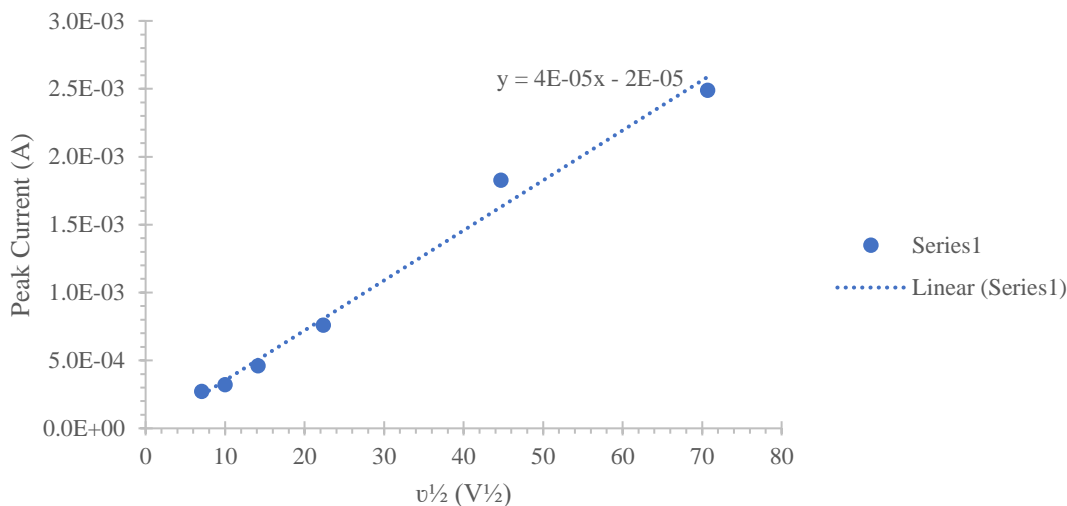
Figure 2. 11 Measurement of electrochemically active surface area for a PDDA, CTAB coated gold nanorod modified bipolar gold electrode

From the slope of this graph, the electrochemically active surface area of the

PDDA, CTAB coated gold nanorod modified gold electrode was calculated, as here D has a value

of 7.6×10^{-6} cm^2s^{-1} [19] which is for the diffusion co-efficient of $K_3Fe(CN)_6$, C is the concentration

(mol cm^{-3}) of $K_3Fe(CN)_6$ and the rest of the symbols have meaning of their own. This gave the

value for the electrochemically active surface area of the modified electrode, which is 0.26 cm^2,

whether the geometric surface area of bare gold electrode was 0.27 cm^2.

So, from the cyclic voltammetric analysis it was observed that, in the presence of gold

nanorod, the electrochemically active surface area increased twice compared to that of the bare

gold electrode which explains the ECL enhancement in the presence of CTAB coated gold

nanorods. The ECL enhancement was up to 12-17 times upon applying gold nanorod on gold electrode due to both plasmonic enhancement and the increase of reaction rate by increasing the surface area. [3]

2.7 Observation of surface plasmon resonance enhancement of ECL by gold nanorods:

2.7.1 Comparison of ECL experiments from bare gold electrode; PDDA, CTAB coated gold nanorod modified gold electrode and PDDA, CTAB coated gold nanoparticles modified gold electrode:

ECL experiments were done by modifying the gold electrode with PDDA, gold nanorods and PDDA, gold nanoparticles. It was found that ECL intensity observed when gold electrode was modified with PDDA, gold nanorods was higher compared to the other modified electrode and bare gold electrode. The result was due to the surface plasmon resonance of gold nanorods [4] and also due to the increase of ECL reaction rate by the increase of the surface area by applying PDDA, CTAB coated gold nanorods on gold electrode. The enhancement of the ECL was also found for the electrode modified with PDDA, CTAB coated gold nanoparticles compared to that of the bare gold electrode. This enhancement was probably due to the increase of surface area in case of gold nanoparticles causing rate of ECL reaction to increase which eventually increases ECL intensity.

90

Comparison of ECL from different modified electrode
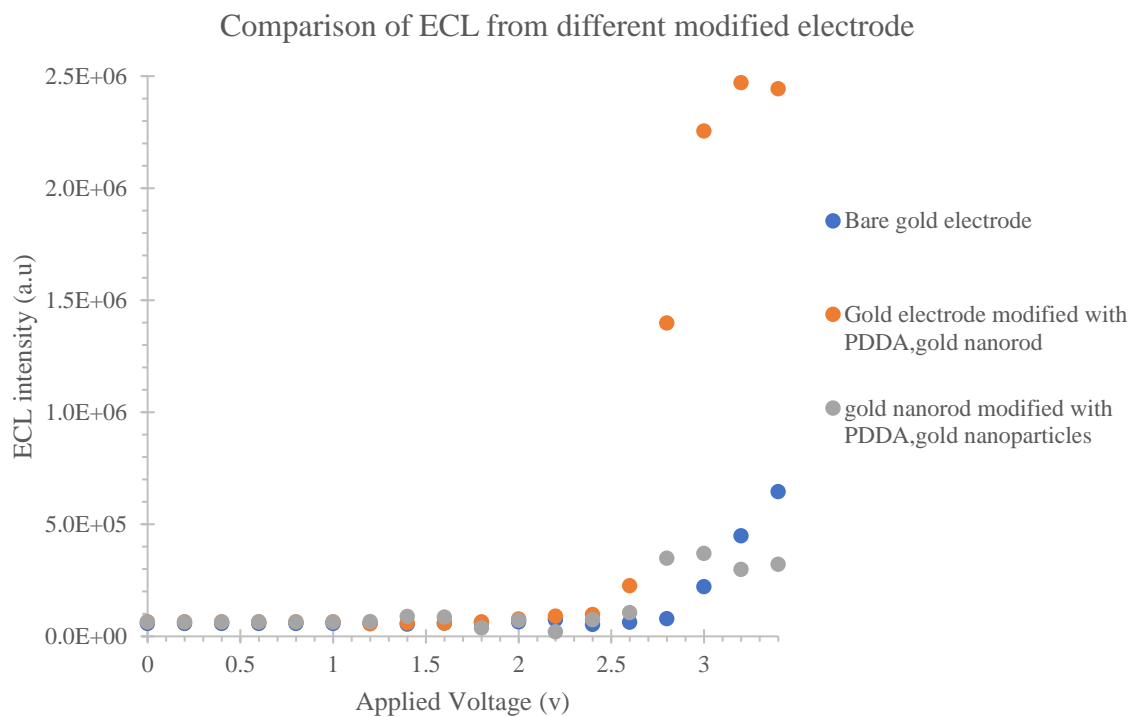
Figure 2. 12 ECL data at different modified and bare gold electrodes

Table 2. 1 Comparison of ECL curves

Types of electrodes showing the ECL curves and on which ECL experiments were done for the ECL solution of Ru(bpy)$_3$Cl$_2$	ECL intensity (a.u)	Area under the curve compared with bare gold electrode
Area under the curve for Bare Gold electrode in the potential range from 2.8V-3.4V	6.8×10^5	1
Area under the curve for Gold electrode modified with PDDA, gold nanoparticles in the potential range of 2.6V-3.4 V	6.7×10^6	10
Area under the curve for Gold electrode modified with PDDA, gold nanorods in the potential range of 2.4V-3.4 V	1.1×10^7 a.u	17

The increase of ECL intensity in case of PDDA, CTAB coated gold nanoparticle modified gold electrode was probably due to rate of increase of the ECL reaction by the increase of surface area by applying PDDA, CTAB coated gold nanoparticles on gold electrode. These observations proved that surface plasmon resonance effect and rate of increase of the ECL reaction by the increase of surface area upon applying PDDA, CTAB coated gold nanorod were responsible for the ECL enhancement to occur [3]. Here with respect to two times increment of the surface area seventeen times enhancement of ECL was observed in case of PDDA, CTAB coated modified gold electrode compared to bare gold electrode.

2.7.2 Comparison of ECL experiments from bare gold electrode; CTAB coated gold nanorod modified gold electrode; PDDA modified gold electrode and PDDA, CTAB coated gold nanorod modified gold electrode:

In the graph 2.13, it was observed that when gold electrode was modified with PDDA first, after that with CTAB capped gold nanorods, then the ECL intensity observed was even higher. This result was possibly due to increase of concentration of the gold nanorods in the surface of gold as PDDA which worked as a binder used to bind more gold nanorods onto the surface, increasing the surface area twice compared to that of the bare gold electrode as was observed in cyclic voltammetric experiments. However, when gold electrode was modified with CTAB coated gold nanorod without the PDDA, the ECL observed was still higher compared to the bare gold electrode, due to the surface plasmon resonance effect and also due to the increase of ECL intensity upon increasing the ECL reaction rate as a result of increase of surface area by gold nanorods, but less than the one electrode which was modified with PDDA, gold nanorod probably due to the lesser density of the gold nanorod attached to the gold electrode without the

PDDA. Electrode modified with PDDA showed a much weaker ECL due to the surface blocking

tendency of the PDDA causing reduction of the surface area.
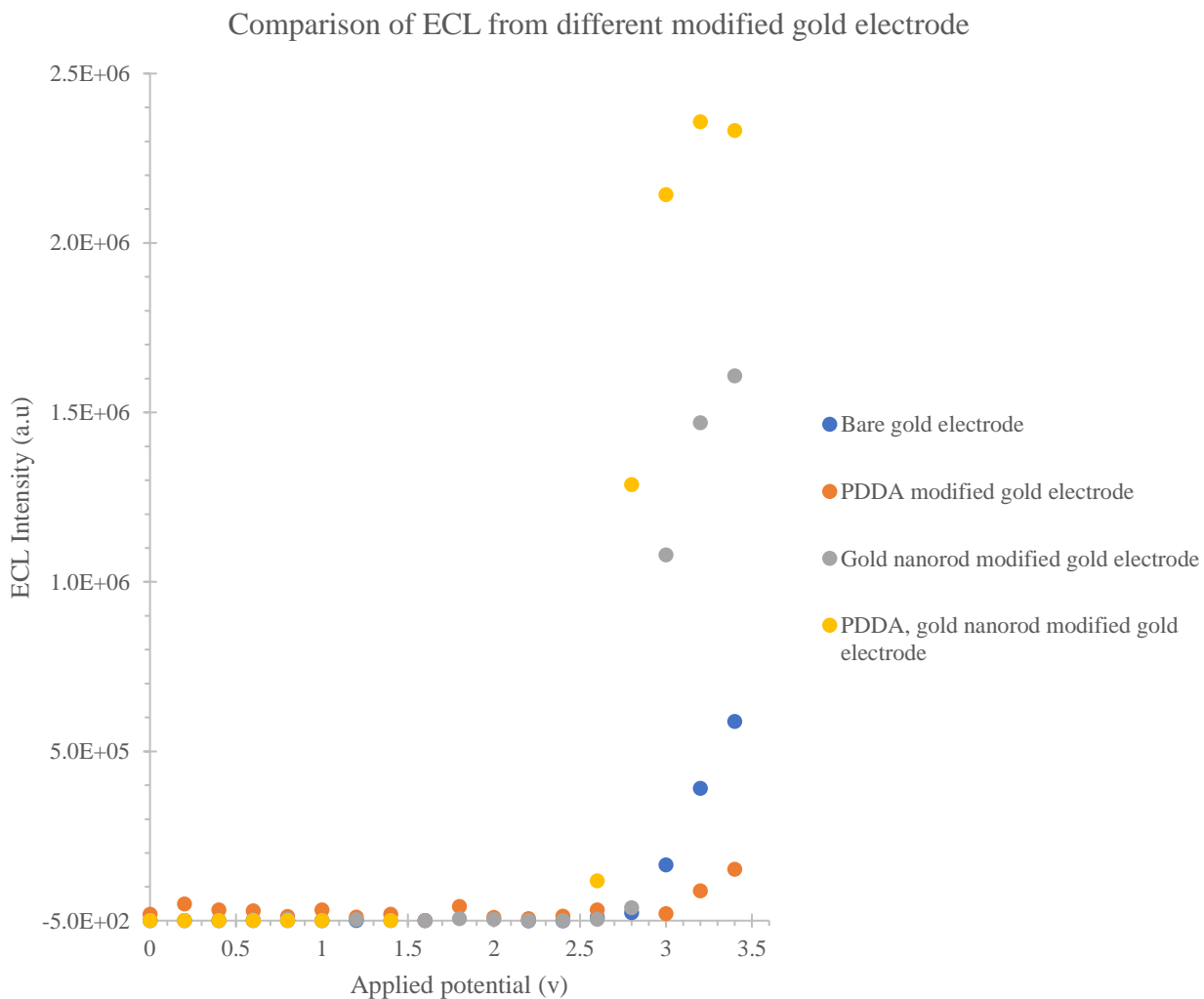
Figure 2. 13 Comparison of ECL enhancement at different modified gold electrodes

Table 2. 2 Comparison of the ECL from different modified electrode

Types of electrodes showing the ECL curves and on which ECL experiments were done for the ECL solution of Ru(bpy)$_3$Cl$_2$	ECL intensity (a.u)	Area under the curve compared with the gold electrode

Area under the curve for Bare gold electrode in the potential range of 2.8V-3.4 V	8.0×10^4	1.0
Area under the curve for Electrode modified with PDDA in the potential range of 3.0 V-3.4V	1.8×10^4	2.2×10^{-1}
Area under the curve for Electrode modified with gold nanorods in the potential range of 2.8 V-3.4 V	4.1×10^5	5.2
Area under the curve for Electrode modified with PDDA, gold nanorods in the potential range of 2.0 V-3.4 V	1.0×10^6	12

These observations proved that surface plasmon resonance effect and rate of increase of the ECL reaction by the increase of surface area by applying PDDA, CTAB coated gold nanorod on gold electrode were responsible for the ECL enhancement [3]. Here with respect to two times increment of the surface area twelve times enhancement of ECL was observed in case of PDDA, CTAB coated modified gold electrode compared to bare gold electrode.

2.7.3 Comparison of ECL experiments from bare gold electrode; CTAB coated gold nanorod modified gold electrode; PDDA modified gold electrode and PDDA, CTAB coated gold nanorod modified gold electrode:

In the graph 2.14 it was shown that, Gold electrode was also modified with PDDA and different volumes of gold nanorod solution and it was found that ECL intensity was larger in case of gold electrode modified with PDDA and gold nanorod solution of different concentrations due to surface plasmon resonance effect and increase of ECL reaction rate by increase of surface area by applying PDDA,CTAB coated gold nanorods on gold electrode. However, the variation of volumes of gold nanorod solution did not change the ECL intensity that much. Gold electrode was

also modified with CTAB solution and it was found that ECL intensity decreased profoundly compared to the bare gold electrode, signifying the fact that CTAB has a surface blocking effect.
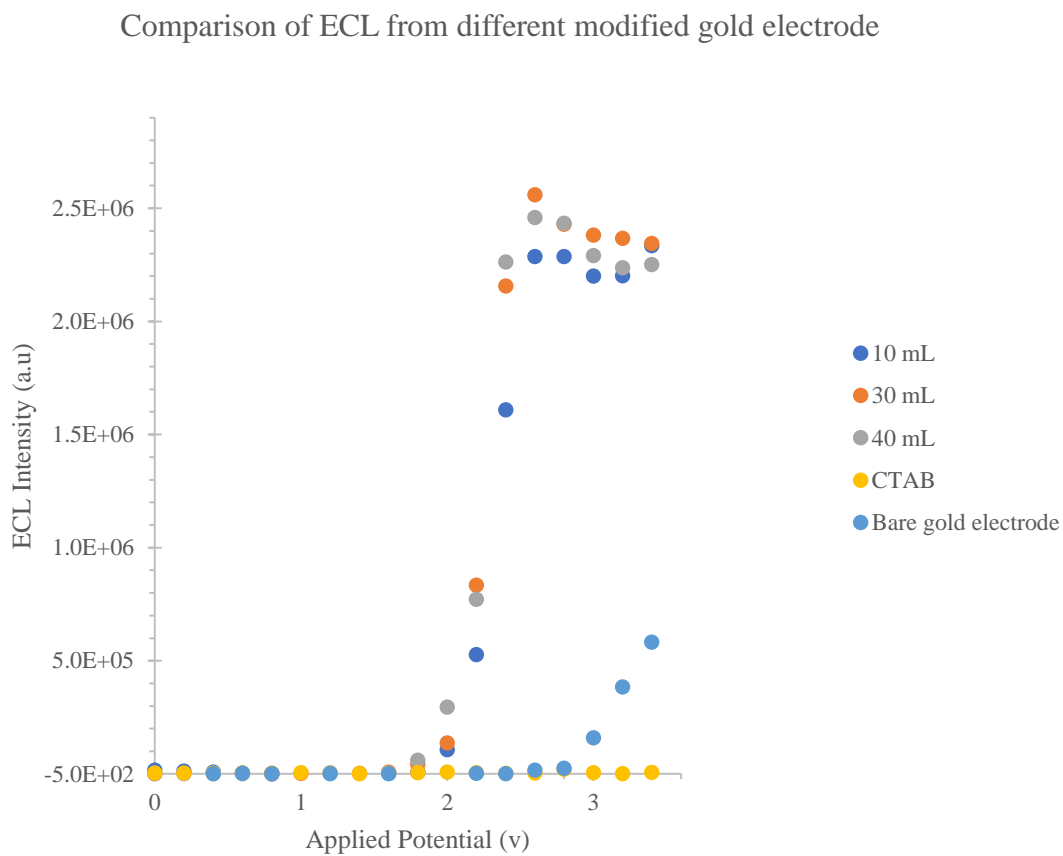
Figure 2. 14 Comparison of ECL in different modified gold electrode with different volumes of gold nanorods

Table 2. 3 Comparison of the ECL from different modified electrode

Types of Electrodes showing the ECL curves and on which ECL experiments were done for the ECL solution of $Ru(bpy)_3Cl_2$	ECL intensity (a.u)	Area under the curve compared with bare gold electrode
Area under the curve for Bare gold electrode in the potential range 2.8V-3.4 V	$1.3x10^5$	1
Area under the curve for Gold electrode modified with CTAB in the potential range 2.8V-3.4 V	$3.1x10^4$	$2.4x10^{-1}$
Area under the curve for Gold electrode modified with 10 µL gold nanorods in the potential range 1.8V-3.4V	$2.1x10^6$	7.0
Area under the curve for Gold electrode modified with 30 µL gold nanorods in the potential range 1.8V-3.4V	$2.4x10^6$	18
Area under the curve for Gold electrode modified with 40 µL gold nanorods in the potential range 1.8V-3.4 V	$2.3x10^6$	18

These observations proved that surface plasmon resonance effect and rate of increase of the ECL reaction by the increase of surface area upon applying PDDA, CTAB coated gold nanorod were responsible for the ECL enhancement to occur.[3] Here with respect to two times increment of the surface area, eighteen times enhancement of ECL was observed in case of PDDA, CTAB coated gold nanorod modified gold electrode compared to bare gold electrode.

2.7.4 Comparison of ECL experiments from bare gold electrode; PDDA, CTAB coated gold nanorod modified gold electrode; PDDA modified gold electrode and from solution of Ru(bpy)$_3$Cl$_2$ mixed with CTAB coated gold nanorods on bare gold electrode:

In the graph of 2.15, the effect of gold nanorod suspended into the Ru(bpy)$_3$Cl$_2$ solution was analyzed and a higher ECL intensity was found compared to the bare gold electrode. But, as the gold nanorods were suspended in solution, there were inhomogeneity in distance between gold nanorod molecules and Ru(bpy)$_3$Cl$_2$ which resulted in a decrease in ECL intensity compared to that of the Ru(bpy)$_3$Cl$_2$ molecules staying at a fixed distance from the gold nanorods. The electrode, which was modified with PDDA, did not show much ECL intensity which signified the fact that ECL was inhibited by the surface blocking tendency of PDDA.
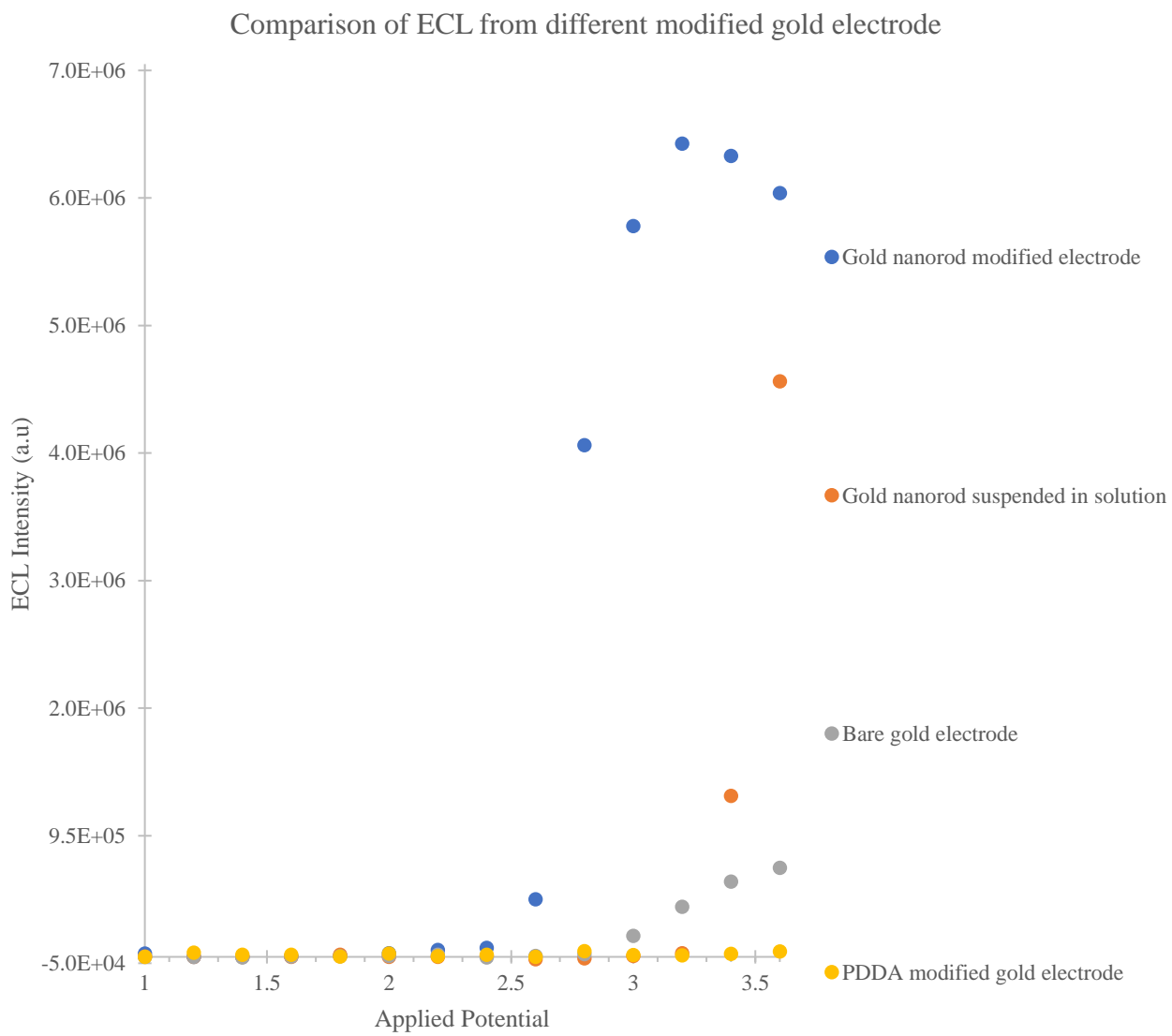
Figure 2. 15 Comparison of different modified gold electrodes

Table 2. 4 Comparison of the ECL intensity for different modified electrodes

Types of electrode showing ECL curves and on which ECL experiments were done for the ECL solution of Ru(bpy)$_3$Cl$_2$	Area under the curve	Area under the curve compared to the area under the curve of bare gold electrode
Area under the curve for Bare gold electrode in the potential range of 2.8V-3.6V	3×10^5 a.u	1.0
Area under the curve for PDDA, gold nanorod modified electrode in the potential range of 2.2V-3.6V	5×10^6 a.u	1.7
Area under the curve for Gold nanorod suspended in solution in the potential range of 3.0V-3.6V	7.1×10^5 a.u	2.3
Area under the curve for PDDA modified electrode in the potential range of 2.8 V-3.6 V	4.6×10^4 a.u	0.15

These observations proved that surface plasmon resonance effect and rate of increase of the ECL reaction by the increase of surface area by applying PDDA, CTAB coated gold nanorod were responsible for the ECL enhancement to occur [3]. Here with respect to two times increment of the surface area seventeen times enhancement of ECL was observed in case of PDDA, CTAB coated gold nanorod modified gold electrode compared to bare gold electrode.

2.7.5 Comparison of ECL experiments from bare gold electrode and cystein, CTAB coated gold nanorod modified gold electrode:

The other type of self-assembled monolayer, for example self-assembled monolayer of cysteine was also tested to see the ECL enhancement upon modification of the gold electrode with CTAB coated gold nanorods. 0.1M cysteine solution was prepared in PBS buffer solution.

The cysteine solution was added on top of the electrode and the electrode was kept in dark along with the cysteine solution, which allowed the self-assembled monolayer of cysteine to form on gold electrode. 25 µL gold nanorod was added on top of the modified electrode and the electrode was kept in dark for four hours which initiated the bonding of cysteine with the gold nanorod [21]. In case of cysteine modified gold electrode, much lower enhancement factor compared to that of the PDDA modified electrode was observed as shown in the graph of 2.16. This was probably, the result of different tunneling co-efficient of different types of self-assembled monolayer systems [22].

Comparison of ECL of a bare gold and cystein-gold nanorod modified gold electrode at pH=7.4
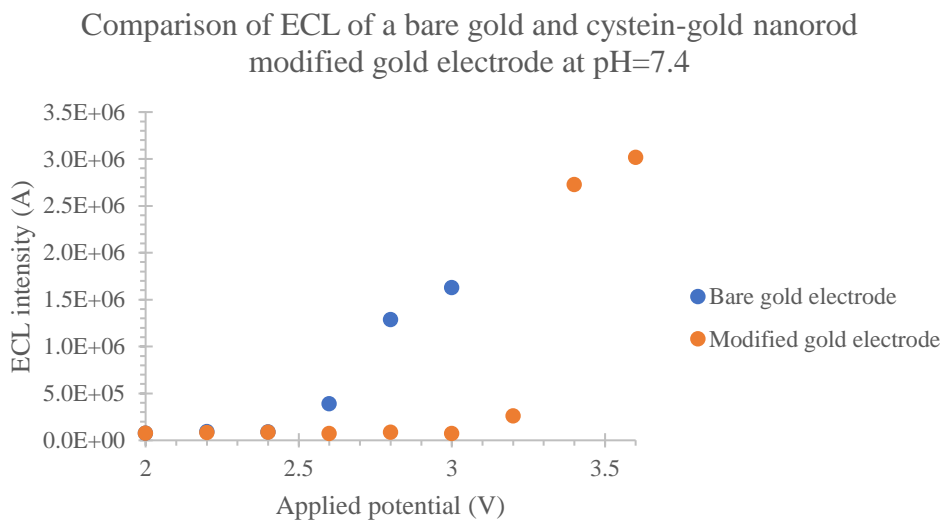
Figure 2. 16 Comparison of ECL curve of bare gold electrode and cysteine, gold nanorod modified electrode

Table 2. 5 Comparison of the ECL intensity for different modified electrode

Types of electrode showing ECL curves and on which ECL experiments were done for the ECL solution of $Ru(bpy)_3Cl_2$	ECL Intensity (a.u)	Area under the curve compared to the area under the curve of bare gold electrode
Area under the curve for Bare gold electrode in the potential range 2.4V-3.0V	5.4×10^5 a.u	1.0

Area under the curve for Cystein, gold nanorod modified electrode in the potential range 3.0V-3.6V	9.9×10^5 a.u	1.8

These observations proved that surface plasmon resonance effect and rate of increase of the ECL reaction by the increase of surface area by applying PDDA, CTAB coated gold nanorod were responsible for the ECL enhancement to occur [3]. Here with respect to two times increment of the surface area 1.8 times enhancement of ECL was observed in case of PDDA, CTAB coated gold nanorod modified gold electrode compared to bare gold electrode.

2.7.6 Summary of the ECL experiments:

From the ECL experiments it was observed that when gold electrode was modified with PDDA, CTAB coated gold nanorods twelve to eighteen times enhancement of the ECL was observed compared to the bare gold electrode for the ECL solution of $Ru(bpy)_3Cl_2$ in water mainly due to plasmonic enhancement of ECL by gold nanorods and also due to the increase of ECL reaction rate by twice the surface area enlargement upon applying PDDA, CTAB coated gold nanorods on gold electrode.

2.8 Fluorescence enhancement of $Ru(bpy)_3Cl_2$ by gold nanorods:

Fluorescence enhancement of $Ru(bpy)_3Cl_2$ in the presence of gold nanorods was also tested. These experiments were done to measure the surface plasmon resonance effect of gold nanorods on the ECL enhancement [23] as noble metals such as Au, Ag tend to show surface plasmon resonance effect which can enhance the ECL or fluorescence intensity. [23] Compared to the fluorescence spectrum of $Ru(bpy)_3Cl_2$, the fluorescence spectrum of $Ru(bpy)_3Cl_2$ along with PSS coated gold nanorods were measured. The system was excited by the light of wavelength 450 nm and the emission wavelength was analyzed from a wavelength of 500 nm to 750 nm. It was

found that fluorescence spectrum of Ru(bpy)$_3$Cl$_2$ along with PSS coated gold nanorods were enhanced compared to that of the fluorescence spectrum of Ru(bpy)$_3$Cl$_2$ which was varied depending on the concentration of Ru(bpy)$_3$Cl$_2$. It was found that with the increase of concentration of Ru(bpy)$_3$Cl$_2$, enhancement decreased due to dye-dye loading. With the decreasing concentration of dyes, the dye-dye distance increased so fluorescence quenching due to FRET decreased [6], which helped to increase the probability of enhancement effect due to surface plasmon resonance of gold nanorods.

Based on the calibration curve of Ru(bpy)$_3$Cl$_2$, it was found that fluorescence intensity increased linearly with increasing concentration of Ru(bpy)$_3$Cl$_2$ up to a concentration of 100 nm of Ru(bpy)$_3$Cl$_2$. But at a higher concentration, the calibration curve shows nonlinearity which is a deviation from the Beer lambert law [24]. So, the concentration of up to 100 nM of Ru(bpy)$_3$Cl$_2$ was used to do the fluorescence measurement.
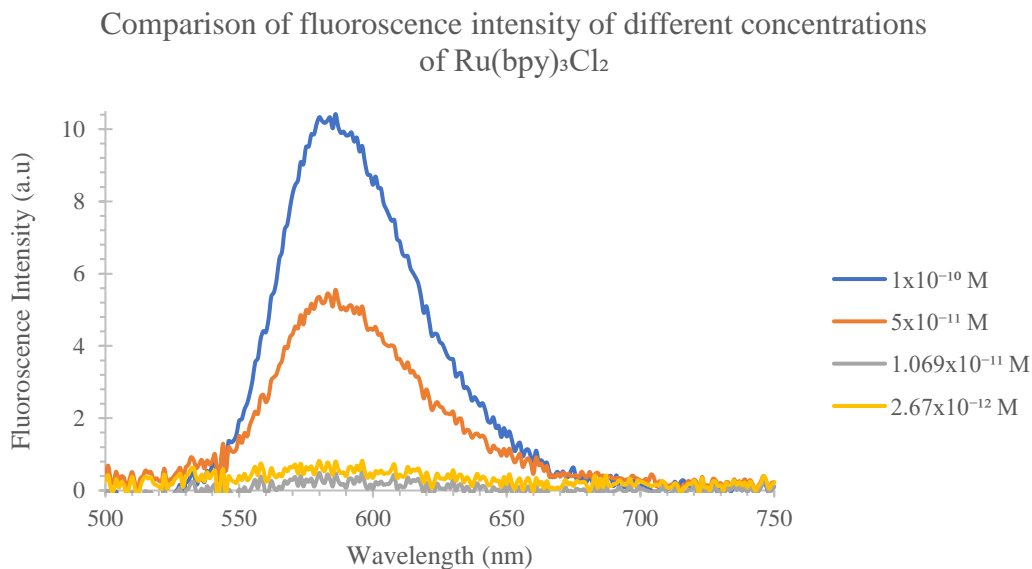
Figure 2. 17 Fluorescence spectrum of solutions of different concentrations of Ru(bpy)$_3$Cl$_2$

Calibration curve for different concentration of Ru(bpy)$_3$Cl$_2$
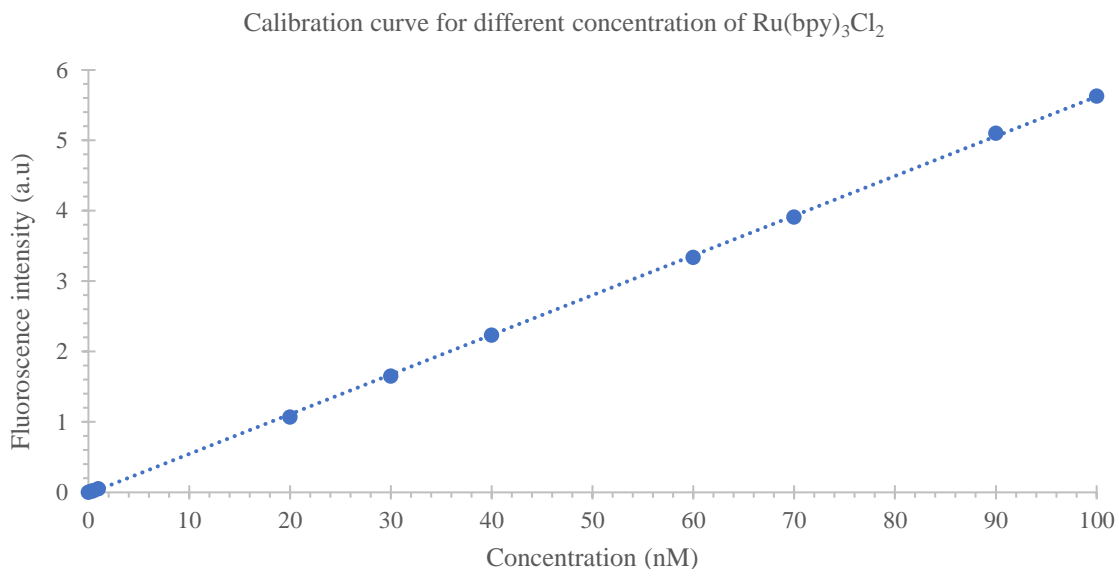
Figure 2. 18 Calibration curve of Ru(bpy)$_3$Cl$_2$

2.8.1 Chemicals:

Tris (2,2'-bipyridyl) dichlororuthenium (II) hexahydrate (Ru(bpy)$_3$Cl$_2$) (99.95% trace metals basis, Aldrich Chemical Co.), hexadecyltrimethylammonium bromide (CH$_3$(CH$_2$)$_{15}$N(Br)(CH$_3$)$_3$) ($\geq$98%, Aldrich Chemical Co.), Poly (sodium 4-styrenesulfonate) (C$_8$H$_7$NaO$_3$S)$_n$ (M$_w$=70,000, Aldrich Chemical Co.). All the solutions were prepared by 0.8 mM CTAB solution as the gold nanorods were stable in CTAB solution.

2.8.2 Apparatus used:

All the fluorescence measurements were done in RF 5301 spectrofluorometer where 150W Xenon lamp was used as a source of light, concave-blazed holographic grating having 1300 grooves/mm was used to produce monochromatic radiation and it could produce fluorescence spectrum in the range of 220-900 nm.

Fluorescence measurements were done at different concentrations of Ru(bpy)$_3$Cl$_2$, in the presence and in the absence of PSS, CTAB coated gold nanorods to measure the enhancement of fluorescence in the presence of PSS, CTAB coated gold nanorods.

2.8.3 Preparation of the solutions:

The gold nanorod solution was added to 2 g/L PSS solution having 6 mM NaCl added to the aqueous solution of PSS. The mixture was shaken for 3 hours to be mixed properly before centrifuging the solution to remove the excess PSS. This PSS, CTAB coated gold nanorod was precipitated out and the supernatant solution was decanted. The PSS, CTAB coated gold nanorod was dissolved in 0.8 mM CTAB solution as the gold nanorod was found to be unstable in water [25].

Different concentrations of Ru(bpy)$_3$Cl$_2$ solution was made using 0.8 mM CTAB[6] as a solvent. 50 µL of gold nanorod was added to 950 µL of the Ru(bpy)$_3$Cl$_2$ solution and the solution was made to 10 mL by adding 0.8 mM CTAB solution. This mixture was left undisturbed overnight for doing the fluorescence measurement [25].
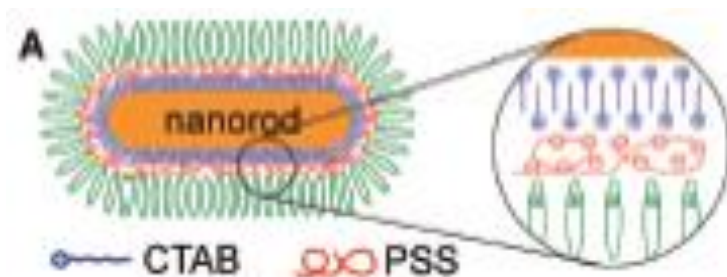
Figure 2. 19 Dye attached to PSS, CTAB coated gold nanorods [26]

From the fluorescence spectrum of different concentrations of Ru(bpy)$_3$Cl$_2$ attached to the gold nanorods it was observed that the main emission band of the Ru(bpy)$_3$Cl$_2$ splits also the position of the peak and the intensity of the peak changes in the presence of gold

nanorods. This splitting of peak caused by the interaction of different interband transition state within the gold nanorods and the emission band of the $Ru(bpy)_3Cl_2$.[26] The gold nanorod tends to increase the rate of radiative decay and decrease the rate of non-radiative decay thus enhancing the fluorescence of $Ru(bpy)_3Cl_2$. Along with the main emission band of $Ru(bpy)_3Cl_2$ at 586 nm and nearby split peaks, the fluorescence spectrum of $Ru(bpy)_3Cl_2$ added with gold nanorods showed additional peak at 693 nm. This peak in the infrared region was caused by the intraband transition of gold nanorods and possibly by transition of higher order such as electric quadrupole or octupole moments of gold nanorods. The energy forbidden intraband transition becomes feasible due to enlargement of electric field caused by the surface plasmon resonance effect of the gold nanorods. The lower intensity of the infrared emission was due to decreasing number of holes and decreasing transmission co-efficient of light emitted in the infrared region [27].

2.8.4 Experimental results and discussions:

2.8.4.1 Fluorescence experiment with $1.1x10^{-11}$ M $Ru(bpy)_3Cl_2$ solution:

Fluorescence spectrum of $1.1x10^{-11}$ M $Ru(bpy)_3Cl_2$ and the fluorescence spectrum of $1.1x10^{-11}$ M $Ru(bpy)_3Cl_2$ along with PSS, CTAB coated gold nanorods were compared and when integrated peak area were measured fluorescence spectrum of $1.1x10^{-11}$ M $Ru(bpy)_3Cl_2$ along with PSS, CTAB coated gold nanorods were found to show 5.4 times higher fluorescence intensity compared to the fluorescence spectrum of $1.1x10^{-11}$ M $Ru(bpy)_3Cl_2$. This enhancement was due to the surface plasmon resonance effect of gold nanorods. The splitting of the emission band of $Ru(bpy)_3Cl_2$ to peaks of 574 nm, 596 nm and 618 nm and also its movement from 585 nm to 596 nm caused by the interaction of different interband transition state within the gold nanorods and the emission band of the $Ru(bpy)_3Cl_2$.[26] The gold nanorod tends to increase the rate of radiative decay and decrease the rate of non-radiative decay thus enhancing the fluorescence of $Ru(bpy)_3Cl_2$.

Along with the main emission band of Ru(bpy)$_3$Cl$_2$ at 586 nm and nearby split peaks, the fluorescence spectrum of Ru(bpy)$_3$Cl$_2$ added with gold nanorods showed additional peak at 700 nm. This peak in the infrared region was caused by the intraband transition of gold nanorods and possibly by transition of higher order such as electric quadrupole or octupole moments of gold nanorods. The energy forbidden intraband transition becomes feasible due to enlargement of electric field caused by the surface plasmon resonance effect of the gold nanorods. The lower intensity of the infrared emission was due to decreasing number of holes and decreasing transmission co-efficient of light emitted in the infrared region [27] The peak at 517 nm was due to the transverse band of gold nanorods in case of the 1.1x10^{-11} M Ru(bpy)$_3$Cl$_2$ solution with PSS, CTAB coated gold nanorods. [15]

Comparison of fluoroscence spectrum of 1.1x10^{-11} M Ru(bpy)$_3$Cl$_2$ with 1.1x10^{-11} M Ru(bpy)$_3$Cl$_2$ and PSS, CTAB coated gold nanorods

Figure 2. 20 Comparison of fluorescence spectrum of 1.1x10^{-11} M Ru(bpy)$_3$Cl$_2$ with the fluorescence spectrum of Ru(bpy)$_3$Cl$_2$ and PSS coated gold nanorods

Table 2. 6 Comparison of fluorescence spectrum data

Types of solution showing fluorescence curves and on which fluorescence experiments were done	Fluorescence Intensity (a.u)	Area under the curve compared with just the Ru(bpy)$_3$Cl$_2$
Area under the curve for 1.1x10^{-11} M Ru(bpy)$_3$Cl$_2$ solution in the wavelength range 528 nm-669 nm	1.1x10^2	1.0
Area under the curve for 1.1x10^{-11} M Ru(bpy)$_3$Cl$_2$ with pss coated gold nanorods in the wavelength range 528nm-669 nm	6.2x10^2	5.4

Here, the surface plasmon resonance effect of the gold nanorods helped to increase the fluorescence intensity of the Ru(bpy)$_3$Cl$_2$ solution in the presence of gold nanorods. [23]

2.8.4.2 Fluorescence experiment with 1x10^{-10} M Ru(bpy)$_3$Cl$_2$ solution:

Fluorescence spectrum of 1x10^{-10} M Ru(bpy)$_3$Cl$_2$ and the fluorescence spectrum of 1x10^{-10} M Ru(bpy)$_3$Cl$_2$ along with PSS, CTAB coated gold nanorods were compared and when integrated peak area were measured fluorescence spectrum of 1x10^{-10} M Ru(bpy)$_3$Cl$_2$ along with PSS, CTAB coated gold nanorods were found to show 1.6 times higher fluorescence intensity compared to the fluorescence spectrum of 1x10^{-10} M Ru(bpy)$_3$Cl$_2$. This enhancement was due to the surface plasmon resonance effect of gold nanorods. The splitting of the emission band of Ru(bpy)$_3$Cl$_2$ due to the interaction of different interband transition state within the gold nanorods and the emission band of the Ru(bpy)$_3$Cl$_2$ [26] was less probable here due to the higher concentration of Ru(bpy)$_3$Cl$_2$. The gold nanorod tends to increase the rate of radiative decay and decrease the rate of non-radiative decay thus enhancing the fluorescence of Ru(bpy)$_3$Cl$_2$. Along with the main emission band of Ru(bpy)$_3$Cl$_2$ at 586 nm, the fluorescence spectrum of Ru(bpy)$_3$Cl$_2$ added with

gold nanorods showed additional peak at 700 nm. This peak in the infrared region was caused by the intraband transition of gold nanorods and possibly by transition of higher order such as electric quadrupole or octupole moments of gold nanorods. The energy forbidden intraband transition becomes feasible due to enlargement of electric field caused by the surface plasmon resonance effect of the gold nanorods. The lower intensity of the infrared emission was due to decreasing number of holes and decreasing transmission co-efficient of light emitted in the infrared region [27]. The peak at 517 nm was due to the transverse band of gold nanorods in case of the $1x10^{-10}$ M Ru(bpy)$_3$Cl$_2$ solution with PSS, CTAB coated gold nanorods. [15]

Figure 2. 21 Fluorescence enhancement with gold nanorods

Table 2. 7 Comparison of fluorescence spectrum

Types of solutions showing fluorescence curve and on which fluorescence experiments were done	Area under the curve	Area under the curve compared with just the Ru(bpy)$_3$Cl$_2$
Area under the curve for $1x10^{-10}$ M Ru(bpy)$_3$Cl$_2$ solution in the wavelength range 534 nm-674 nm	$6.5x10^2$ a.u	1.0

Area under the curve for 1×10^{-10} M Ru(bpy)$_3$Cl$_2$ with PSS coated gold nanorods solution in the wavelength range 534 nm-674 nm	1.0×10^3 a.u	1.6

Here, the surface plasmon resonance effect of the gold nanorods helped to increase the fluorescence intensity of the Ru(bpy)$_3$Cl$_2$ solution in the presence of gold nanorods. [23]

2.8.4.3 Fluorescence experiment with 2.7×10^{-12} M Ru(bpy)$_3$Cl$_2$ solution:

Fluorescence spectrum of 2.7×10^{-12} M Ru(bpy)$_3$Cl$_2$ and the fluorescence spectrum of 2.7×10^{-12} M Ru(bpy)$_3$Cl$_2$ along with PSS, CTAB coated gold nanorods were compared and when integrated peak area were measured fluorescence spectrum of 2.7×10^{-12} M Ru(bpy)$_3$Cl$_2$ along with PSS, CTAB coated gold nanorods were found to show 7.4 times higher fluorescence intensity compared to the fluorescence spectrum of 2.7×10^{-12} M Ru(bpy)$_3$Cl$_2$. This enhancement was due to the surface plasmon resonance effect of gold nanorods. The possible splitting of the emission band of Ru(bpy)$_3$Cl$_2$ to peaks of 564 nm, 574 nm and 590 nm and also its movement from 585 nm to 574 nm caused by the interaction of different interband transition state within the gold nanorods and the emission band of the Ru(bpy)$_3$Cl$_2$.[26] The gold nanorod tends to increase the rate of radiative decay and decrease the rate of non-radiative decay thus enhancing the fluorescence of Ru(bpy)$_3$Cl$_2$. Along with the main emission band of Ru(bpy)$_3$Cl$_2$ at 586 nm and nearby split peaks, the fluorescence spectrum of Ru(bpy)$_3$Cl$_2$ added with gold nanorods showed additional peak at 700 nm. This peak in the infrared region was caused by the intraband transition of gold nanorods and possibly by transition of higher order such as electric quadrupole or octupole moments of gold nanorods. The energy forbidden intraband transition becomes feasible due to enlargement of electric field caused by the surface plasmon resonance effect of the gold nanorods. The lower

intensity of the infrared emission was due to decreasing number of holes and decreasing transmission co-efficient of light emitted in the infrared region [27]. The peak at 517 nm was due to the transverse band of gold nanorods in case of the 2.7×10^{-12} M Ru(bpy)$_3$Cl$_2$ solution with PSS, CTAB coated gold nanorods. [15]

Comparison of fluoroscence inetnsity of 2.7×10^{-12} M Ru(bpy)$_3$Cl$_2$ with 2.7×10^{-12} M Ru(bpy)$_3$Cl$_2$ and PSS,CTAB coated gold nanorods
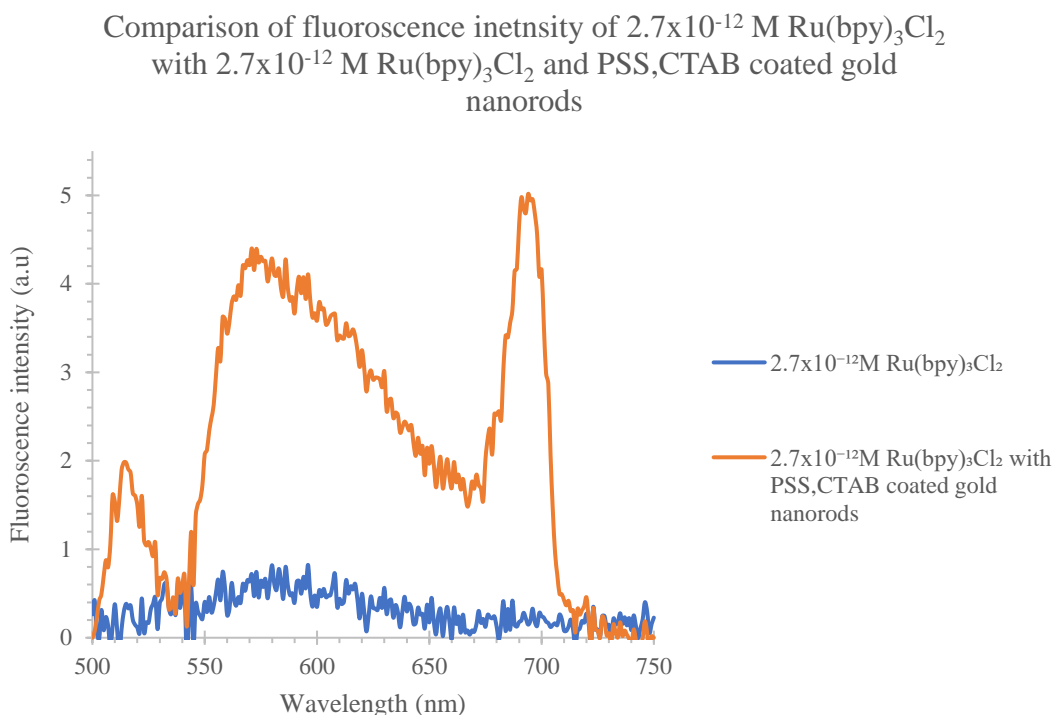
Figure 2. 22 Comparison of the fluorescence with and without the presence of gold nanorods

Table 2. 8 Comparison of the fluorescence spectrum

Types of solutions showing fluorescence curve and on which fluorescence experiments were done	Fluorescence Intensity (a.u)	Area under the curve compared with just Ru(bpy)$_3$Cl$_2$
Area under the curve for 2.67×10^{-12} M Ru(bpy)$_3$Cl$_2$ solution in the wavelength range of 542 nm- 674 nm	5.2×10^1 a.u	1.0

Area under the curve for 2.67×10^{-12} M $Ru(bpy)_3Cl_2$ with gold nanorods in the wavelength range of 542 nm-674 nm	4.0×10^2 a.u	7.4

Here, the surface plasmon resonance effect of the gold nanorods helped to increase the fluorescence intensity of the $Ru(bpy)_3Cl_2$ solution in the presence of gold nanorods. [23]

2.8.4.4 Fluorescence experiment with 2.7×10^{-13} M $Ru(bpy)_3Cl_2$ solution:

Fluorescence spectrum of 2.7×10^{-13} M $Ru(bpy)_3Cl_2$ and the fluorescence spectrum of 2.7×10^{-13} M $Ru(bpy)_3Cl_2$ along with PSS, CTAB coated gold nanorods were compared and when integrated peak area were measured fluorescence spectrum of 2.7×10^{-13} M $Ru(bpy)_3Cl_2$ along with PSS, CTAB coated gold nanorods were found to show 3.3 times higher fluorescence intensity compared to the fluorescence spectrum of 2.7×10^{-13} M $Ru(bpy)_3Cl_2$. This enhancement was due to the surface plasmon resonance effect of gold nanorods. The possible splitting of the emission band of $Ru(bpy)_3Cl_2$ to peaks of 572 nm, 596 nm and 617 nm and also its movement from 585 nm to 596 nm caused by the interaction of different interband transition state within the gold nanorods and the emission band of the $Ru(bpy)_3Cl_2$.[26] The gold nanorod tends to increase the rate of radiative decay and decrease the rate of non-radiative decay thus enhancing the fluorescence of $Ru(bpy)_3Cl_2$. Along with the main emission band of $Ru(bpy)_3Cl_2$ at 586 nm and nearby split peaks, the fluorescence spectrum of $Ru(bpy)_3Cl_2$ added with gold nanorods showed additional peak at 700 nm. This peak in the infrared region was caused by the intraband transition of gold nanorods and possibly by transition of higher order such as electric quadrupole or octupole moments of gold nanorods. The energy forbidden intraband transition becomes feasible due to enlargement of electric field caused by the surface plasmon resonance effect of the gold nanorods. The lower

intensity of the infrared emission was due to decreasing number of holes and decreasing transmission co-efficient of light emitted in the infrared region [27]. The peak at 517 nm was due to the transverse band of gold nanorods in case of the 2.7×10^{-13} M Ru(bpy)$_3$Cl$_2$ solution with PSS, CTAB coated gold nanorods. [15]

Comparison of Fluoroscence Intensity of 2.7×10^{-13} M Ru(bpy)$_3$Cl$_2$ with 2.7×10^{-13} M Ru(bpy)$_3$Cl$_2$ and PSS,CTAB coated gold nanorod
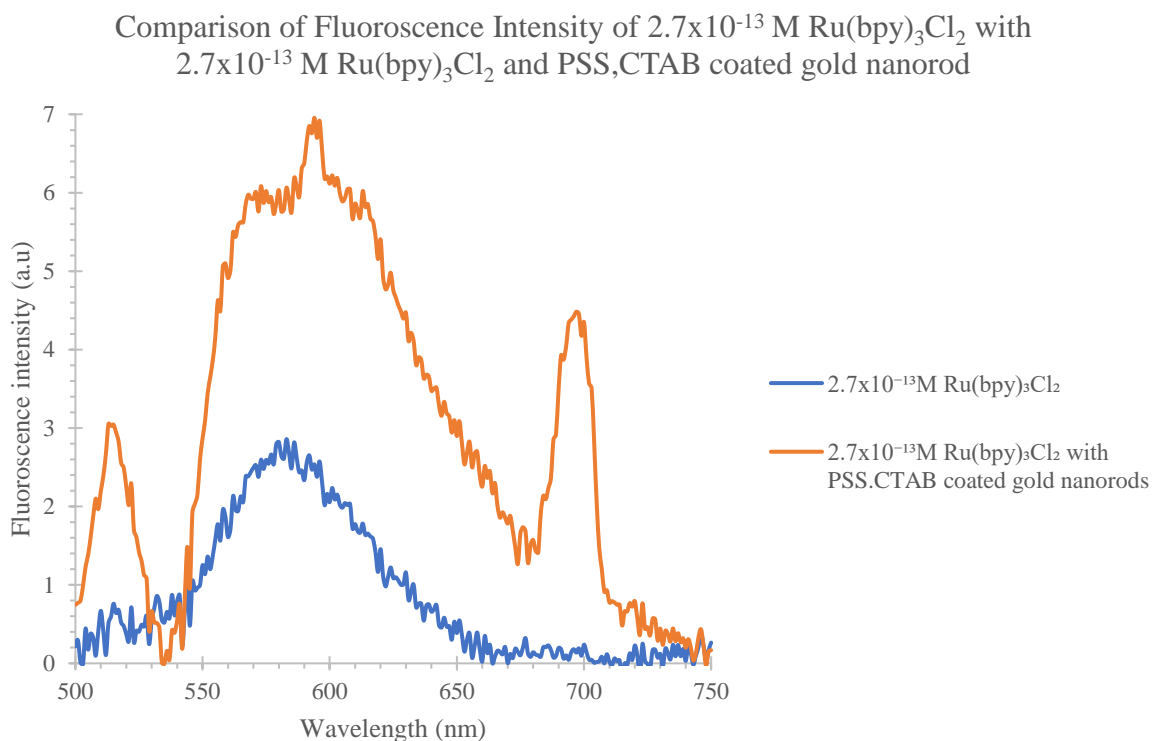
Figure 2. 23 Comparison of Fluorescence spectrum with and without the presence of PSS, CTAB coated gold nanorods in case of Ru(bpy)$_3$Cl$_2$ of concentration 2.7×10^{-13} M

Table 2. 9 Comparison of the fluorescence data

Types of solution showing Fluorescence curve and on which fluorescence experiments were done	Fluorescence Intensity (a.u)	Area under the curve compared to that of just the Ru(bpy)$_3$Cl$_2$
Area under the curve for 2.7×10^{-13} M Ru(bpy)$_3$Cl$_2$ solution in the wavelength range 535nm-678nm	1.8×10^2	1.0

Area under the curve for 2.7×10^{-13} M Ru(bpy)$_3$Cl$_2$ with PSS, CTAB coated gold nanorods in the wavelength range 535 nm-678nm	5.9×10^2	3.3

Here, the surface plasmon resonance effect of the gold nanorods helped to increase the fluorescence intensity of the Ru(bpy)$_3$Cl$_2$ solution in the presence of gold nanorods [23]

2.8.4.5 Fluorescence experiment with 5×10^{-11} M Ru(bpy)$_3$Cl$_2$ solution:

Fluorescence spectrum of 5×10^{-11} M Ru(bpy)$_3$Cl$_2$ and the fluorescence spectrum of 5×10^{-11} M Ru(bpy)$_3$Cl$_2$ and PSS, CTAB coated gold nanorods were compared and when integrated peak area was measured fluorescence spectrum of 5×10^{-11} M Ru(bpy)$_3$Cl$_2$ and PSS, CTAB coated gold nanorods were found to show 2.8 times higher fluorescence intensity compared to the fluorescence spectrum of 5×10^{-11} M Ru(bpy)$_3$Cl$_2$. This enhancement was due to the surface plasmon resonance effect of gold nanorods. The possible splitting of the emission band of Ru(bpy)$_3$Cl$_2$ to peaks of 576 nm, 594 nm and 615 nm and also its movement from 585 nm to 594 nm caused by the interaction of different interband transition state within the gold nanorods and the emission band of the Ru(bpy)$_3$Cl$_2$.[26] The gold nanorod tends to increase the rate of radiative decay and decrease the rate of non-radiative decay thus enhancing the fluorescence of Ru(bpy)$_3$Cl$_2$. Along with shifting the main emission band of Ru(bpy)$_3$Cl$_2$ at 586 nm and nearby split peaks, the fluorescence spectrum of Ru(bpy)$_3$Cl$_2$ added with gold nanorods showed additional peak at 700 nm. This peak in the infrared region was caused by the intraband transition of gold nanorods and possibly by transition of higher order such as electric quadrupole or octupole moments of gold nanorods. The energy forbidden intraband transition becomes feasible due to enlargement of electric field caused by the surface plasmon resonance effect of the gold nanorods. The lower

intensity of the infrared emission was due to decreasing number of holes and decreasing transmission co-efficient of light emitted in the infrared region [27]. The peak at 517 nm was due to the transverse band of gold nanorods in case of the 5×10^{-11} M Ru(bpy)$_3$Cl$_2$ solution with PSS, CTAB coated gold nanorods. [15]
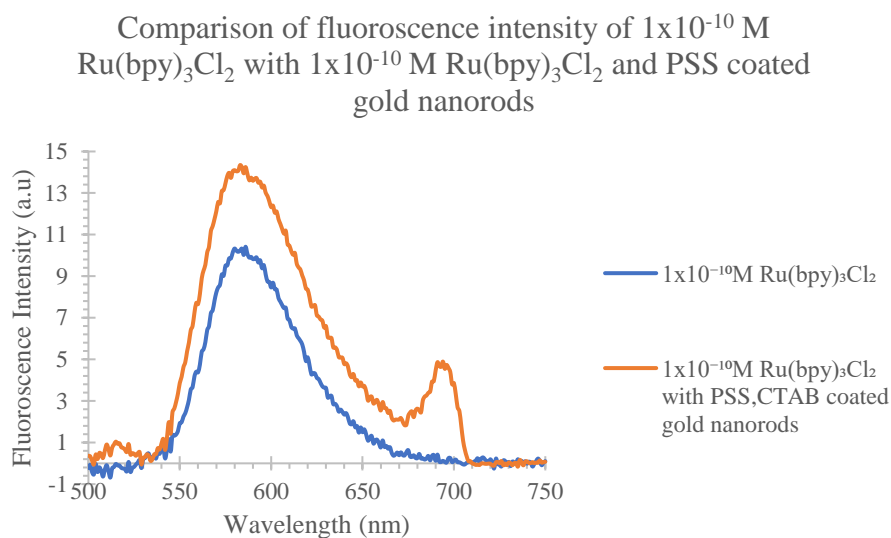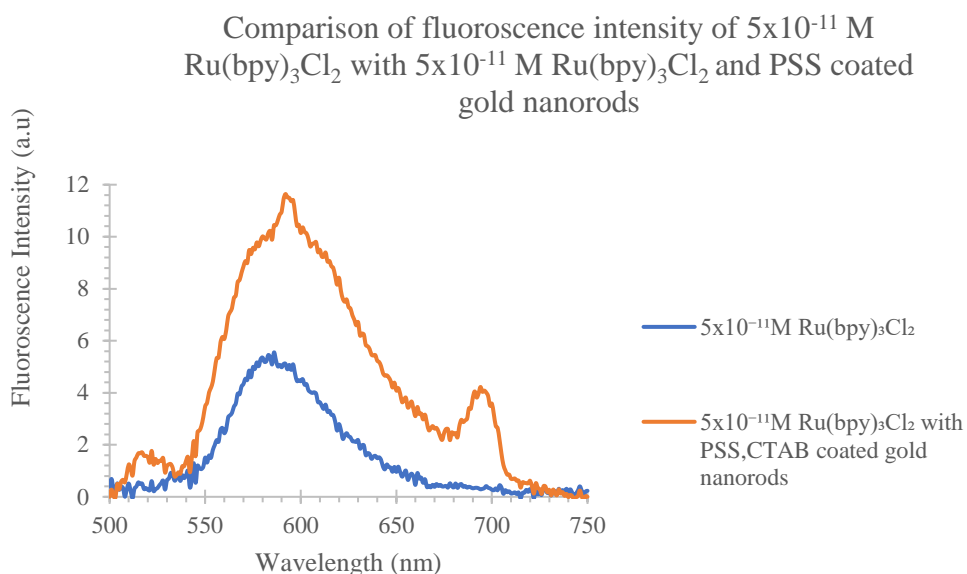

Figure 2. 24 Comparison of the fluorescence spectrum in the presence and absence of PSS, CTAB coated gold nanorods in case of Ru(bpy)$_3$Cl$_2$ of concentration 5×10^{-11} M

Table 2. 10 Comparison of the fluorescence data

Types of Fluorescence Solution showing fluorescence curve and on which fluorescence experiments were done	Fluorescence Intensity (a.u)	Area under then curve compared to that of just the Ru(bpy)$_3$Cl$_2$
Area under the curve for 5×10^{-11} M Ru(bpy)$_3$Cl$_2$ solution in the wavelength range 537nm-678nm	2.9×10^2	1

Area under the curve for 5×10^{-11} M Ru(bpy)$_3$Cl$_2$ with PSS, CTAB coated gold nanorods in the wavelength range 537nm-678 nm	8.0×10^2	2.8

Here, the surface plasmon resonance effect of the gold nanorods helped to increase the fluorescence intensity of the Ru(bpy)$_3$Cl$_2$ solution in the presence of gold nanorods. [23]

2.8.4.6 Fluorescence experiment with 100×10^{-9} M Ru(bpy)$_3$Cl$_2$ solution:

Fluorescence spectrum of 100×10^{-9} M Ru(bpy)$_3$Cl$_2$ and the fluorescence spectrum of 100×10^{-9} M Ru(bpy)$_3$Cl$_2$ along with PSS, CTAB coated gold nanorods were compared and when integrated peak area were measured fluorescence spectrum of 100×10^{-9} M Ru(bpy)$_3$Cl$_2$ along with PSS, CTAB coated gold nanorods were found to show 0.65 times fluorescence intensity compared to the fluorescence spectrum of 100×10^{-9} M Ru(bpy)$_3$Cl$_2$. Here, due to the smaller dye to dye separation, fluorescence decreased by the FRET mechanism upon addition of gold nanorods.[6] The fluorescence spectrum of Ru(bpy)$_3$Cl$_2$ added with gold nanorods showed additional peak at 700 nm. This peak in the infrared region was caused by the intraband transition of gold nanorods and possibly by transition of higher order such as electric quadrupole or octupole moments of gold nanorods. The energy forbidden intraband transition becomes feasible due to enlargement of electric field caused by the surface plasmon resonance effect of the gold nanorods. The lower intensity of the infrared emission was due to decreasing number of holes and decreasing transmission co-efficient of light emitted in the infrared region [27].

Comparison of fluoroscence spectrum of 100×10^{-9}M Ru(bpy)$_3$Cl$_2$ with 100×10^{-9}M Ru(bpy)$_3$Cl$_2$ and PSS,CTAB coated gold nanorods
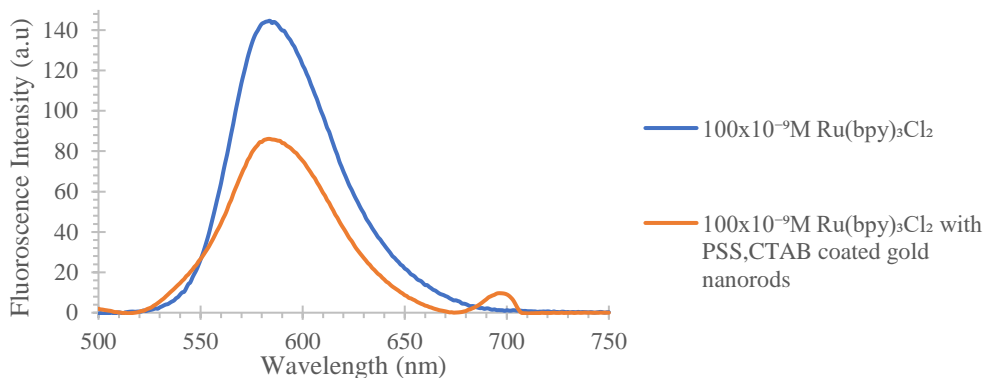
Figure 2. 25 Comparison of the fluorescence spectrum in the presence and absence of PSS, CTAB coated gold nanorods in case of Ru(bpy)$_3$Cl$_2$ of concentration 100×10^{-9} M

Table 2. 11 Comparison of the fluorescence data

Types of Solutions showing Fluorescence curves and on which fluorescence experiments were done	Fluorescence Intensity (a.u)	Area under then curve compared to that of just the Ru(bpy)$_3$Cl$_2$
Area under the curve for 100 nM Ru(bpy)$_3$Cl$_2$ solution in the wavelength range of 524nm-680nm	8.7×10^3	1.0
Area under the curve for 100 nM Ru(bpy)$_3$Cl$_2$ with pss coated gold nanorods in the wavelength range of 524nm-680nm	5.7×10^3	6.5×10^{-1}

Here, due to the higher concentration of Ru(bpy)$_3$Cl$_2$ number of Ru(bpy)$_3$Cl$_2$ molecules per gold nanorod was higher which caused FRET effect that dominated any plasmonic effect of gold nanorods. [6]

2.9 Relationship of fluorescence enhancement factor with the concentration of Ru(bpy)₃Cl₂:

Based on these experiments, it can be concluded that, upon decreasing the concentration of $Ru(bpy)_3Cl_2$, fluorescence increased in the presence of PSS, CTAB coated gold nanorods. At a higher concentration of dyes present in solution, the dye to dye separation decreases which result in a fluorescence quenching due to transfer of Forster resonance energy which is created by the transfer of energy by non-radiative coupling between donor and acceptor.[6] As the theory says, as the concentration of $Ru(bpy)_3Cl_2$ increases, the dye to dye separation bonded to the gold nanorod decreases.[6] So, tendency of transfer of Forster resonance energy between neighboring $Ru(bpy)_3Cl_2$ molecules increases. So, energy is transferred from a donor to an acceptor $Ru(bpy)_3Cl_2$ molecules. As a result, fluorescence intensity decreases. [6]
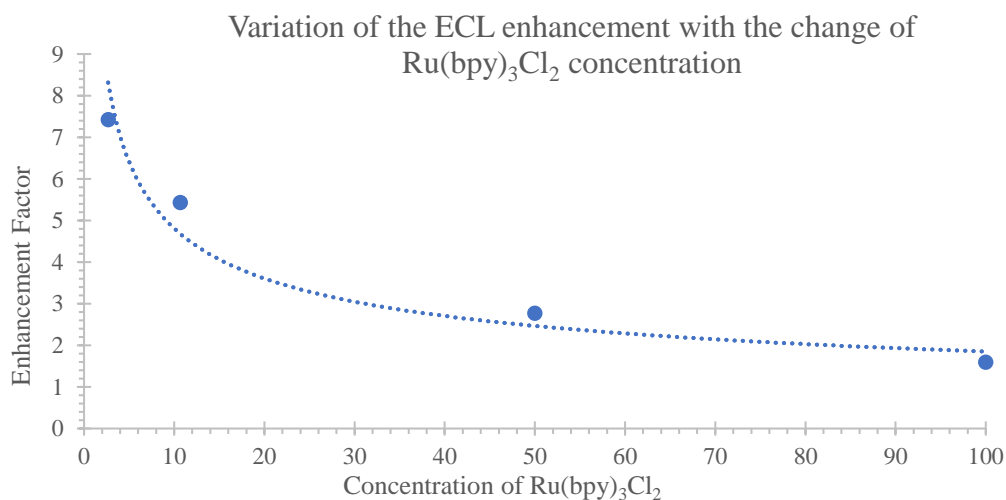
Figure 2. 26 Fluorescence enhancement with different concentrations of $Ru(bpy)_3Cl_2$ along with PSS, CTAB coated gold nanorods compared to that of $Ru(bpy)_3Cl_2$

2.10 Relationship of fluorescence enhancement factor with the number of Ru(bpy)$_3$Cl$_2$ molecules attached to each gold nanorod molecule:

With the increasing concentration of Ru(bpy)$_3$Cl$_2$, the number of Ru(bpy)$_3$Cl$_2$ attached to the surface of each gold nanorod molecule also increased. So, the enhancement factor was found to be decreased with the change of the number of Ru(bpy)$_3$Cl$_2$ molecules attached with the surface of each of the gold nanorods molecule. Here, the number of Ru(bpy)$_3$Cl$_2$ attached to each of the gold nanorods was measured from the number of nanorods present in 50 µL of PSS, CTAB coated gold nanorods and from the ratio of the area of the fluorescence intensity found from the Ru(bpy)$_3$Cl$_2$ solution and Ru(bpy)$_3$Cl$_2$, along with PSS, CTAB coated gold nanorod solution [28]

2.10.1 Calculation:

Here, the number of gold nanorod molecules in 50 µL 4.1×10^{-17} M gold nanorod is 1.05×10^8

The number of Ru(bpy)$_3$Cl$_2$ molecules in 950 µL Ru(bpy)$_3$Cl$_2$ solution of 1.1×10^{-11} M is 6.1×10^9

The number of Ru(bpy)$_3$Cl$_2$ molecule bonded to gold nanorod was calculated from the ratio of the total Ru(bpy)$_3$Cl$_2$ molecules present in the solution to that of the fluorescence enhancement factor= $6.1 \times 10^9 / 5.4 = 1.1 \times 10^9$ (for the Ru(bpy)$_3$Cl$_2$ solution of concentration 1.1×10^{-11} M)

So, the number of Ru(bpy)$_3$Cl$_2$ molecules present per gold nanorod molecule was= $1.1 \times 10^9 / 1.05 \times 10^8 = 108$ (for the Ru(bpy)$_3$Cl$_2$ solution of concentration 1.1×10^{-11} M)

Similarly, for other solutions of Ru(bpy)$_3$Cl$_2$, number of Ru(bpy)$_3$Cl$_2$ molecules bound to each gold nanorod molecule was calculated.

Variation of the enhancement factor with the number of Ru(bpy)$_3$Cl$_2$ attached per PSS, CTAB coated gold nanorod
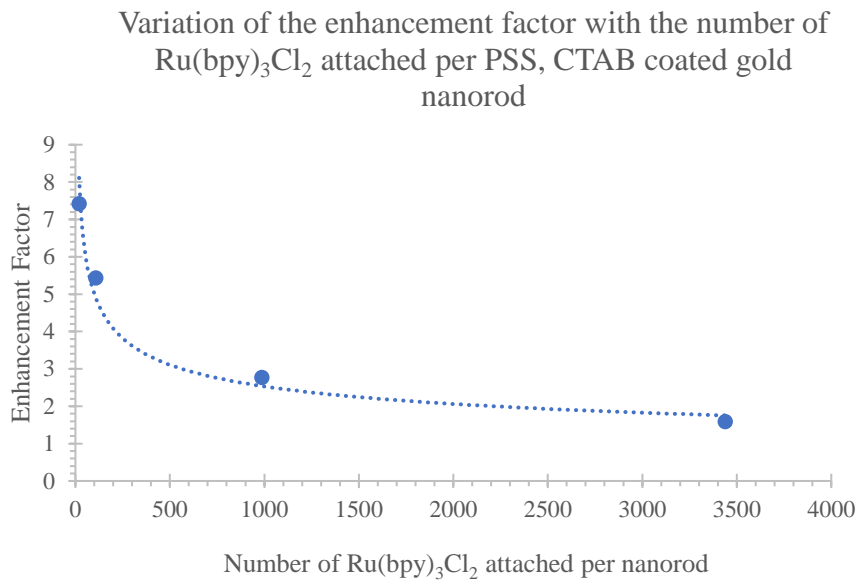
Figure 2. 27 Variation of the enhancement factor with the number of Ru(bpy)$_3$Cl$_2$ attached per PSS, CTAB coated gold nanorod

As the theory says as the concentration of Ru(bpy)$_3$Cl$_2$ increases, the number of Ru(bpy)$_3$Cl$_2$ molecules per molecules of gold nanorods also increases. [6] So, tendency of transfer of Forster resonance energy between neighboring Ru(bpy)$_3$Cl$_2$ molecules increases. So, energy is transferred from a donor to an acceptor Ru(bpy)$_3$Cl$_2$ molecules. As a result, fluorescence intensity decreases. [6]

2.11 Linear relationship of fluorescence intensity with concentration of Ru(bpy)$_3$Cl$_2$:

On the other hand, when the fluorescence spectrum of different concentrations of Ru(bpy)$_3$Cl$_2$ mixed with PSS, CTAB coated gold nanorods were compared, it was found that fluorescence intensity was increased with the increase of the concentration of the dye which is the basic principle of Beer Lambert Law.[24] The fluorescence spectrum of Ru(bpy)$_3$Cl$_2$ added with gold nanorods showed additional peak at 700 nm. This peak in the infrared region was caused by the intraband transition of gold nanorods and possibly by transition of higher order such as electric

119

quadrupole or octupole moments of gold nanorods. The energy forbidden intraband transition becomes feasible due to enlargement of electric field caused by the surface plasmon resonance effect of the gold nanorods. The lower intensity of the infrared emission was due to decreasing number of holes and decreasing transmission co-efficient of light emitted in the infrared region [27]

Comparison of fluoroscence different concentration of Ru(bpy)$_3$Cl$_2$ with PSS,CTAB coated gold nanorods
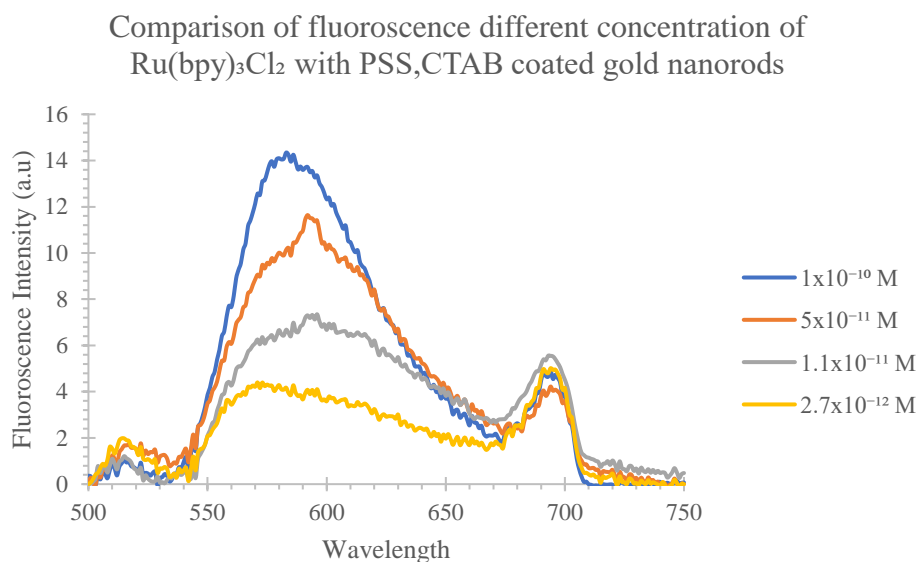
Figure 2. 28 Comparison of the fluorescence spectrum of different concentrations of Ru(bpy)$_3$Cl$_2$ in the presence of PSS, CTAB coated gold nanorods

Table 2. 12 Comparison of the fluorescence data

Solutions types showing fluorescence curves and on which fluorescence experiments were done	Fluorescence Intensity (a.u)	Area under the curve compared to 2.67x10^{-12} M Ru(bpy)$_3$Cl$_2$ in the presence of PSS, CTAB coated gold nanorods
Area under the curve of 2.7x10^{-12} M Ru(bpy)$_3$Cl$_2$ with PSS, CTAB coated gold nanorods solution in the wavelength range 537nm-674nm	3.9x10^2	1.0

Area under the curve of 1.1×10^{-11} M Ru(bpy)$_3$Cl$_2$ with PSS, CTAB coated gold nanorods solution in the wavelength range 537nm-674nm	6.2×10^2	1.7
Area under the curve of 5×10^{-11} M Ru(bpy)$_3$Cl$_2$ with PSS, CTAB coated gold nanorods in the wavelength range 537nm-674nm	8.0×10^2	2.1
Area under the curve of 1.0×10^{-10} M Ru(bpy)$_3$Cl$_2$ with PSS, CTAB coated gold nanorods in the wavelength range 537 nm-674 nm	1.0×10^3 a.u	2.7

Again, when the fluorescence spectrum of different concentrations of Ru(bpy)$_3$Cl$_2$ were compared, it was found that fluorescence intensity was increased with the increase of the concentrations of the dye which is the basic principle of Beer Lambert Law. [24]
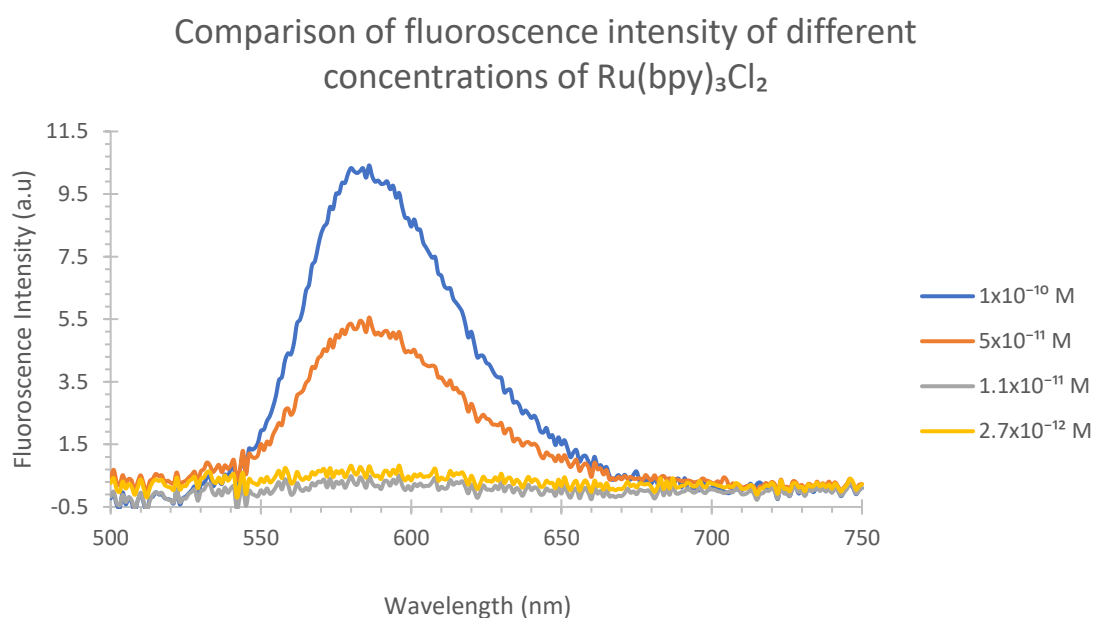
Figure 2. 29 Comparison of the fluorescence of different concentrations of Ru(bpy)$_3$Cl$_2$

Table 2. 13 Comparison of the fluorescence data

Solution types showing fluorescence curves and on which fluorescence experiments were done	Fluorescence Intensity (a.u)	Area under the curve compared to the fluorescence spectrum of 2.67×10^{-12} M Ru(bpy)$_3$Cl$_2$
Area under the curve of 5×10^{-11} M Ru(bpy)$_3$Cl$_2$ solution in the wavelength range 529 nm-682 nm	2.9×10^2	5.5
Area under the curve of 1.069×10^{-11} M Ru(bpy)$_3$Cl$_2$ solution in the wavelength range 529 nm-682 nm	1.1×10^2	2.2
Area under the curve of 2.67×10^{-12} M Ru(bpy)$_3$Cl$_2$ solution in the wavelength range 529 nm-682 nm	5.3×10^1	1.0
Area under the curve of 1×10^{-10} M Ru(bpy)$_3$Cl$_2$ solution in the wavelength range 529 nm-682 nm	6.5×10^2	12

As here, in the figure 2.33 we can see that with increasing concentration of Ru(bpy)$_3$Cl$_2$ fluorescence intensity was found to be increased. This is the basic principle of Beer Lambert's Law. [24]

2.12 Overall findings:

The preferred reagent for producing ECL is Ru(bpy)$_3^{2+}$ and its derivatives as they are highly soluble in water, highly stable electrochemically and can be repeatedly regenerated in multiple cycles of ECL reaction [1]. However, the efficiency of ECL solution made of Ru(bpy)$_3^{2+}$ is very low, 3.5-6% [2]. The target of improving sensitivity of the bipolar electrochemical sensor was achieved by increasing bipolar electrochemical sensitivity based on plasmonic enhancement of ECL also the rate of ECL reaction by increasing surface area which increases the ECL intensity.

For this purpose gold nanorod of aspect ratio 2.6 was synthesized which shows its

longitudinal band at 650 nm that can overlap with the emission of Ru(bpy)$_3$Cl$_2$, 620 nm [4] to show the plasmonic enhancement of ECL from Ru(bpy)$_3$Cl$_2$ and gold nanoparticles was also synthesized. The ECL experiment was done in a closed bipolar cell having 5 mM Ru(bpy)$_3^{2+}$, 25 mM TPA and 0.1 M phosphate buffer solution in the reporting compartment and 5 mM K$_3$Fe(CN)$_6$, 0.1 M KNO$_3$ in the sensing compartment [2]. The efficiency of the ECL solution of Ru(bpy)$_3^{2+}$ was tested for bare gold electrode and also by modifying the electrodes with PDDA-CTAB coated gold nanoparticles modified gold electrode, PDDA-CTAB coated gold nanorods modified gold electrode, PDDA, CTAB etc. In the cases of gold electrode modified with PDDA-CTAB coated gold nanorods, PDDA-CTAB coated gold nanoparticles, CTAB coated gold nanorods ECL was found to be increased compared with the bare gold electrode mainly due to the surface plasmon resonance effect and also due to the increasing rate of ECL reaction by increasing surface area by applying PDDA, CTAB coated gold nanorods on gold electrode. However, for the gold electrode modified with PDDA, CTAB the ECL signal was also found to be decreased mainly due to the surface blocking effect of the surfactants which reduces the surface area.

To analyze the ECL enhancement by increasing ECL reaction rate surface area enhancement was tested upon modifying the gold electrode with PDDA, CTAB coated gold nanorods and comparing the result with that of bare gold electrode. Fluorescence experiments were done in the presence and absence of CTAB coated gold nanorods to verify any plasmonic enhancement.

For the surface area measurement, cyclic voltammetric experiments were done on bare gold electrode and gold electrode modified with PDDA, gold nanorod in 1.0 mM K$_3$Fe(CN)$_6$ mixed with 0.5 M KCl in water. For both bare gold and PDDA-gold nanorod modified gold electrode CV measurements were done by measuring current at different scan rate

for the potential range of 0 to 500 mV. From the slope of the graph, oxidation peak current vs √Scan rate, electrochemically active surface area of the electrode was calculated based on the equation

$I_P = 0.4463nF(nF/RT)^{1/2} AD^{1/2}v^{1/2}C$ [5]

From the comparison of the surface area of the bare gold electrode (13 cm^2) and surface area of the PDDA-gold nanorod modified gold electrode (26 cm^2) it was found that due to the gold nanorods the electrode has two times higher surface area compared to the bare gold electrode. This explained the fact that, due to the enhancement of the surface area, rate of ECL reaction increases as the number of active sites increases which ultimately increases the ECL intensity.

In the fluorescence experiments, fluorescence intensity was found to be increased 2.8-7.4 times in case of Ru(bpy)$_3$Cl$_2$ solution in the presence of CTAB coated gold nanorods compared to the Ru(bpy)$_3$Cl$_2$ solution without gold nanorods. Fluorescence experiments were done for solutions of different concentrations of Ru(bpy)$_3$Cl$_2$ and it was found that enhancement factor decreases with increasing the concentration of Ru(bpy)$_3$Cl$_2$ due to the FRET effect [6]. The maximum enhancement was observed for a solution of Ru(bpy)$_3$Cl$_2$ concentration 2.6×10^{-12} M and 7.4 times fluorescence enhancement was observed for a solution containing Ru(bpy)$_3$Cl$_2$ and PSS,CTAB coated gold nanorods compared to the fluorescence emission observed for a solution of Ru(bpy)$_3$Cl$_2$ only. On the other hand, minimum enhancement was observed for a solution of Ru(bpy)$_3$Cl$_2$ concentration 1×10^{-10} M and 1.6 times fluorescence enhancement was observed for a solution containing Ru(bpy)$_3$Cl$_2$ and PSS,CTAB coated gold nanorods compared to the fluorescence emission observed for a solution of Ru(bpy)$_3$Cl$_2$ only.

These fluorescence experiments proved the plasmonic enhancement of gold nanorods to increase the ECL efficiency of $Ru(bpy)_3Cl_2$. [7]

Reference 2:

(1)   Wang, D.; Guo, L.; Huang, R.; Qiu, B.; Lin, Z.; Chen, G. Surface Enhanced Electrochemiluminescence of Ru(Bpy)32+. *Sci. Rep.* **2015**, *5* (1), 7954. https://doi.org/10.1038/srep07954.

(2)   Wallace, W. L.; Bard, A. J. Electrogenerated Chemiluminescence. 35. Temperature Dependence of the ECL Efficiency of Tris(2,2'-Bipyridine)Rubidium(2+) in Acetonitrile and Evidence for Very High Excited State Yields from Electron Transfer Reactions. *J. Phys. Chem.* **1979**, *83* (10), 1350–1357. https://doi.org/10.1021/j100473a022.

(3)   Holdren, G. R.; Speyer, P. M. Reaction Rate-Surface Area Relationships during the Early Stages of Weathering—I. Initial Observations. *Geochim. Cosmochim. Acta* **1985**, *49* (3), 675–681. https://doi.org/10.1016/0016-7037(85)90162-0.

(4)   Murphy, C. J.; Gole, A. M.; Hunyadi, S. E.; Stone, J. W.; Sisco, P. N.; Alkilany, A.; Kinard, B. E.; Hankins, P. Chemical Sensing and Imaging with Metallic Nanorods. *Chem Commun* **2008**, No. 5, 544–557. https://doi.org/10.1039/B711069C.

(5)   Bard, A. J.; Faulkner, L. R. *Electrochemical Methods: Fundamentals and Applications*, 2nd ed.; Wiley: New York, 2001.

(6)   Abadeer, N. S.; Brennan, M. R.; Wilson, W. L.; Murphy, C. J. Distance and Plasmon Wavelength Dependent Fluorescence of Molecules Bound to Silica-Coated Gold Nanorods. *ACS Nano* **2014**, *8* (8), 8392–8406. https://doi.org/10.1021/nn502887j.

(7)   Nikoobakht, B.; El-Sayed, M. A. Preparation and Growth Mechanism of Gold Nanorods (NRs) Using Seed-Mediated Growth Method. *Chem. Mater.* **2003**, *15* (10), 1957–1962. https://doi.org/10.1021/cm020732l.

(8)   Mavré, F.; Chow, K.-F.; Sheridan, E.; Chang, B.-Y.; Crooks, J. A.; Crooks, R. M. A Theoretical and Experimental Framework for Understanding Electrogenerated Chemiluminescence (ECL) Emission at Bipolar Electrodes. *Anal. Chem.* **2009**, *81* (15), 6218–6225. https://doi.org/10.1021/ac900744p.

(9)   Yu, S.; Mehrgardi, M.; Shannon, C. A Bipolar Electrochemical Sensor with Square Wave Excitation and ECL Readout. *Electrochem. Commun.* **2018**, *88*, 24–28. https://doi.org/10.1016/j.elecom.2018.01.013.

(10)   Wu, M.-S.; Liu, Z.; Shi, H.-W.; Chen, H.-Y.; Xu, J.-J. Visual Electrochemiluminescence Detection of Cancer Biomarkers on a Closed Bipolar Electrode Array Chip. *Anal. Chem.* **2015**, *87* (1), 530–537. https://doi.org/10.1021/ac502989f.

(11)   Ulrich, C.; Andersson, O.; Nyholm, L.; Björefors, F. Formation of Molecular Gradients on Bipolar Electrodes. *Angew. Chem. Int. Ed.* **2008**, *47* (16), 3034–3036. https://doi.org/10.1002/anie.200705824.

(12)   Creutz, C.; Sutin, N. Reaction of Tris(Bipyridine)Ruthenium(III) with Hydroxide and Its
       Application in a Solar Energy Storage System. *Proc. Natl. Acad. Sci.* **1975**, *72* (8), 2858–
       2862. https://doi.org/10.1073/pnas.72.8.2858.

(13)   Maness, K. M.; Bartelt, J. E.; Wightman, R. M. Effects of Solvent and Ionic Strength on the
       Electrochemiluminescence of 9,10-Diphenylanthracene. *J. Phys. Chem.* **1994**, *98* (15),
       3993–3998. https://doi.org/10.1021/j100066a015.

(14)   Greber, G. Vogel's Textbook of Practical Organic Chemistry (5th Ed.), Revised by Brian S.
       Furniss, Antony J. Hannaford, Peter W. G. Smith, and Austin R. Tatchell, John Wiley &
       Sons, New York, 1514 Pp. Price: $84.95. *J. Polym. Sci. Part Polym. Chem.* **1991**, *29* (8),
       1223–1223. https://doi.org/10.1002/pola.1991.080290821.

(15)   Chang, H.-H.; Murphy, C. J. Mini Gold Nanorods with Tunable Plasmonic Peaks beyond
       1000   Nm.   *Chem.   Mater.*   **2018**,   *30*   (4),   1427–1435.
       https://doi.org/10.1021/acs.chemmater.7b05310.

(16)   Mayer, K. M.; Lee, S.; Liao, H.; Rostro, B. C.; Fuentes, A.; Scully, P. T.; Nehl, C. L.;
       Hafner, J. H. A Label-Free Immunoassay Based Upon Localized Surface Plasmon
       Resonance   of   Gold   Nanorods.   *ACS   Nano*   **2008**,   *2*   (4),   687–692.
       https://doi.org/10.1021/nn7003734.

(17)   Scarabelli, L.; Sánchez-Iglesias, A.; Pérez-Juste, J.; Liz-Marzán, L. M. A "Tips and Tricks"
       Practical Guide to the Synthesis of Gold Nanorods. *J. Phys. Chem. Lett.* **2015**, *6* (21), 4270–
       4279. https://doi.org/10.1021/acs.jpclett.5b02123.

(18)   Elgrishi, N.; Rountree, K. J.; McCarthy, B. D.; Rountree, E. S.; Eisenhart, T. T.; Dempsey,
       J. L. A Practical Beginner's Guide to Cyclic Voltammetry. *J. Chem. Educ.* **2018**, *95* (2),
       197–206. https://doi.org/10.1021/acs.jchemed.7b00361.

(19)   Grewal, Y. S.; Shiddiky, M. J. A.; Gray, S. A.; Weigel, K. M.; Cangelosi, G. A.; Trau, M.
       Label-Free Electrochemical Detection of an Entamoeba Histolytica Antigen Using Cell-
       Free   Yeast-ScFv   Probes.   *Chem.   Commun.*   **2013**,   *49*   (15),   1551.
       https://doi.org/10.1039/c2cc38882k.

(20)   Milkani, E.; Khaing, A. M.; Morais, S.; Lambert, C. R.; McGimpsey, W. G. SPR-Based
       Single Nucleotide Mismatch Biosensor. *Anal Methods* **2011**, *3* (1), 122–132.
       https://doi.org/10.1039/C0AY00492H.

(21)   Dong, Y.-P.; Cui, H.; Wang, C.-M. Electrogenerated Chemiluminescence of Luminol on a
       Gold-Nanorod-Modified Gold Electrode. *J. Phys. Chem. B* **2006**, *110* (37), 18408–18414.
       https://doi.org/10.1021/jp062396s.

(22)   Furst, A. L.; Smith, M. J.; Francis, M. B. Direct Electrochemical Bioconjugation on Metal
       Surfaces.   *J.   Am.   Chem.   Soc.*   **2017**,   *139*   (36),   12610–12616.
       https://doi.org/10.1021/jacs.7b06385.

(23)   Sun, S.; Wu, L.; Bai, P.; Png, C. E. Fluorescence Enhancement in Visible Light: Dielectric or Noble Metal? *Phys. Chem. Chem. Phys.* **2016**, *18* (28), 19324–19335. https://doi.org/10.1039/C6CP03303B.

(24)   Swinehart, D. F. The Beer-Lambert Law. 3.

(25)   Ni, W.; Chen, H.; Su, J.; Sun, Z.; Wang, J.; Wu, H. Effects of Dyes, Gold Nanocrystals, PH, and Metal Ions on Plasmonic and Molecular Resonance Coupling. *J. Am. Chem. Soc.* **2010**, *132* (13), 4806–4814. https://doi.org/10.1021/ja910239b.

(26)   Ni, W.; Yang, Z.; Chen, H.; Li, L.; Wang, J. Coupling between Molecular and Plasmonic Resonances in Freestanding Dye−Gold Nanorod Hybrid Nanostructures. *J. Am. Chem. Soc.* **2008**, *130* (21), 6692–6693. https://doi.org/10.1021/ja8012374.

(27)   Beversluis, M. R.; Bouhelier, A.; Novotny, L. Continuum Generation from Single Gold Nanostructures through Near-Field Mediated Intraband Transitions. *Phys. Rev. B* **2003**, *68* (11), 115433. https://doi.org/10.1103/PhysRevB.68.115433.

(28)   Reineck, P.; Gómez, D.; Ng, S. H.; Karg, M.; Bell, T.; Mulvaney, P.; Bach, U. Distance and Wavelength Dependent Quenching of Molecular Fluorescence by Au@SiO$_2$ Core–Shell Nanoparticles. *ACS Nano* **2013**, *7* (8), 6636–6648. https://doi.org/10.1021/nn401775e.

Chapter Three

Possible Improvements

3.1 Raman signal enhancement by gold nanorods:

Surface plasmon resonance of gold nanorods can be applied to enhance the Raman signal. Raman spectroscopy is associated with the change of polarizability of the molecule. In the presence of nanomaterial, polarizability of a molecule changes as charge is transferred between the molecule and the metal. Surface enhanced Raman scattering follows two mechanisms. Electromagnetic enhancement and chemical enhancement[1]. Electromagnetic enhancement occurs when by using nanoparticles there is a significant overlap between the plasmon band and wavelength of the excitation source, chemical enhancement occurs due to the surface curvature of the nanoparticles. The high enhancement due to surface curvature is known as lightening rod effect.

If the incident light has energy equal to the difference in energy of the molecular orbital of the molecule adsorbed to the nanomaterial and the fermi level of the metal, then Raman enhancement occurs [1].

The type of contact amongst the nanomaterial and the adsorbate has the effect on charge transfer mechanism. For example, the Schottky contact blocks the recombination of electron and hole, whereas the ohmic contact allows the transfer of electrons throughout the interface into the adsorbate [1].

The enhancement in Raman signal can be calculated by the equation of enhancement factor (EF).

$$EF= [I_{SERS}]/ [I_{Raman}] \times [M_{bulk}]/ [M_{ads}]\ [2]$$

Where the number of molecules is represented by M_{bulk}, the number of adsorbed molecules is represented by M_{ads}, intensity of a signal in Raman spectra is I_{Raman} and intensity of a Raman signal in the presence of gold nanorods is I_{SERS} [2]

3.1.1 Chemical enhancement of Raman signal:

For example enhancement of the Raman signal was observed, when 4-MBA formed self- assembled monolayer (SAM) on gold coated glass slide and different nanoparticle solution was added on top of the SAM to compare the Raman signal enhancement of gold nanospheres, gold nanorod of aspect ratio 3.2, gold nanorod of aspect ratio 4.4, gold nanorod of aspect ratio 16, gold nanocubes, gold nanoblocks, gold tetrapods and gold dogbones when 25 mW helium neon laser with a wavelength of 633 nm was applied in the system. The peak at 1070 cm^{-1} which was due to the ring breathing of C-C bond in 4-MBA was compared to measure the enhancement factor. Despite the fact that, the absorption band of gold tetrapods and gold nanorod of aspect ratio 3.2 have the absorption band closer to the wavelength of the laser excitation, the enhancement found was maximum in cases of gold nanocubes, gold blocks and gold dogbones as these nanomaterials have more sharper corners than that of gold tetrapods or gold nanorod of aspect ratio 3.2 [2]. This is a result of chemical enhancement.
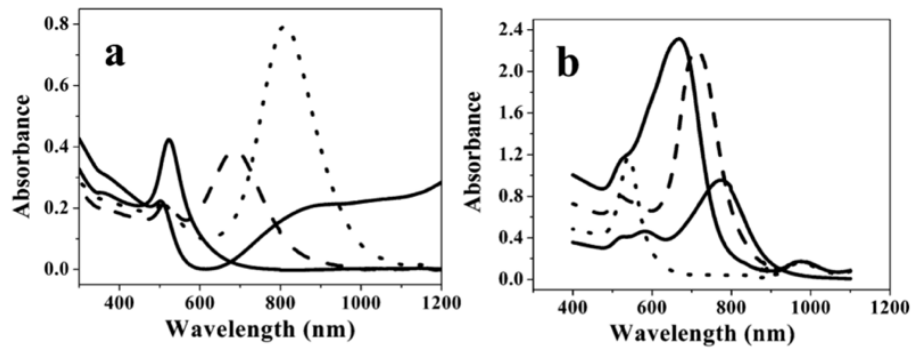
Figure 3. 1 UV-Visible spectrum of   a) gold nanosphere (-), gold nanorod having aspect ratio 3.2

(- - -), gold nanorod having aspect ratio 4.4, gold nanorod having aspect ratio 16 (-), b) gold

dogbones (-), gold cubes (…), gold tetrapods (-) and gold blocks (- - -) [2]

(Reprinted with permission from Ref.2. Copyright © 2005, Analytical Chemistry)
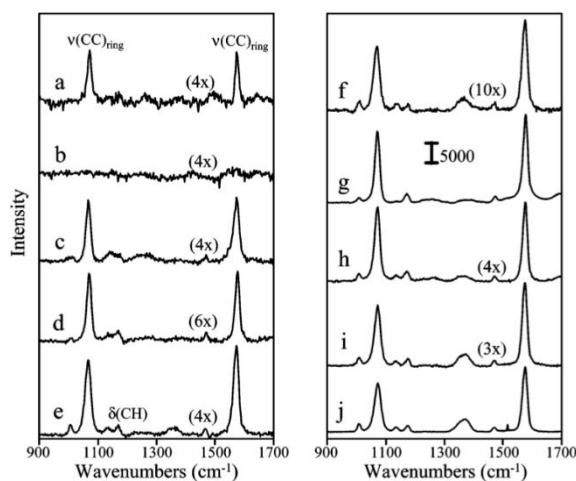
Figure 3. 2 Raman spectrum of a) 4-MBA of concentration 0.01 M, b) SAM of 0.01 M 4-MBA on

gold, c) SAMs of 4-MBA on gold with gold nanospheres, d) SAMs of 4-MBA on gold with gold

nanorod of aspect ratio 3.2, e) SAMs of 4-MBA on gold with gold nanorod of aspect ratio 4.4, f)

SAMs of 4-MBA on gold with gold nanorod of aspect ratio 16, g) SAMs of 4-MBA on gold with

gold nanocubes, h) SAMs of 4-MBA on gold with gold nanoblocks, i) SAMs of 4-MBA on gold

with gold tetrapods, j) SAMs of 4-MBA on gold with gold dogbones [2]

(Reprinted with permission from Ref.2. Copyright © 2005, Analytical Chemistry)

Raman signal enhancement was also observed when the binding of pyridine with

gold nanorods and gold nanoparticles were compared. As gold nanorod has {110} facet which is

absent in gold nanoparticles and which has a higher surface energy, pyridine strongly binds to the

gold nanorods and 10^4-10^5 times enhancement of the ring breathing vibration of pyridine occurs

compared to that of the pyridine bonded to the gold nanoparticles when 1064 nm Nd:YAG laser was used to excite the system [3].

3.1.2 Electromagnetic enhancement of Raman signal:

Raman signal enhancement was also observed for 2,2'-bipyridine, 4-aminobiophenol, 4-mercaptopyridine bonded to gold and silver nanorods of different aspect ratios.[4] In those cases, electromagnetic mechanism acted to have the enhanced Raman signal. For that case dilute solution was used to prevent aggregation of the nanorods. HeNe laser of wavelength 632.8 nm was used to excite the system and the silver nanorod of aspect ratio 10 and gold nanorod of aspect ratio 1.7 showed the maximum enhancement as their absorption band significantly overlapped with the excitation source [4].
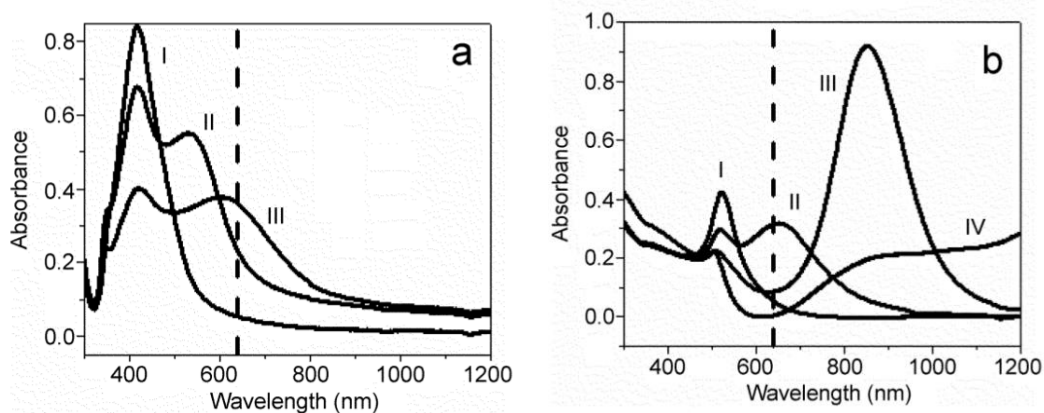
Figure 3. 3 UV-Visible spectrum of a) Ag nanorods of aspect ratio I) 1, II)3.5, III)10, b) Gold nanorod of aspect ratio I)1, II)1.7, III) 4.5, IV)16 [4]

(Reprinted with permission from Ref.4. Copyright © 2006, Physical Chemistry Chemical Physics)

It was found that thiol molecules showed higher Raman enhancement compared to that of 2,2'- bipyridine due to their stronger binding ability with the nanorods due to electrostatic

interaction between negatively charged thiol molecules and positively charged CTAB coating of the nanorods [4].

3.2 ECL enhancement in case of Iridium complexes:

ECL from Iridium complexes can be an alternative to ECL from $Ru(bpy)_3^{2+}$ because they produce ECL of higher quantum efficiency compared to that of the ECL from $Ru(bpy)_3^{2+}$. The high quantum efficiency of Iridium complexes is due to the fact that they can be excited to a triplet state whether ruthenium complexes can be excited to singlet state [5]. Quantum efficiency of $Ru(bpy)_3^{2+}$ complex is 0.05 whether the quantum efficiency of $Ir(ppy)_3^{3+}$ is 0.75.[6] The ECL of $[(ppy)_2Ir(dcbpy)]^+.PF_6^-$ complex (ppy=2-phenylpyridyl; dcbpy=4,4'-dicarboxy-2,2'-bipyridyl) was used to detect the K562 cells.[7] Here the Con A@Au/Ir-MSN nanoprobe was used to be bonded with the mannose group of the K562 cell and resulted the ECL. The ECL of this iridium complex was enhanced due to the presence of material of graphene which has larger surface area.

Here, the mechanism for the ECL reaction was[7]:

$Ir \rightarrow Ir^+ + e^-$

$TPA \rightarrow TPA^{·+} + e^-$

$Ir^+ + TPA \rightarrow Ir + TPA^{·+}$

$TPA^{·+} \rightarrow TPA^· + H^+$

$TPA^· + Ir^+ \rightarrow Ir^* + TPA$

$Ir^* \rightarrow Ir + hv$
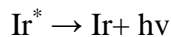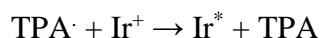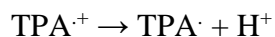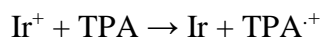
Here, the construction of the nanoprobe was monitored by UV-Visible spectroscopy and fluorescence measurement. Here for the mesoporous silica nanoparticles no absorption band was found which was curve a in the following figure. Au nanoparticle has transverse absorption

133

band at 520 nm which was showed in curve b of the following figure. The characteristic absorption

peak of 258 nm and 369 nm was found for the Ir-complex which was curve c of the figure and

when this Ir complex was added with the nanoprobe curve d was observed. Due to the addition of

Au nanoparticles, the characteristic absorption peak for the Au nanoparticles was also observed

which was curve c. When Au Nps was added to the mixture three peaks, two for the Ir complex

and one for the Au NPs was observed in the UV-Visible spectrum (curve-d). [7]
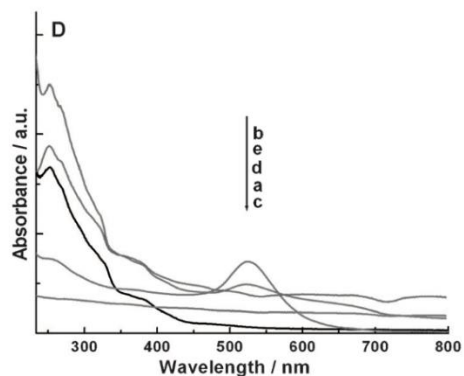
Figure 3. 4 UV-Visible spectrum for the formation of nanoprobe [7]

(Reprinted with permission from Ref.7. Copyright © 2014, Chemistry-A European Journal)

Also, in the fluorescence spectroscopy it was found that, there was no

luminescence for the mesoporous silica nanoparticles alone (curve a). However, for the Ir complex

a luminescence peak at 575 was observed (curve b) which was also present when Ir complex was

added with mesoporous silica nanoparticles (curve c). [7]

Similarly, Ru nanoprobe complex was formed to compare the ECL with that of Ir nanoprobe complex. ECL experiment was done for both the complexes when TPA was present as the co-reactant and it was found that ECL found from Ir-nanoprobe was 24 times larger than the ECL observed from Ru-nanoprobe [7].

The ECL of other Ir complex such as $(pq)_2Ir(acac)$, $(pq)_2Ir(tmd)$, $(ppy)_2Ir(phen)^+$, $(ppy)_2Ir(bpy)^+$ was also compared to that of the ECL from $Ru(bpy)_3^{2+}$ [8]. It was found that due to the higher oxidation potential and the closeness of the HOMO of the TPA to that of the LUMO of the emitter 77 times and 49 times higher ECL was observed for $(pq)_2Ir(acac)$ and $(pq)_2Ir(tmd)$ complexes compared to that of the $Ru(bpy)_3^{2+}$ complex respectively. But due to the rigidity of the phenyl groups, the ECL of $(pq)_2Ir(acac)$ and $(pq)_2Ir(tmd)$ was just 2 and 4 times higher than that of the $Ru(bpy)_3^{2+}$ complex.
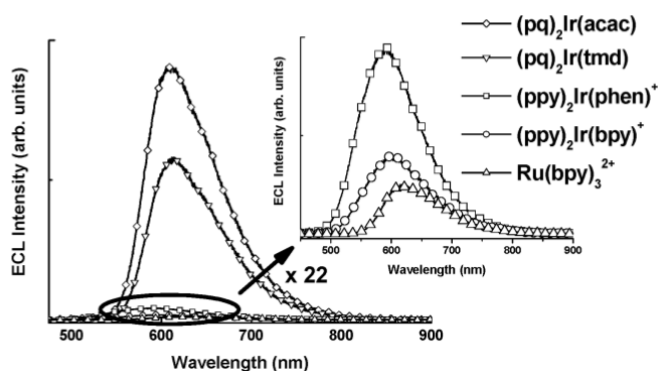
Figure 3. 6 Comparison of the ECL spectrum of $Ru(bpy)_3^{2+}$ complex to that of the IR complex [8]

3.3 Directional ECL enhancement of Ru(bpy)₃Cl₂:

The longitudinal band of the gold nanorod can enhance the electromagnetic field and to excite the longitudinal band the excitation light needs to be parallel to the length axis and the scattering from the gold nanorod is also parallel to the length axis of the gold nanorod [9]. So, the fluorescence can be turned on and off by changing the angle of excitation light [9].
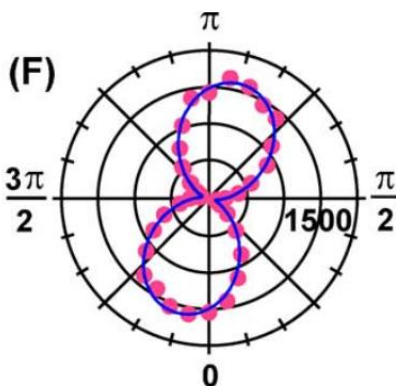
Figure 3. 7 Change of fluorescence intensity with the variation of excitation light angle [9]

(Reprinted with permission from Ref.9. Copyright © 2010, Nano Today)

This dependence of ECL enhancement on the direction of longitudinal band of gold nanorod can be controlled for single molecular experiment. In the presence of multiple molecules in the solution it is difficult to have the p-polarised excitation for all the molecule as in the solution molecules can have different orientations. So, to observe enhancement it is important to work with single molecule and to excite the molecule in a direction parallel to the longitudinal plasmonic band of the gold nanorods. [9]

3.4 Alternatives to gold nanorods to get ECL enhancement:

3.4.1 Use of silver nanorods instead of gold nanorods to get ECL enhancement:

By using silver nanorods instead of gold nanorods it is possible to get much higher enhancement. As the interband transition is in higher energy, Ag nanospheres show

strongest electric field compared to that gold and Cu. The interband transition in case of Au nanospehere is at 530 nm and the plasmonic band is at 520 nm, so there is resonance damping in the Au nanospheres and again same problem happened in the case of Cu [10].
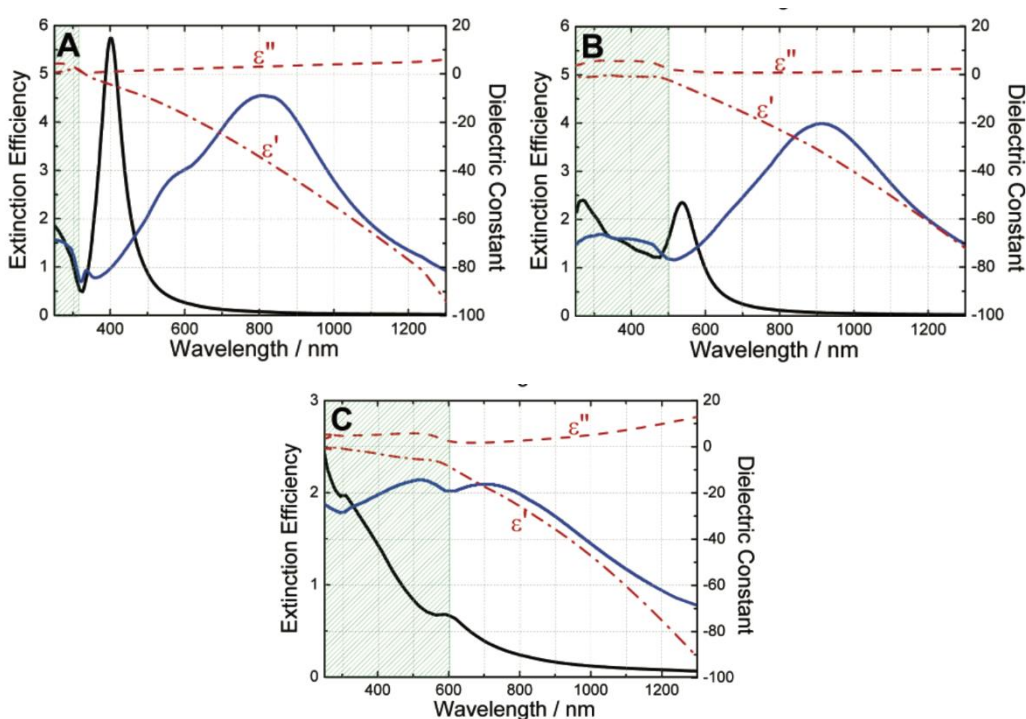
Figure 3. 8 UV-Visible spectrum of A) Ag nanosphere (black), nanoshell (blue), B) Gold nanosphere (Black), nanoshell (blue), C) Cu nanospehere(black), nanoshell (blue) [10]

(Reprinted with permission from Ref.10. Copyright © 2005, Physical Chemistry)

Also, based on the comparison of the electronegativities of Ag, S and Au it can be postulated that the Ag-S bond is more ionic compared to that of the Au-S bond. So, upon adsorption of the monolayers, the change of charge distribution was higher than that of Au.[11]

Silver nanospheres shows higher Raman sensitivity than gold nanosphere as in silver nanosphere the interband transition region is at lower wavelength compared to the plasmonic band so there is no overlap of the plasmonic band with that of the interband transition so there is

no plasmonic damping but in case of gold nanosphere due to overlap of the plasmonic band and interband transition damping of the plasmon and a lowering of the electric field occurs.[12] However, the interband transition does not impact the electric fields of silver or gold nanorods as the longitudinal band of silver nanorods and gold nanorods are at much higher wavelength compared to that of the interband transition region. However, the plasmonic band is sharper in silver than that of gold. So, oscillation of conduction electrons due to the incident light occurs for a longer time in silver. So, from the DDA calculation it was found that electric field in silver nanorods is five time higher than that of gold nanorod. Moreover, due to the incident light's surface plasmon resonance effect, the probability of scattering is higher in gold compared to the light absorption, but the opposite trend is true for silver. So, upon irradiation with laser gold nanorod looks brighter than that of silver nanorod. [12]
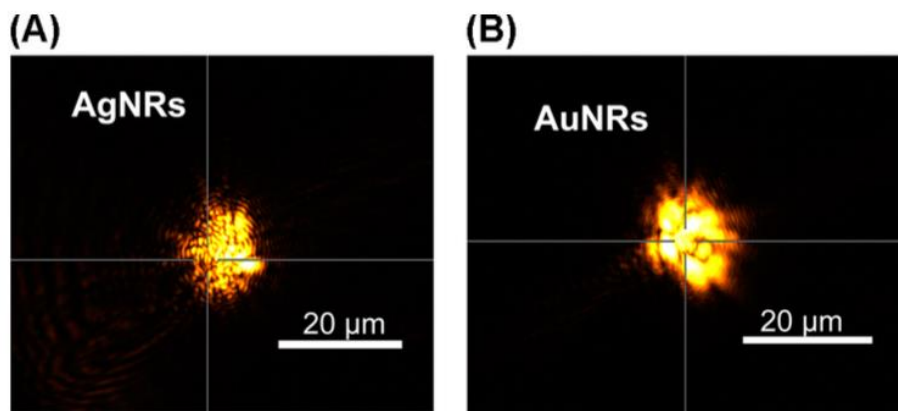
Figure 3. 9 Scattering form A) AgNRs and B) AuNRs upon irradiation by laser [12]

(Reprinted with permission from Ref.12. Copyright © 2013, Physical Chemistry Letters)

However, the problem dealing with silver nanorods are that silver nanorods of small aspect ratio are not stable in light due to the tendency of oxidation of the Ag to Ag^+ [13]

3.4.2: Surface plasmon polaritons to get ECL enhancement:

ECL can also be enhanced by surface plasmon polaritons generated in the metallic surface by grating or prism. If we compare the LSPR with propagating surface plasmon, then we find that, peak in propagating surface plasmons are narrow and the phase lag is long whether the peak in localized surface plasmon resonance is broad and there is an electric field which is concentrated in both sides of the grooves.[14]

When light incidents on a metallic surface it cannot generate surface plasmon polaritons as the wavevector of the incident light and the wavevector of the plasmon is different. So, to match the wavevectors prism or grating can be used. SPR occurs when there is a parallel relationship between the wavevector of the incident light and the metallic plane. This light is known as p polarized light. But when there is a perpendicular relationship between the wavevector of the incident light and the metallic surface, then the light is known as s polarized light and for the s polarized light, surface plasmon resonance does not occur.[15]

The surface plasmon polaritons are generated when the wavevector of the surface plasmon k_{sp} equals to the wavevector of the incident light k_x based on the following equation-

$K_{sp} = k_x = k_0 np \sin \theta_{sp}$ [15]

$Sin\theta_I$ is the modification parameter which should be achieved by introducing prism or grating for surface plasmon resonance to occur. [15]
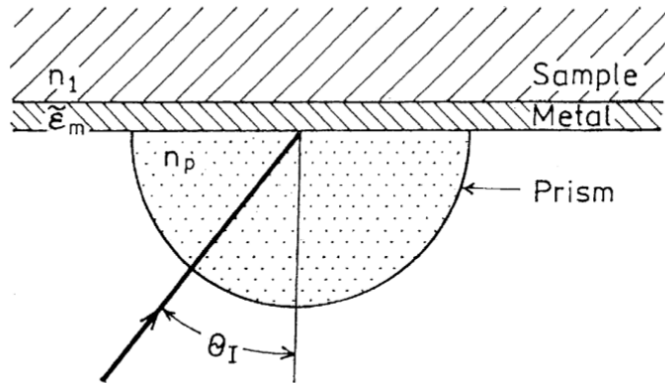
Figure 3. 10 Surface plasman polariton instrumentation [15]

(Reprinted with permission from Ref.15. Copyright © 2004, Chemical Physics Letters)

When the incident light couples to the metallic surface through prism, it completely gets reflected in the interface of prism-metal layer and an evanescent wave is generated which moves through the interface. This phenomenon is applied in Attenuated Total Reflection method.
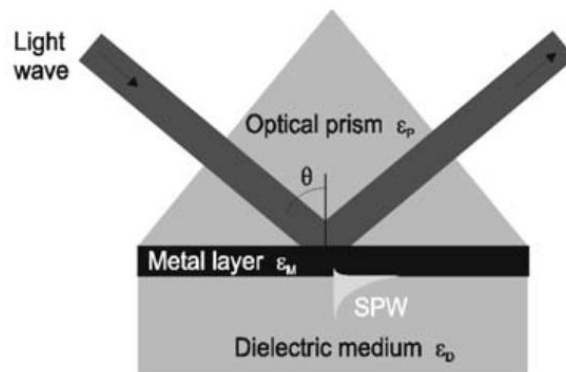
Figure 3. 11 Instrumentation of Attenuated Total Reflection [15]
(Reprinted with permission from Ref.15. Copyright © 2004, Chemical Physics Letters)

In the diffraction grating method, the waves that are diffracted and parallel to the metallic surface is increased and the enhancement is inversely proportional to the number of gratings.
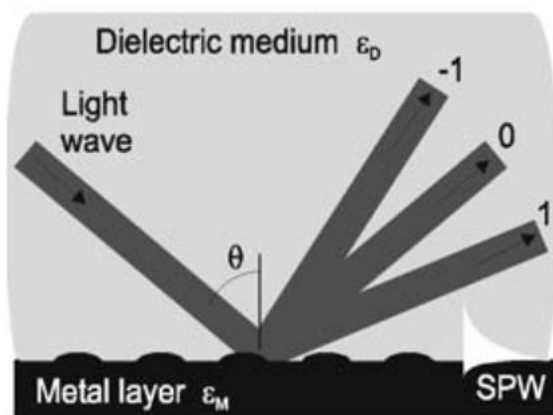
Figure 3. 12 Instrumentation for the diffraction grating [15]

(Reprinted with permission from Ref.15. Copyright © 2004, Chemical Physics Letters)

Fluorescence of a molecule can be enhanced by using diffraction grating. For example, the fluorescence of R6G was enhanced by using Ag grating. R6G shows an absorption band at 540 nm and emission band at 550 nm.[16] By changing the period of grating it is possible to change the incidence angle and emission angle which can cause the enhancement based on surface plasmon polariton. [16]

Both the enhancement due to absorption band and emission band was observed for Rhodamine 6G dye on Ag grating and two types of grating with different periods of 300 nm and 375 nm were compared to observe the fluorescence enhancement. [16]
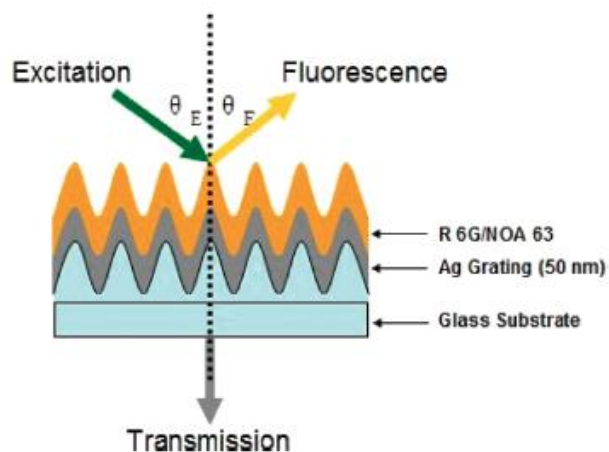
Figure 3. 13 Fluorescence enhancement of R6G dye by surface plasmon polariton technique [16]

(Reprinted with permission from Ref.16. Copyright © 2011,Physical Chemistry)

When light of 539 nm wavelength was incident onto the Rhodamine 6G sample over the Ag grating having a period of 300 nm, enhancement was observed with a maximum of 14 times compared to that of the bare 300 nm grating when the incident light angle, θ_E was 5^0 relative to the plane of the grating which was observed at the transient absorption spectra of the grating system. The enhancement was observed to decrease with the increase of angle, as in the incidence angle of 5^0 surface plasmon polariton occurred, so enhancement found was maximum. This type of trend was also observed in spectrum of decay rate with the maximum decay occurred when light was absorbed by the Ag grating due to surface plasmon polariton. And the maximum enhancement found in the decay rate was two times compared to that of the decay rate for the grating without the presence of metallic Ag [16].
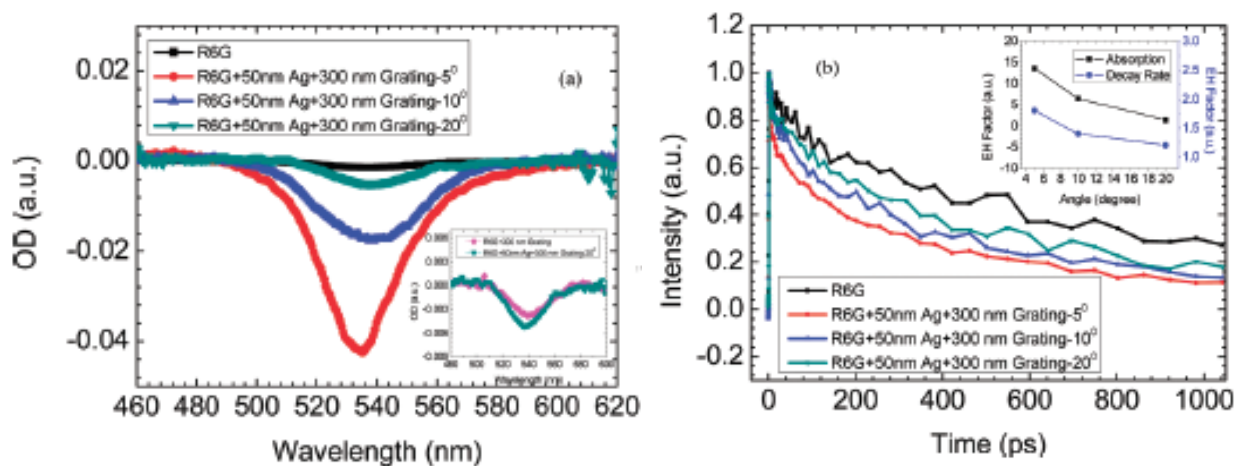
Figure 3. 14 a) Transient absorption spectra, b) spectrum of decay rate of fluorescence for the Rhodamine 6G molecule coated on Ag grating having a period of 300 nm [16].

(Reprinted with permission from Ref.16. Copyright © 2011,Physical Chemistry)

Similarly, for the grating having a period of 350 nm, maximum enhancement in the transition spectra was observed for an incident light angle, θ_E of 23^0 compared to the plane of grating and the decay rate found was maximum for that angle of 23^0. However, the overall enhancement found for the grating having a period of 375 nm was less than that of grating of period 300 nm, as the coupling between the incident light and frequency of the oscillation of conduction electrons was weaker [16].
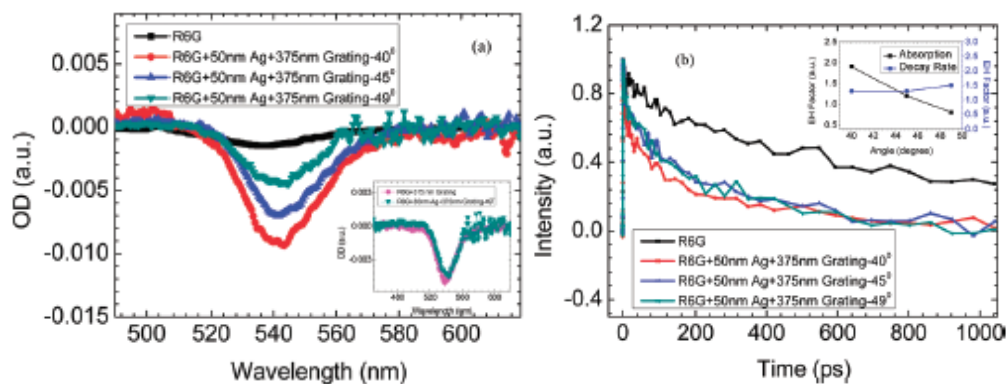
Figure 3. 15 a) Transient absorption spectra and b) Spectrum of decay rate of fluorescence for Rhodamine 6G coated on Ag grating of period 375 nm [16]

The fluorescence peak for the Rhodamine 6G was observed at the wavelength of 552 nm and for the grating of period of 300 nm. Maximum fluorescence was observed when the emission light formed an angle of 23^0 relative to the plane of the grating and the area of the peak was found to be enhanced 9 times and the intensity of the peak was found to be enhanced 10 times compared to that of the fluorescence found from the grating without the Ag metal [16].
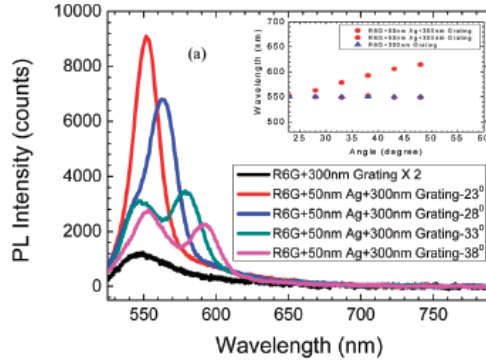
Figure 3. 16 Fluorescence spectrum of Rhodamine 6G in the presence and in the absence of Ag grating having 300 nm period [16]

(Reprinted with permission from Ref.16. Copyright © 2011,Physical Chemistry)

Similarly, the fluorescence enhancement was also observed for the grating having period of 375 nm. The maximum enhancement was observed when the emitted light formed an angle of 5^0 compared to the surface of the grating. The fluorescence peak area was found to be enhanced 30 times and fluorescence peak intensity was found to be enhanced 60 times compared to that of the grating without the Ag metal. The higher enhancement of fluorescence in case of the grating of 375 nm period was because of the fact that higher percentage of spectral overlap amongst the surface plasmon polaritons and peak of the fluorescence spectrum which is the basis of surface plasmon coupled emission to occur [16].
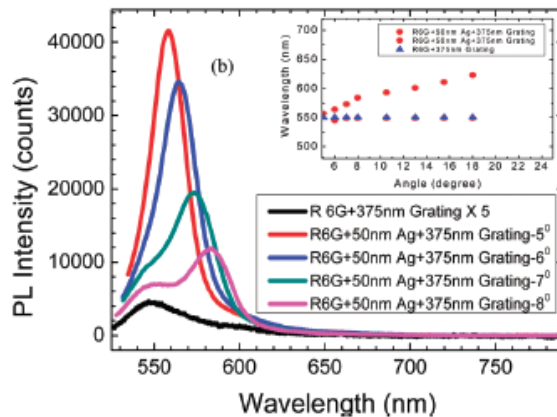
Figure 3. 17 Fluorescence spectrum of Rhodamine 6G in the presence of Ag grating having a period of 375 nm [16]

(Reprinted with permission from Ref.16. Copyright © 2011,Physical Chemistry)

When a fluorophore is excited through a prism (Kretchman configuration) or excited through air (Reverse Kretchman configuration), bright emission from the fluorophore can be observed which can go back to the prism and the prism can re-emit the radiation which is p-polarised and can form a symmetrical cone surrounding the plane perpendicular to the prism. This re-emitted radiation is known as surface plasmon coupled emission [17].
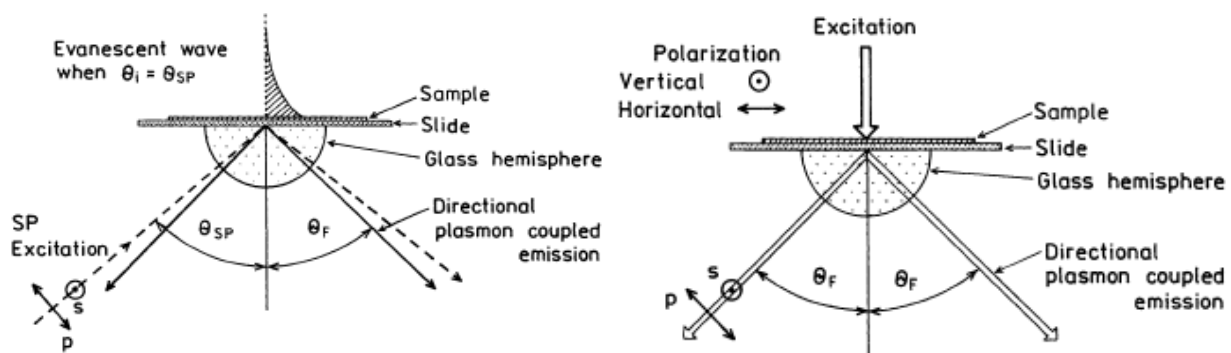
Figure 3. 18 SPCE from Kretchmann configuration (left) and Reverse Kretchmann configuration (Right) [17]

(Reprinted with permission from Ref.17. Copyright © 2004,Physical Chemistry)

The angle created in surface plasmon coupled emission is dependent on the thickness of the dye layer absorbed on the prism. And interestingly, the polarization dependence of the SPCE also changed with the thickness of the PVA attached to 50 nm silver film on prism. For example, when the thickness of the PVA film was 290 nm, then both the p-polarization dependence and s-polarization dependence of the SPCE was observed [17].

145
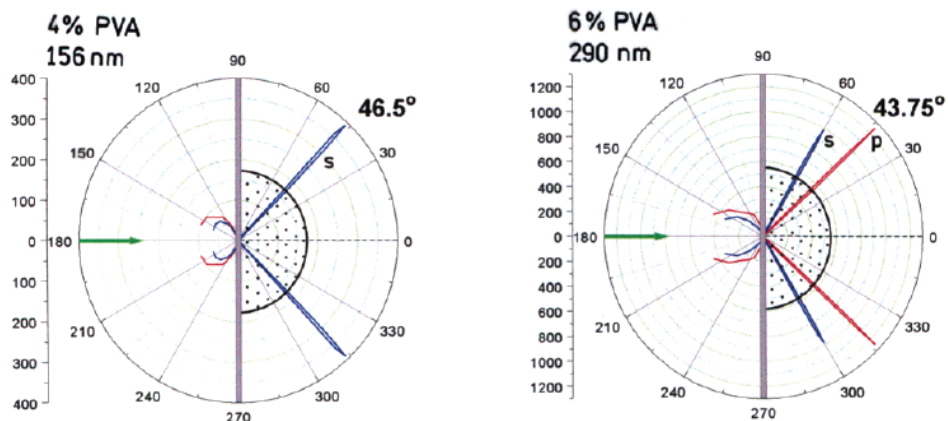
Figure 3. 19 Change of polarization dependence of the SPCE with the change of thickness of PVA film [17]

(Reprinted with permission from Ref.17. Copyright © 2004,Physical Chemistry)

So, two types of alternate SPCE ring was observed in the photographs. [17]
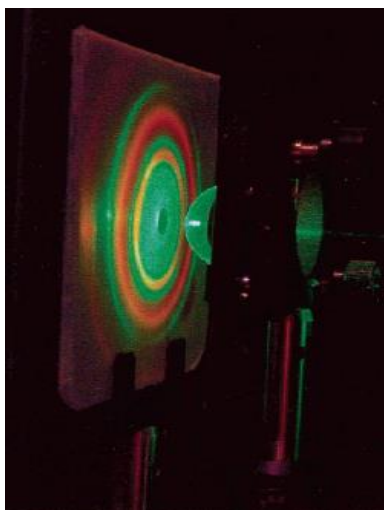
Figure 3. 20 Surface plasmon coupled emission observed for PVA of 290 nm thick attached to Ag metal on prism [17]

(Reprinted with permission from Ref.17. Copyright © 2004,Physical Chemistry)

By using different polarizers, the two types of rings were separated. [17]

s oriented polarizer   p oriented polarizer
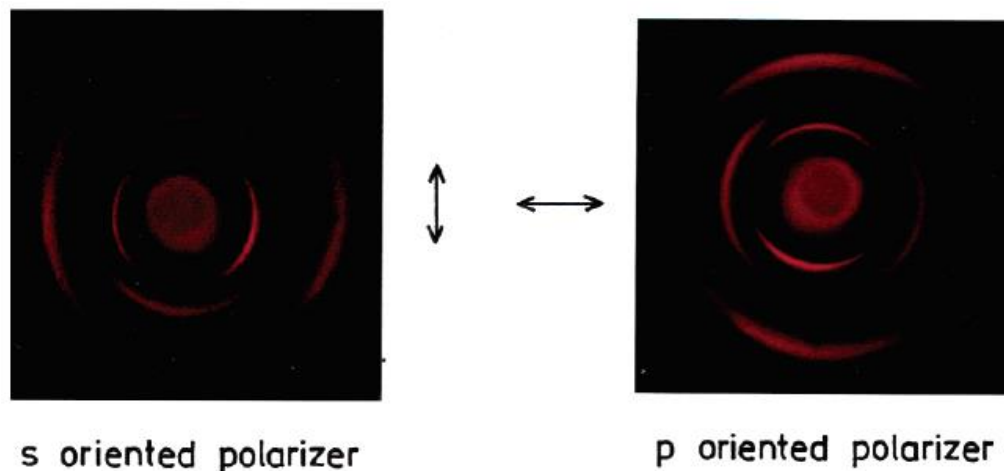
Figure 3. 21 SPCE from a horizontal polarizer (left), SPCE from a vertical polarizer (Right) [17] (Reprinted with permission from Ref.17. Copyright © 2004,Physical Chemistry)

Self-assembled monolayer system can be useful to attach gold nanorods with the gold electrode and to observe the surface plasmon resonance enhancement of the ECL. By employing different types of self-assembled monolayer system and also by changing the thickness of the gold nanorods along with replacing CTAB of the gold nanorods by other reagents like mercapto-carboxylic acids, DNA it is possible to control the distance between the gold nanorods and gold electrode which is a critical parameter to observe enhancement in the ECL signal of $Ru(bpy)_3Cl_2$

3.5 Self-assembled monolayer for a better control of distance:

The process of formation of nanometer sized layers from a reagent is known as self-assembled monolayer. The reagent taking part in self-assembly process forms a complex layer. The molecules in the self-assembled monolayer have a linking group, a main chain and an active group. The headgroup forms a bond with the attached metal surface, the main chain helps to pack the monolayer and the stability of the monolayer is also dependent on the main chain and

the property of the monolayer, it can be cationic or anionic depending on the terminal active group and based on the terminal group, so molecules can bind to the surface of the monolayer. The stability of the monolayer is also dependent on the type of the gold substrate. The adsorption time of the monolayer is different, where alkanethiols having long chain can form the monolayer within 2-12 hours, on the other hand, alkanethiols having short chains can form the monolayer by 24 hours.[18] The alkanethiols having long chain are found to form more stable self-assembled monolayer system.[19] The adsorption process of the monolayer involves, physisorption of the monolayer and then chemisorption process of molecules involves in the formation of self-assembled monolayers and at the final stage crystalline monolayers form. Alkanethiols by their tendency to form vander waals interaction with the physisorbed surface and with their sulfur headgroups can be chemisorbed on to the attached surface are considered to be an excellent candidate to form self-assembled monolayers on gold surface [18].
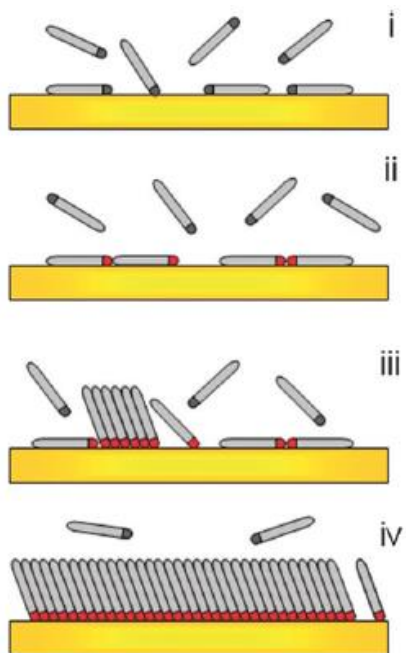
Figure 3. 22 Stepwise formation of self-assembled monolayer system [18]

(Reprinted with permission from Ref.18. Copyright © 2010, Chemical Society Review)

The reaction involving the absorption of thiols is [20]-

$$2RSH + 2Au \rightarrow RSSRAu_2$$
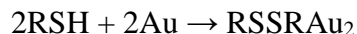
Thiols are absorbed as the form of disulfides and the desorption of the disulfide can occur by the process [20]

$$RSSRAu_2 \rightarrow RSSR + 2Au$$
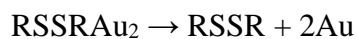
To destroy the monolayer of thiols and to get the electrode in its initial state piranha solution can be used. If the electrode with the thiol monolayer is soaked under piranha solution for ten minutes 98% thiol monolayer can be removed. On the other hand, if the thiol monolayer is exposed in the UV then, the sulfur of the thiol can be converted to sulfoxide, which can further be converted to sulfates. Rinsing the electrode with water can remove the sulfates.[20] SAMs can also be destroyed by applying potential. For example, SAM of thioctic acid on gold electrode can be damaged by applying triple pulse potential of (+1.6, 0.0, -0.8 V) each for 100 ms.[19]

From the measurement of the surface coverage, the alignment of the thiols can be assumed. The thiols have the upright alignment, however the dithiols due to its two –SH group can form bond with the attached gold electrode with its two thiol groups, as a result they tend to form loop conformation resulted in the lying down conformation of the dithiols. This is especially true for the case of long chain thiols. However, for hexanedithiol as it is short chained, the dithiol was found to form upright conformation as was found when reduction peak of hexanethiol and hexanedithiol were compared.[21]However, contradictory theory was also found that short chain alkanethiols forming self-assembled monolayer that is lying down conformation [18].
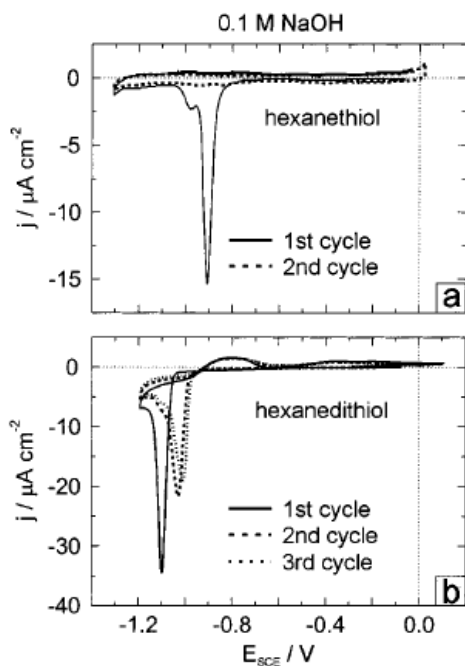
Figure 3. 23 CV of a) haxanethiol, b) haxanedithiol on Au (111) [21]

(Reprinted with permission from Ref.21. Copyright © 2001, Langmuir)

The thiols can be arranged depending on the time involved in the thiol formation process, length of the hydrocarbon chain, types of terminal group involved in the reagent molecule, purity of the surface also temperature of the reagent solution. The terminal groups such as –SH, -COOH, -OH, -NH_2 reduces the homogeneity of the SAM on the surface [18].

In the complex of gold nanorods attached to gold electrode by a self-assembled monolayer, the electrochemical process used to occur by three steps: gold nanorods gets charged up by consuming electrons from the electrochemical solution, electron moves across the nanorod and electron moves through the self-assembled monolayer towards the gold electron by forming tunnels [22].
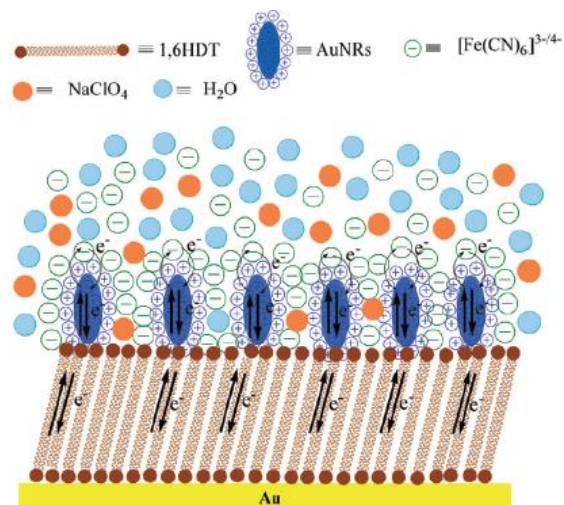
Figure 3. 24 Electronic movement from the electrolyte solution toward the electrode in a self-assembled monolayer system [22]

(Reprinted with permission from Ref.22. Copyright © 2017, American Chemical Society)

From the comparison of the CV responses and integration of the reduction peak of gold nanorod modified electrode and normal gold electrode in 1 M H_2SO_4, it is possible to find the surface area enhancement due to gold nanorod compared to the planer gold electrode [23].
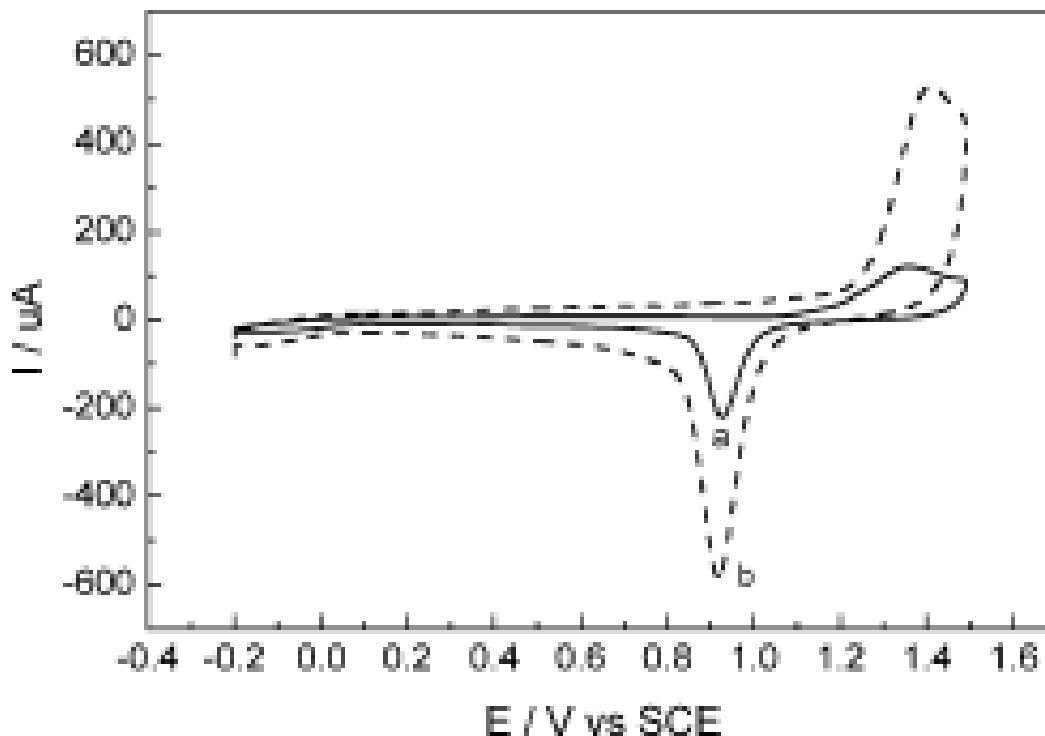
Figure 3. 25 Comparison of CV of (a) normal gold electrode and (b) gold nanorod modified electrode in 1 M H$_2$SO$_4$ [23]

(Reprinted with permission from Ref.23. Copyright © 2005, Electrochimica Acta)

The reduction process belongs to the reaction

RS-Au + e$^-$ → RS$^-$ [18]
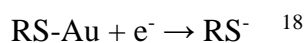
CTAB coated gold nanorods can be bonded to the gold electrode by electrostatic interaction or by forming covalent bonds.

For example, mercaptohexanoic acid with its thiol group can be bonded with the hydrophobic surface of planer gold electrode and with its carboxylic acid group which is deprotonated at a pH=6.5. At this stage, mercaptohexanoic acid can be bonded with the positively charged CTAB group of the gold nanorod, in this way a sandwich structure between gold electrode

and CTAB coated gold nanorods can be formed by 16-mercaphexanoic acid self-assembled monolayer system. [24]
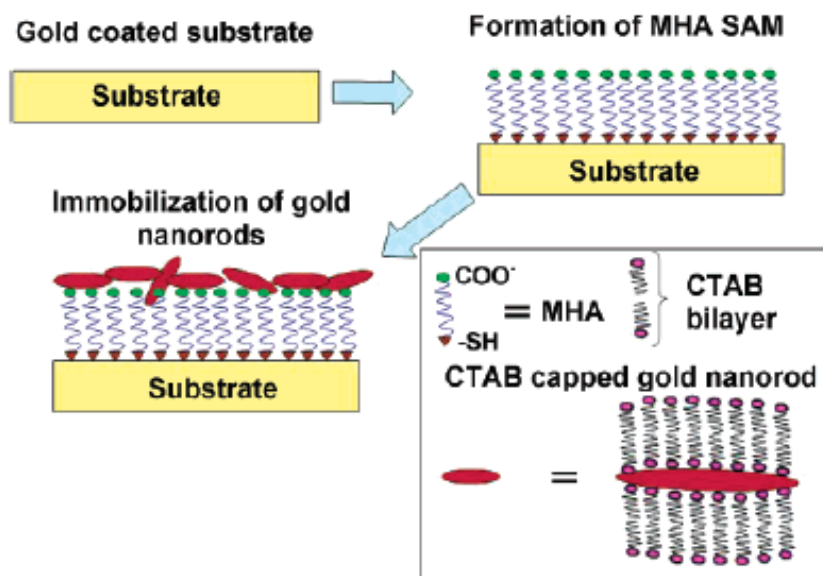
Figure 3. 26 Formation of sandwich structure between gold coated glass slide and CTAB coated gold nanorods by 16-Mercaptohexanoic acid [24]

(Reprinted with permission from Ref.24. Copyright © 2004, American Chemical Society)

The immobilization of gold nanorods toward the gold electrode can be characterized by AFM and FTIR methods. The gold nanorods are sensitive towards the pH change of the solution. At higher pH gold nanorods tend to form aggregates, as the ionic strength of the solution increases [24].

Similar electrostatic interactions can also be observed for adipic acid, which can aggregate gold nanorods by forming electrostatic interactions with the positively charged CTAB coated gold nanorods by having carboxylic terminals in both of their ends at a pH of 7, when the molecules are completely deprotonated. Similar effect was not observed for hexanoic acid as the molecule of hexanoic acid have just one carboxylic acid at one end also the effect was not true for

dodecanedioic acid, even though they have two carboxylic acids at two ends but due to their higher length, dodecanedioic acid forms loop conformation, so both of the terminal's carboxylic groups tend to form bond with the same gold nanorod. [25]
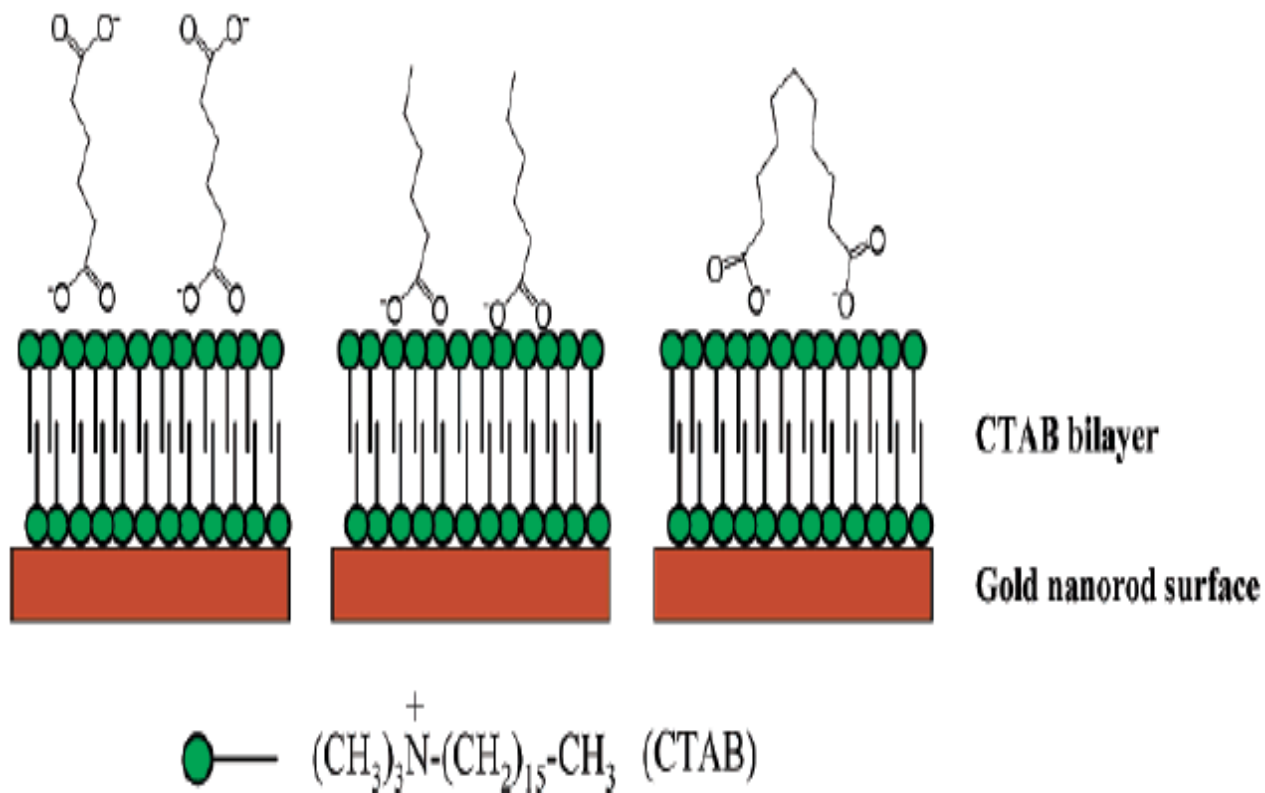
Figure 3. 27 Adsorption process of adipic acid (left one), hexanoic acid (middle one), dodecanedioic acid (right one) on the surface of CTAB coated gold nanorods [25]

(Reprinted with permission from Ref.25. Copyright © 2005, Langmuir)

This electrostatic interaction can be used to form alternate coatings of anionic surfactant, poly(sodium-4-styrenesulfonate) and cationic surfactant, PDDA on the positively charged CTAB coated gold nanorods [26]. In this way, it is possible to change the distance between the gold nanorods and the gold electrode which is a crucial factor for observing enhancement in the ECL due to surface plasmon resonance. The gold nanorods can be bound to the oppositely

154

charged glass slides either by cationic or anionic interactions. Here, PSS and PDDA was chosen to coat the nanorod as their chain length matched with the dimension of the nanorods. Salt was added so that the polymers can perfectly wrap around the nanorods.
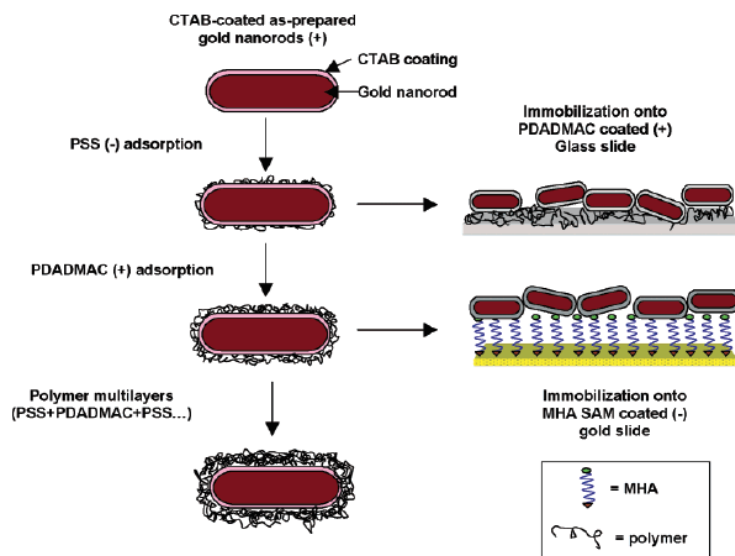
Figure 3. 28 Multiple coating phenomena on gold nanorods by alternating layers of PSS and PDDA[26]

(Reprinted with permission from Ref.26. Copyright © 2005, American Chemical Society)

3.6 Exchanging CTAB of gold nanorods to control the distance of Ru(bpy)$_3$Cl$_2$ with gold nanorods:

Replacement of CTAB can be done by exchanging the CTAB with other ligands. For that process, gold nanorods used to be dissolved in a solvent which increases the CMC of CTAB, which can result in precipitation of the nanorods. Afterwards, the precipitates can be dissolved in organic solvent. For example, CTAB coated gold nanorods were reacted with dodecanethiol (DDT) in acetone which formed DDT coated gold nanorod in the organic phase and the colorless CTAB solution was formed in the aqueous phase.[27] The DDT coated gold nanorods

were further treated with mercaptocarboxylic acids of different chain lengths in toluene as a result, gold nanorods were coated with carboxylic groups and were able to be dissolved in buffer system of tris-borate-EDTA complex.[27] The carboxylic acid group of the gold nanorods can be further transferred by PEG, thiolated DNA molecules [27]. The carboxylic acid can be activated to form NHS ester which can react with antibody such as anti-cTnl molecule. [28]

Figure 3. 29 A) Replacement of CTAB of gold nanorods by different ligands, B) Change of absorption band of gold nanorod upon changing the coating ligand from CTAB to MUDA [28]

(Reprinted with permission from Ref.28. Copyright © 2013, Angewandte Chemie)

CTAB ligand can also be exchanged by the reaction between thiolated DNA and CTAB coated gold nanorods at a molar ratio of 1000 molecules of DNA to 1 molecule of CTAB coated gold nanorod in a buffer solution composed of 0.02% Sodium dodecyl sulfate, Tris/borate/EDTA complex and 500 mM NaCl.[29] After shaking the mixture for 10 minutes and

centrifugation, the precipitate was dispersed in the buffer system. This process formed thiolated

DNA coated gold nanorods [29].
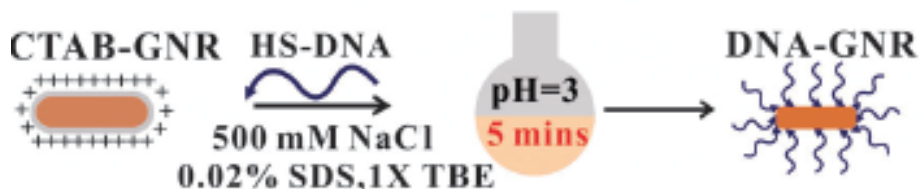
Figure 3. 30 Process of replacement of CTAB by DNA in gold nanorods [29]

(Reprinted with permission from Ref.29. Copyright © 2013, Royal Society of Chemistry)

When CTAB is replaced by DNA, the number of DNA that can be attached to the surface of the gold nanorods can be effected by the concentration of salt added [30].
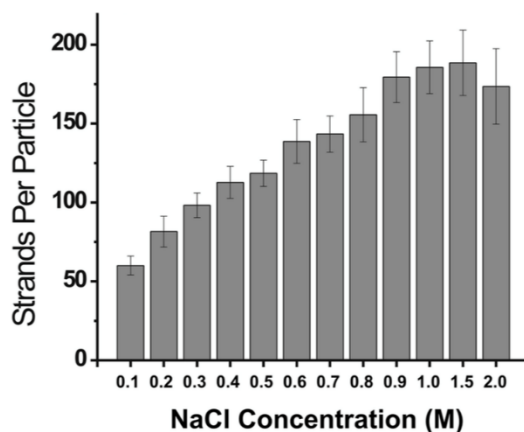
Figure 3. 31 Variation of the numbers of DNA that can be bonded with the gold nanorod upon change of salt concentration [30]

(Reprinted with permission from Ref.30. Copyright © 2009, ACS Nano)

Upon changing the ligand of the gold nanorods, thickness of the gold nanorods changes. For example, CTAB has a thickness of about 3.9 nm, but when PSS is added to the CTAB

coated gold nanorod solution, then thickness of the gold nanorods changes to about 5.9 nm. Again, when CTAB is replaced by mercaptoundecanoic acid, then the thickness of the gold nanorod changed to 1.69 nm [28].

Figure 3. 32 Changes of the thickness of the gold nanorods upon changing the ligands [28]
(Reprinted with permission from Ref.28. Copyright © 2013, Angewandte Chemie)

CTAB can be replaced by thiolated PEG but due to the large size of the thiolated PEG, it cannot totally replace the CTAB also due to the large size of thiolated PEG it increases the distance between the analyte and the gold nanorod. So, instead of thiolated PEG, 11-mercaptoundecanoic acid and cysteamine can be used to replace CTAB [31].

It is possible to monitor the ligand exchange process by ^{1}H NMR. The peak of 1.3 ppm in the NMR spectrum due to the –CH_2- group and the peak at 3.1 ppm in the NMR spectrum due to the –$N(CH_3)_3$- group, characteristic of the CTAB coated gold nanorod can be disappeared when molecules like dodecanethiol replaces CTAB from the gold nanorod. The removal of CTAB can also be monitored by the complete removal of m/z=284.33 peak in the mass

spectrum of gold nanorod when molecule like dodecanethiol reacts with the CTAB coated gold nanorods in acetone [27].

To avoid aggregation of the gold nanorod, after the replacement of CTAB temperature of the solution should be increased, but too much high temperature can cause flocculation of the gold nanorods. The gold nanorod solution can be sonicated as well to avoid the aggregation to formed [32].

The thermal conductance of the gold nanorods can be determined by a term, G. Hydrophobic ligands such as CTAB and mercaptocarboxylic acids prevent water to flow to the gold nanorod core. On the other hand, hydrophilic ligands such as PEG, polyelectrolyte ligands tend to allow water to flow to the gold nanorod core which forms an ordered structure. So, transport of heat is easier when gold nanorods are coated by hydrophilic ligands compared to that of the hydrophobic ligands [33].

It is also possible to attach thiolated DNA with the gold electrode. For example, the o-quinones functionalized gold electrode which was formed by electrochemical oxidation of catechol attached to the gold electrode. By the conjugation of the terminal aniline with that of the o-quinones, it is possible to attach DNA on the surface of the gold electrode. Due to the possible interactions of DNA bases with the metal surface, functionalized DNA can be used to form self-assembled monolayer on the gold surface [22].

Reference 3:

(1)   Zhan, C.; Chen, X.-J.; Yi, J.; Li, J.-F.; Wu, D.-Y.; Tian, Z.-Q. From Plasmon-Enhanced Molecular Spectroscopy to Plasmon-Mediated Chemical Reactions. *Nat. Rev. Chem.* **2018**, *2* (9), 216–230. https://doi.org/10.1038/s41570-018-0031-9.

(2)   Orendorff, C. J.; Gole, A.; Sau, T. K.; Murphy, C. J. Surface-Enhanced Raman Spectroscopy of Self-Assembled Monolayers: Sandwich Architecture and Nanoparticle Shape Dependence. *Anal. Chem.* **2005**, *77* (10), 3261–3266. https://doi.org/10.1021/ac048176x.

(3)   Nikoobakht, B.; Wang, J.; El-Sayed, M. A. Surface-Enhanced Raman Scattering of Molecules Adsorbed on Gold Nanorods: Off-Surface Plasmon Resonance Condition. *Chem. Phys. Lett.* **2002**, *366* (1–2), 17–23. https://doi.org/10.1016/S0009-2614(02)01492-6.

(4)   Orendorff, C. J.; Gearheart, L.; Jana, N. R.; Murphy, C. J. Aspect Ratio Dependence on Surface Enhanced Raman Scattering Using Silver and Gold Nanorod Substrates. *Phys Chem Chem Phys* **2006**, *8* (1), 165–170. https://doi.org/10.1039/B512573A.

(5)   Nishimura, K.; Hamada, Y.; Tsujioka, T.; Shibata, K.; Fuyuki, T. Solution Electrochemiluminescent Cell Using Tris(Phenylpyridine) Iridium. *Jpn. J. Appl. Phys.* **2001**, *40* (Part 2, No. 9A/B), L945–L947. https://doi.org/10.1143/JJAP.40.L945.

(6)   Kapturkiewicz, A.; Angulo, G. Extremely Efficient Electrochemiluminescence Systems Based on Tris(2-Phenylpyridine)Iridium(Iii). *Dalton Trans.* **2003**, No. 20, 3907. https://doi.org/10.1039/b308964a.

(7)   Zhou, H.; Yang, Y.; Li, C.; Yu, B.; Zhang, S. Enhanced Iridium Complex Electrochemiluminescence Cytosensing and Dynamic Evaluation of Cell-Surface Carbohydrate Expression. *Chem. - Eur. J.* **2014**, *20* (45), 14736–14743. https://doi.org/10.1002/chem.201403470.

(8)   Kim, J. I.; Shin, I.-S.; Kim, H.; Lee, J.-K. Efficient Electrogenerated Chemiluminescence from Cyclometalated Iridium(III) Complexes. *J. Am. Chem. Soc.* **2005**, *127* (6), 1614–1615. https://doi.org/10.1021/ja043721x.

(9)   Chen, H.; Ming, T.; Zhao, L.; Wang, F.; Sun, L.-D.; Wang, J.; Yan, C.-H. Plasmon–Molecule Interactions. *Nano Today* **2010**, *5* (5), 494–505. https://doi.org/10.1016/j.nantod.2010.08.009.

(10)   Wang, H.; Tam, F.; Grady, N. K.; Halas, N. J. Cu Nanoshells: Effects of Interband Transitions on the Nanoparticle Plasmon Resonance. *J. Phys. Chem. B* **2005**, *109* (39), 18218–18222. https://doi.org/10.1021/jp053863t.

(11)   Hutter, E.; Fendler, J. H.; Roy, D. Surface Plasmon Resonance Studies of Gold and Silver Nanoparticles Linked to Gold and Silver Substrates by 2-Aminoethanethiol and 1,6-Hexanedithiol. *J. Phys. Chem. B* **2001**, *105* (45), 11159–11168. https://doi.org/10.1021/jp011424y.

(12)   Mahmoud, M. A.; El-Sayed, M. A. Different Plasmon Sensing Behavior of Silver and Gold Nanorods. *J. Phys. Chem. Lett.* **2013**, *4* (9), 1541–1545. https://doi.org/10.1021/jz4005015.

(13)   Murphy, C. J.; Sau, T. K.; Gole, A. M.; Orendorff, C. J.; Gao, J.; Gou, L.; Hunyadi, S. E.; Li, T. Anisotropic Metal Nanoparticles: Synthesis, Assembly, and Optical Applications. *J. Phys. Chem. B* **2005**, *109* (29), 13857–13870. https://doi.org/10.1021/jp0516846.

(14)   Liu, W.-C.; Tsai, D. P. Optical Tunneling Effect of Surface Plasmon Polaritons and Localized Surface Plasmon Resonance. *Phys. Rev. B* **2002**, *65* (15), 155423. https://doi.org/10.1103/PhysRevB.65.155423.

(15)   Zhang, J.; Gryczynski, Z.; Lakowicz, J. R. First Observation of Surface Plasmon-Coupled Electrochemiluminescence. *Chem. Phys. Lett.* **2004**, *393* (4–6), 483–487. https://doi.org/10.1016/j.cplett.2004.06.050.

(16)   Jiang, Y.; Wang, H.-Y.; Wang, H.; Gao, B.-R.; Hao, Y.; Jin, Y.; Chen, Q.-D.; Sun, H.-B. Surface Plasmon Enhanced Fluorescence of Dye Molecules on Metal Grating Films. *J. Phys. Chem. C* **2011**, *115* (25), 12636–12642. https://doi.org/10.1021/jp203530e.

(17)   Gryczynski, I.; Malicka, J.; Nowaczyk, K.; Gryczynski, Z.; Lakowicz, J. R. Effects of Sample Thickness on the Optical Properties of Surface Plasmon-Coupled Emission. *J. Phys. Chem. B* **2004**, *108* (32), 12073–12083. https://doi.org/10.1021/jp0312619.

(18)   Vericat, C.; Vela, M. E.; Benitez, G.; Carro, P.; Salvarezza, R. C. Self-Assembled Monolayers of Thiols and Dithiols on Gold: New Challenges for a Well-Known System. *Chem. Soc. Rev.* **2010**, *39* (5), 1805. https://doi.org/10.1039/b907301a.

(19)   Dijksma, M.; Kamp, B.; Hoogvliet, J. C.; van Bennekom, W. P. Formation and Electrochemical Characterization of Self-Assembled Monolayers of Thioctic Acid on Polycrystalline Gold Electrodes in Phosphate Buffer PH 7.4. *Langmuir* **2000**, *16* (8), 3852–3857. https://doi.org/10.1021/la991387q.

(20)   Schlenoff, J. B.; Li, M.; Ly, H. Stability and Self-Exchange in Alkanethiol Monolayers. *J. Am. Chem. Soc.* **1995**, *117* (50), 12528–12536. https://doi.org/10.1021/ja00155a016.

(21)   Esplandiú, M. J.; Hagenström, H.; Kolb, D. M. Functionalized Self-Assembled Alkanethiol Monolayers on Au(111) Electrodes: 1. Surface Structure and Electrochemistry. *Langmuir* **2001**, *17* (3), 828–838. https://doi.org/10.1021/la001139q.

(22) Furst, A. L.; Smith, M. J.; Francis, M. B. Direct Electrochemical Bioconjugation on Metal Surfaces. *J. Am. Chem. Soc.* **2017**, *139* (36), 12610–12616. https://doi.org/10.1021/jacs.7b06385.

(23) Liu, S.; Li, X.; Li, Y.; Li, Y.; Li, J.; Jiang, L. The Influence of Gold Nanoparticle Modified Electrode on the Structure of Mercaptopropionic Acid Self-Assembly Monolayer. *Electrochimica Acta* **2005**, *51* (3), 427–431. https://doi.org/10.1016/j.electacta.2005.04.038.

(24) Gole, A.; Orendorff, C. J.; Murphy, C. J. Immobilization of Gold Nanorods onto Acid-Terminated Self-Assembled Monolayers via Electrostatic Interactions. 6.

(25) Orendorff, C. J.; Hankins, P. L.; Murphy, C. J. PH-Triggered Assembly of Gold Nanorods. *Langmuir* **2005**, *21* (5), 2022–2026. https://doi.org/10.1021/la047595m.

(26) Gole, A.; Murphy, C. J. Polyelectrolyte-Coated Gold Nanorods: Synthesis, Characterization and Immobilization. *Chem. Mater.* **2005**, *17* (6), 1325–1330. https://doi.org/10.1021/cm048297d.

(27) Indrasekara, A. S. D. S.; Wadams, R. C.; Fabris, L. Ligand Exchange on Gold Nanorods: Going Back to the Future. *Part. Part. Syst. Charact.* **2014**, *31* (8), 819–838. https://doi.org/10.1002/ppsc.201400006.

(28) Casas, J.; Venkataramasubramani, M.; Wang, Y.; Tang, L. Replacement of Cetyltrimethylammoniumbromide Bilayer on Gold Nanorod by Alkanethiol Crosslinker for Enhanced Plasmon Resonance Sensitivity. *Biosens. Bioelectron.* **2013**, *49*, 525–530. https://doi.org/10.1016/j.bios.2013.05.057.

(29) Shi, D.; Song, C.; Jiang, Q.; Wang, Z.-G.; Ding, B. A Facile and Efficient Method to Modify Gold Nanorods with Thiolated DNA at a Low PH Value. *Chem. Commun.* **2013**, *49* (25), 2533. https://doi.org/10.1039/c3cc39093d.

(30) Hill, H. D.; Millstone, J. E.; Banholzer, M. J.; Mirkin, C. A. The Role Radius of Curvature Plays in Thiolated Oligonucleotide Loading on Gold Nanoparticles. *ACS Nano* **2009**, *3* (2), 418–424. https://doi.org/10.1021/nn800726e.

(31) Cao, J.; Sun, T.; Grattan, K. T. V. Gold Nanorod-Based Localized Surface Plasmon Resonance Biosensors: A Review. *Sens. Actuators B Chem.* **2014**, *195*, 332–351. https://doi.org/10.1016/j.snb.2014.01.056.

(32) Yu, C.; Varghese, L.; Irudayaraj, J. Surface Modification of Cetyltrimethylammonium Bromide-Capped Gold Nanorods to Make Molecular Probes. *Langmuir* **2007**, *23* (17), 9114–9119. https://doi.org/10.1021/la701111e.

(33) Alper, J.; Hamad-Schifferli, K. Effect of Ligands on Thermal Dissipation from Gold Nanorods. *Langmuir* **2010**, *26* (6), 3786–3789. https://doi.org/10.1021/la904855s.

Chapter four

Conclusion

Bipolar electrochemistry belongs to the branch of electrochemistry where cathodic and anodic processes are coupled. As there can no direct contact be established between the bipolar electrodes and electrical connection, the best way to measure the current produced in the bipolar electrode system is by analyzing the electrochemiluminescence produces by passing the voltage across the bipolar electrode system from an external source such as a potentiostat. $Ru(bpy)_3Cl_2$ is the preferred reagent which shows ECL (electrochemiluminescence) as it is electrochemically stable [1] but it has very lower ECL efficiency 3.5-6% [2]. So, the motivation of the research came from the improvement of the sensitivity of the ECL based sensor system. ECL based Bipolar electrochemistry has application in different fields such as clinical diagnostics including thyroid, hormone, tumor, cardiac, diabetes diseases & other diseases causing infections, food testing, water testing, detection of biowarfare, detection of electrolytes and heavy metals, in detecting explosives, in batteries [1] etc.

The tendency of the gold nanorods to show surface plasmon resonance was used to improve the efficiency of the $Ru(bpy)_3Cl_2$. The condition for the surface plasmon resonance can be occurred for the nanomaterials of gold, silver, copper, because for these materials real part of the dielectric function has a negative value which produces high electric field based on the Mie theory [3].

Gold nanorods was synthesized by the seed mediated method [4] which has an aspect ratio of 2.6 and it has a longitudinal plasmon band at 650 nm for its oscillation along with the longer axis and a transverse plasmon band at 520 nm for its oscillation along with the shorter axis. There was a partial overlap between the emission band of the $Ru(bpy)_3Cl_2$ and longitudinal band of the gold nanorods. Surface plasmon resonance occurs when the incident light is parallel

to the longitudinal axis of the gold nanorod and when the absorption band of the gold matches with the wavelength of the incident light, in that case enhancement of absorption light occurs and if the scattered light's wavelength matches with the emission band of the $Ru(bpy)_3Cl_2$, then intensity of the light emitted also enhances due to the surface plasmon resonance effect [5]. In the presence of gold nanorods, radiative and non-radiative decay rate of $Ru(bpy)_3Cl_2$ changes, that also increases the intensity of light [5].

The bipolar electrochemical cell was made by photolithographic method and was cleaned by piranha solution and electrochemical method [6]. To combat the problem of quenching by oxygen produced in aqueous ECL solution, ECL experiments was tried in non-aqueous ECL system.

The ECL experiment was done by modifying the gold electrode with gold nanorod by different self-assembled monolayers and the ECL was found to be increased compared to that of bare gold electrode due to surface plasmon resonance of gold nanorods. Some lowering of the ECL intensity was also observed when the gold electrode was modified by CTAB or PDDA.

The enhancement of fluorescence in the presence of gold nanorods was also analyzed and due to the hybridization of the molecular orbital of the $Ru(bpy)_3Cl_2$ and different electronic states of the gold nanorods, the fluorescence peak of the $Ru(bpy)_3Cl_2$ not only found to be increased but the peak also splitted into multiple peaks and shifted [7] from their original position. Different amount of fluorescence enhancement was found based on different concentrations of $Ru(bpy)_3Cl_2$ in the presence of PSS, CTAB coated gold nanorods. It was found that enhancement decreased compared to the increase of concentration of $Ru(bpy)_3Cl_2$ as was observed that with increasing dye to dye separation. Higher enhancement was observed in the presence of PSS, CTAB

coated gold nanorods compared to the fluorescence spectrum of $Ru(bpy)_3Cl_2$ in the absence of PSS, CTAB coated gold nanorods [8].

For further improvement in this research, Raman enhancement of $Ru(bpy)_3Cl_2$ in the presence of gold nanorods can be analyzed [9], however higher enhancement can be found for other types of gold nanomaterials as nanomaterials with more edges and sharpness was found to produce higher electromagnetic field [10]. Other type of complexes such as ECL solution of iridium complex can be analyzed which tends to show higher ECL efficiency compared to the complexes of $Ru(bpy)_3^{2+}$ [11]. In case of single $Ru(bpy)_3Cl_2$ molecule, it is possible to excite the molecule in the parallel direction with that of the longitudinal axis of the gold nanorods which is an essential condition for observing the surface plasmon resonance [12]. Silver nanorods instead of gold nanorods can be used to modify the gold electrode or silver electrode as interband transition region is so much smaller in case of silver compared to gold and it does not overlap with the transverse or longitudinal plasmon band of silver nanoparticles. So, resonance damping does not occur in case of silver nanomaterials [13]. ECL enhancement can also be found in the presence of diffraction grating [14] or prism [15] due to the surface plasmon polaritons. Different types of self-assembled monolayer systems can be tested [16] also CTAB of gold nanorods can be replaced [17] to find an optimum metal to dye distance which can be helpful to show ECL enhancement by surface plasmon resonance technique.

Reference 4:

(1) Richter, M. M. Electrochemiluminescence (ECL). *Chem. Rev.* **2004**, *104* (6), 3003–3036. https://doi.org/10.1021/cr020373d.

(2) Wallace, W. L.; Bard, A. J. Electrogenerated Chemiluminescence. 35. Temperature Dependence of the ECL Efficiency of Tris(2,2'-Bipyridine)Rubidium(2+) in Acetonitrile and Evidence for Very High Excited State Yields from Electron Transfer Reactions. *J. Phys. Chem.* **1979**, *83* (10), 1350–1357. https://doi.org/10.1021/j100473a022.

(3) Aslam, U.; Rao, V. G.; Chavez, S.; Linic, S. Catalytic Conversion of Solar to Chemical Energy on Plasmonic Metal Nanostructures. *Nat. Catal.* **2018**, *1* (9), 656–665. https://doi.org/10.1038/s41929-018-0138-x.

(4) Chang, H.-H.; Murphy, C. J. Mini Gold Nanorods with Tunable Plasmonic Peaks beyond 1000 Nm. *Chem. Mater.* **2018**, *30* (4), 1427–1435. https://doi.org/10.1021/acs.chemmater.7b05310.

(5) Li, J.-F.; Li, C.-Y.; Aroca, R. F. Plasmon-Enhanced Fluorescence Spectroscopy. *Chem. Soc. Rev.* **2017**, *46* (13), 3962–3979. https://doi.org/10.1039/C7CS00169J.

(6) Mavré, F.; Chow, K.-F.; Sheridan, E.; Chang, B.-Y.; Crooks, J. A.; Crooks, R. M. A Theoretical and Experimental Framework for Understanding Electrogenerated Chemiluminescence (ECL) Emission at Bipolar Electrodes. *Anal. Chem.* **2009**, *81* (15), 6218–6225. https://doi.org/10.1021/ac900744p.

(7) Ni, W.; Yang, Z.; Chen, H.; Li, L.; Wang, J. Coupling between Molecular and Plasmonic Resonances in Freestanding Dye−Gold Nanorod Hybrid Nanostructures. *J. Am. Chem. Soc.* **2008**, *130* (21), 6692–6693. https://doi.org/10.1021/ja8012374.

(8) Abadeer, N. S.; Brennan, M. R.; Wilson, W. L.; Murphy, C. J. Distance and Plasmon Wavelength Dependent Fluorescence of Molecules Bound to Silica-Coated Gold Nanorods. *ACS Nano* **2014**, *8* (8), 8392–8406. https://doi.org/10.1021/nn502887j.

(9) Zhan, C.; Chen, X.-J.; Yi, J.; Li, J.-F.; Wu, D.-Y.; Tian, Z.-Q. From Plasmon-Enhanced Molecular Spectroscopy to Plasmon-Mediated Chemical Reactions. *Nat. Rev. Chem.* **2018**, *2* (9), 216–230. https://doi.org/10.1038/s41570-018-0031-9.

(10) Orendorff, C. J.; Gole, A.; Sau, T. K.; Murphy, C. J. Surface-Enhanced Raman Spectroscopy of Self-Assembled Monolayers: Sandwich Architecture and Nanoparticle Shape Dependence. *Anal. Chem.* **2005**, *77* (10), 3261–3266. https://doi.org/10.1021/ac048176x.

(11) Kapturkiewicz, A.; Angulo, G. Extremely Efficient Electrochemiluminescence Systems Based on Tris(2-Phenylpyridine)Iridium(Iii). *Dalton Trans.* **2003**, No. 20, 3907. https://doi.org/10.1039/b308964a.

(12) Chen, H.; Ming, T.; Zhao, L.; Wang, F.; Sun, L.-D.; Wang, J.; Yan, C.-H. Plasmon–Molecule Interactions. *Nano Today* **2010**, *5* (5), 494–505. https://doi.org/10.1016/j.nantod.2010.08.009.

(13) Wang, H.; Tam, F.; Grady, N. K.; Halas, N. J. Cu Nanoshells: Effects of Interband Transitions on the Nanoparticle Plasmon Resonance. *J. Phys. Chem. B* **2005**, *109* (39), 18218–18222. https://doi.org/10.1021/jp053863t.

(14) Jiang, Y.; Wang, H.-Y.; Wang, H.; Gao, B.-R.; Hao, Y.; Jin, Y.; Chen, Q.-D.; Sun, H.-B. Surface Plasmon Enhanced Fluorescence of Dye Molecules on Metal Grating Films. *J. Phys. Chem. C* **2011**, *115* (25), 12636–12642. https://doi.org/10.1021/jp203530e.

(15) Zhang, J.; Gryczynski, Z.; Lakowicz, J. R. First Observation of Surface Plasmon-Coupled Electrochemiluminescence. *Chem. Phys. Lett.* **2004**, *393* (4–6), 483–487. https://doi.org/10.1016/j.cplett.2004.06.050.

(16) Esplandiú, M. J.; Hagenström, H.; Kolb, D. M. Functionalized Self-Assembled Alkanethiol Monolayers on Au(111) Electrodes: 1. Surface Structure and Electrochemistry. *Langmuir* **2001**, *17* (3), 828–838. https://doi.org/10.1021/la001139q.

(17) Casas, J.; Venkataramasubramani, M.; Wang, Y.; Tang, L. Replacement of Cetyltrimethylammoniumbromide Bilayer on Gold Nanorod by Alkanethiol Crosslinker for Enhanced Plasmon Resonance Sensitivity. *Biosens. Bioelectron.* **2013**, *49*, 525–530. https://doi.org/10.1016/j.bios.2013.05.057.